Hashemite Kingdom of Jordan

Hashemite University

Jordan Journal of Earth and Environmental Sciences

JJEES

An International Peer-Reviewed Scientific Journal

Financed by the Scientific Research Support Fund

http://jjees.hu.edu.jo/

Volume (6) Number (1) **ISSN 1995-6681** September 2014/Dhu al-Hijjah 1435

The Jordan Journal of Earth and Environmental Sciences (JJEES)

JJEES is an international peer-reviewed research journal, issued by the Deanship of Academic Research and Graduate Studies, the Hashemite University, in corporation with, the Jordanian Scientific Research Support Fund, the Ministry of Higher Education and Scientific Research.

SUBMISSION ADDRESS:

Professor **Eid A. Al-Tarazi**
Deanship of Academic Research and Higher Studies
Hashemite University, P.O. Box 150458, Postal Code 13115, Zarqa, Jordan.
Phone: +962-5-3903333 ext. 4385
E-Mail: jjees@hu.edu.jo

Hashemite Kingdom of Jordan

Hashemite University

Jordan Journal of Earth and Environmental Sciences

JJEES

An International Peer-Reviewed Scientific Journal

Financed by Scientific Research Support Fund

http:// jjees.hu.edu.jo/

ISSN 1995-6681

المجلة الأردنية لعلوم الأرض والبيئة
Jordan Journal of Earth and Environmental Sciences (JJEES)
http://jjees.hu.edu.jo

Hashemite University

Deanship of Scientific Research and Graduate Studies

TRANSFER OF COPYRIGHT AGREEMENT

Journal publishers and authors share a common interest in the protection of copyright: authors principally because they want their creative works to be protected from plagiarism and other unlawful uses, publishers because they need to protect their work and investment in the production, marketing and distribution of the published version of the article. In order to do so effectively, publishers request a formal written transfer of copyright from the author(s) for each article published. Publishers and authors are also concerned that the integrity of the official record of publication of an article (once refereed and published) be maintained, and in order to protect that reference value and validation process, we ask that authors recognize that distribution (including through the Internet/WWW or other on-line means) of the authoritative version of the article as published is best administered by the Publisher.

To avoid any delay in the publication of your article, please read the terms of this agreement, sign in the space provided and return the complete form to us at the address below as quickly as possible.

Article entitled:----------

Corresponding author: ----------

To be published in the journal: Jordan Journal of Earth & Environmental Sciences (JJEES)

I hereby assign to the Hashemite University the copyright in the manuscript identified above and any supplemental tables, illustrations or other information submitted therewith (the "article") in all forms and media (whether now known or hereafter developed), throughout the world, in all languages, for the full term of copyright and all extensions and renewals thereof, effective when and if the article is accepted for publication. This transfer includes the right to adapt the presentation of the article for use in conjunction with computer systems and programs, including reproduction or publication in machine-readable form and incorporation in electronic retrieval systems.
Authors retain or are hereby granted (without the need to obtain further permission) rights to use the article for traditional scholarship communications, for teaching, and for distribution within their institution.

☐ **I am the sole author of the manuscript**

☐ **I am signing on behalf of all co-authors of the manuscript**

☐ **The article is a 'work made for hire' and I am signing as an authorized representative of the employing company/institution**

Please mark one or more of the above boxes (as appropriate) and then sign and date the document in black ink.

Signed:_____ **Name printed:** _____

Title and Company (if employer representative) : _____

Date: _____

Data Protection: By submitting this form you are consenting that the personal information provided herein may be used by the Hashemite University and its affiliated institutions worldwide to contact you concerning the publishing of your article.

Please return the completed and signed original of this form by mail or fax, or a scanned copy of the signed original by e-mail, retaining a copy for your files, to:

Hashemite University
Deanship of Scientific Research and Graduate Studies
Zarqa 13115 Jordan
Fax: +962 5 3903338
Email: jjees@hu.edu.jo

Subscription

Jordan Journal of Earth & Environmental Sciences (ISSN 1995-6681)
An International Peer- Reviewed Research Journal
Published by the deanship of Research and Graduate Studies- The Hashemite University

Name:	الاســـــــــــــم:
Specialty:.....	التخصـــــــــــص:
Address:.....	العنـــــــــــوان:
P.O. Box:.....	صنـــدوق البريـــــد:
City & Postal Code:	المدينة: الرمز البريدي:
Country:.....	الـــــــــــــدولة:
Phone:.....	رقـــم الهاتـــــــف:
Fax No:.....	رقـــم الفاكـــــــس:
E-mail:.....	البريـــد الإلكترونـــي:
Method of payment:	طريقـــــة الدفـــع:
Amount Enclosed:.....	المبلـــــغ المرفـــق:
Signature:.....	التوقيـــــــــــع:

Cheques should be paid to Deanship of Research and Graduate Studies- The Hashemite University

I would like to subscribe to the Journal:

For

- ☐ One year
- ☐ Two years
- ☐ Three years

One year Subscription Rates		
	Inside Jordan	Outside Jordan
Individuals	10JD	70$
Students	5JD	35$
Institutions	20JD	90$

Correspondence

Subscriptions and sales:

Prof. Dr. Eid Al-Tarazi
The Hashemite University
P.O. Box 330127- Zarqa 13115 - Jordan
Tel. +962-(0) 795651567 (mobile)
+962-5-3903333 -4385 (office)
Fax: +962 5 3903338
Email: jjees@hu.edu.jo

JJEES
Jordan Journal of Earth and Environmental Sciences

JJEES

Volume 6, Number 1, September, 2014
ISSN 1995-6681
Pages 1- 7

Jordan Journal of Earth and Environmental Sciences

What Can Be Learnt from Past Disasters? Analysis of the Mw 8.8 Mega Earthquake of Central Chile with MORT

R. Alvarado-Corona [1* 1,2], C. Mota-Hernández [1],
J. L. Félix-Hernández [1,2] and J. Santos-Reyes[1,2]

[1]TESCI, IPN, SEPI - ESIME ZAC., Distrito Federal, México
[2]SARACS Research Group, IPN, SEPI- ESIME, Distrito Federal, México

Received 29 May, 2014; Accepted 27 August, 2014

Abstract

The impact, in its various facets, caused by natural disasters, is increasing sharply. Poor resilience contributes to increasing the impact on society, throughout history; natural disasters have exerted a heavy toll of death and suffering. Given this, natural disasters present a big challenge to society today concerning how they are to be mitigated so as to produce an acceptable risk is a question which has come to the fore in extreme ways recently. The Mw 8.8 Maule earthquake of 27 February 2010 has been studied in detail. The paper presents some preliminary results of the analysis of the Chilean earthquake that occurred in February 2010, by applying the Management Oversight Risk Tree (MORT) model. Some of the key questions that have been addressed are: what can be learnt from mega earthquakes? Can MORT be applied to the analysis of mega earthquakes? The MORT may be regarded as a structured checklist in the form of a complex fault tree model that is intended to ensure that all aspects of an organization's management are looked into when assessing the possible causes of an incident. The MORT accident investigation model has been applied widely to the analysis of accident/incidents that have occurred in industries, such as the oil and gas, nuclear, aviation, etc. It may be argued that the model has the potentiality to be applied to the analysis of natural disasters such as mega earthquakes. It is hoped that by conducting such analysis lessons can be learnt so that the impact of natural disasters such as the Chile´s Mega Earthquake can be mitigated in future similar events.

Keywords: Analysis, Chile, Disasters, Mega Earthquake, MORT.

1. Introduction

The occurrence of natural phenomena, which are part of the processes of our own planet, and the link with a non-resilient society, can promote natural disasters, whose intensity depends on the maturity level of the community in question. It may be argued that once a disaster has occurred, the affected countries or communities tend to recover from it and implement 'measures', in the best cases, intended to be better prepared for future undesirable events. However, there is little evidence of a detailed and explicit analysis of disasters in order to understand what went wrong and what went right, so that lessons can be learnt. Moreover, there is little evidence in the literature concerning explicit models or methodologies aiming at analysis past disasters triggered by natural hazards, such as earthquakes. On the other hand, in the so called socio-technical systems (i.e., nuclear, petrochemical, transport, and aviation industries), a number of accident models and methodologies have been developed to analyze past failure incidents. That is, when a major accident occurs in any of these systems, usually an inquiry is set up to look at it and draw some recommendations aiming at preventing recurrence in the future. Earthquakes have exerted a heavy toll of death and suffering and are increasing in recent years: for example those occurred at Wenchuan province on 12 may 2008, China (Zhao et al., 2009), L. Aquila on 6 April 2009, Italy (Rupakhety and Sigbjornsson, 2010), (Alexander, 2012a) and (Alexander, 2012b), 12 January 2010 Italy, (USGS, 2010), 27 February, Chile (Grant, 2010), and 14 April 2010, China (BBC, 2010a-d). In addition, trends suggest that the impact of natural disasters is intensifying, with an increasing effect on poor nations largely due to growing populations and a greater vulnerability to natural hazards. Researchers, governmental and non-governmental organizations (NGO) have published a vast amount of reports and publications on the management of natural disasters. The above stresses the importance of prevention, mitigation and preparedness including evacuation planning in order to limit the impact of natural disasters. Disaster prevention includes all those activities intended to avoid the adverse impact of natural hazards (e.g. a decision not to build houses in a disaster-prone area). Mitigation, on the other hand, refers to measures that should be taken in advance of a disaster order to decrease its impact on society (e.g. developing building codes). Finally, disaster preparedness includes pre- and post- emergency measures that are intended to minimize the loss of life, and to organize and facilitate timely effective rescue, relief, and rehabilitation in case of disaster (e.g. organizing simulation activities to prepare for an eventual disaster relief operation). We must promote a mature society prone to resilience. This raises the following questions: What can be learnt from past natural disasters?, in particular, What can be learnt from mega earthquakes?

* Corresponding author. e-mail: ralvcor@gmail.com

The paper addresses the analysis of the mega earthquake disaster that occurred off the coast of central Chile on Saturday, 27 February 2010, at 03:34 local time, with a magnitude of 8.8 on the moment magnitude scale, which ranks as the sixth largest earthquake ever to be recorded by a seismograph; the approach has been the application of the Management Oversight Risk Tree (MORT) accident investigation model. The paper gives an accounting of the analysis and application of the MORT model. The present paper argues that approaches such as the Management Oversight Risk Tree (MORT) (NRI-1, 2002) can be applied to such analysis (Santos-Reyes et al., 2010; Alvarado-Corona, and Santos-Reyes, 2012). Accidents may be regarded as unplanned and unintentional events that result in the loss of human life, property, production, etc. (Gavious et al., 2009; LaBelle, 2000). Moreover, these losses increase an organization's operating cost, decrease efficiency, and some undesirable long term effects such as an unfavorable public opinion (Cullen, 1990). A number of accident and seismic analysis tools have been developed to address this, see for example, PRISMA (Van der Schaaf, 1996); STAMP (Leverson, 2004); MORT (Johnson, 1980); Accimap (Rasmussen, 1997; Hopkins, 2000); see also Hale et al. (1997) and Deng et al. (2014). It may be argued that accident analysis tools are intended to help to identify 'root causes' of accidents so that lessons can be learnt and prevent recurrence. Some authors, such as Johnson (2003) has addressed this by proposing some useful causal concepts based on early works on causation by Lewis (1973, 1986) and Mackie (1993). Some authors (Absolon, 1994; Jeynes, 2002), define Risk management as a decision making process that takes into consideration multiple factors with relevant risk assessments relating to a potential hazard, so it is known that every logistic company has a lot of risks (Siu-Lun et al., 2009). Some other analytical tools for service industries, and Risk Based Models, such as Risk Management Model for Merger and Acquisition (Chui, 2011) would be interesting for an extended and preliminary analysis, particularly in changing information technology environments (Tak 2011; Olla and Patel, 2002). It is important to notice Chile's long experience on quakes. A preliminary analysis of an extreme event (mega quake), that occurred in Chile on 27 February 2010 (USGS, 2010), Chile is presented.

2. The 8.8 Mega Earthquake

An 8.8 magnitude mega quake struck the Chilean coast on February 27, 2010, despite the magnitude of the mega earthquake, Chile suffered relatively little impact. Chile´s massive mega earthquake caused widespread damage, knocking down buildings, bridges and roads in many areas, land and water level variations were reported (Farías et al,. 2010), also triggered a tsunami that devastated some coastal areas of the country. Electricity, water and phone lines were cut. The earthquake occurred at the boundary between the Nazca and South American tectonic plates. At least 523 people killed, 24 missing, about 12,000 injured, 800,000 displaced and at least 370,000 houses, 4,013 schools, 79 hospitals and 4,200 boats damaged or destroyed by the earthquake and tsunami in the Valparaiso-Concepcion-Temuco area. In addition, 1.8 million people were affected in Araucania, Bio-Bio, Maule, O'Higgins, Region Metropolitana and Valparaiso. The economic loss in Chile was estimated at 30 billion US dollars. Electricity, telecommunications and water supplies were disrupted and the airports at Concepcion and Santiago suffered minor damage. The tsunami damaged many buildings and roads at Concepcion, Constitucion, Dichato and Pichilemu and damaged boats and a dock in the San Diego area, USA. Maximum acceleration of 0.65g was recorded at Concepcion and more than 2 m of uplift along the coast was observed near Arauco.

The mega earthquake was generated at the gently sloping fault that conveys the Nazca plate eastward and downward beneath the South American plate. The two plates are converging at 7 meters per century. The fault rupture, largely offshore, exceeded 100 km in width and extended nearly 500 km parallel to the coast. The rupture began deep beneath the coast and spread westward, northward, and southward. As it spread, the fault slip generated earthquake shaking. Some investigations have attempted to determine features of the rupture propagation to clarify why the Maule incident became a mega earthquake with the use of GPS technology (Vigny et al., 2011). The fault slip also warped the ocean floor, setting off the tsunami along the fault-rupture area. Liquefaction was observed to have occurred over a large area of Chile affected by the earthquake. The widespread presence of river sediments and the long duration of the event most likely contributed to the large number of observations of liquefaction. This was the strongest earthquake affecting Chile since the magnitude 9.5 1960 Valdivia earthquake (the most energetic earthquake ever measured in the world), and it was the strongest earthquake worldwide since the 2004 Indian Ocean earthquake and until the 2011 Tōhoku earthquake. It is tied with the 1906 Ecuador-Colombia and 1833 Sumatra earthquakes as the sixth strongest earthquake ever measured, approximately 500 times more powerful than the 7.0 Mw earthquake in Haiti in January 2010. Seismologists estimate that the earthquake was so powerful that it may have shortened the length of the day by 1.26 microseconds and moved the Earth's Figure axis by 8 cm. Nearly half the places in the country were declared "catastrophe zones", and curfews were imposed in some areas of looting and public disorder. A day after the mega earthquake, some affected cities were chaotic, with extensive looting of supermarkets in Concepción. Items stolen included not only food and other necessities, but also electronic goods and other durable merchandise. To control vandalism, a special police was sent to disperse rioters with tear gas and water cannons. The outgoing president didn't want to remind people of the Dictatorship years by militarizing the streets, thus failed to provide assistance on time to the city. When the situation became unsustainable and all sectors of the population were demanding actions, the government authorized the use of the military to control the affected cities. Despite these and other government acts, pillaging continued in both urban and rural areas of the affected zones. According to "Shake Map" of the Geological Survey of the United States (NEIC-USGS, 2010), the maximum intensities and the Epicenter of the mega earthquake are shown in Fig 1.

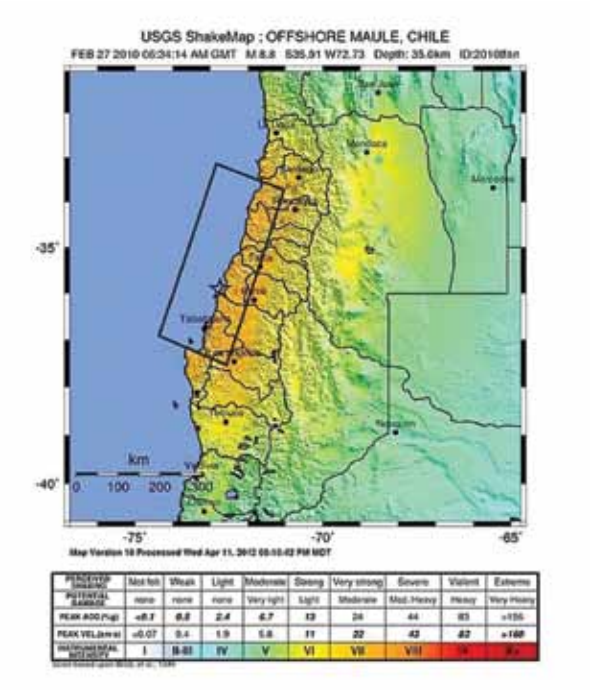

Figure 1: Epicenter of the Mega Earthquake on February 27 in Chile (USGS, 2010).

Several factors contributed overall to the low casualty rate and rapid recovery. A major factor is the strong building code in Chile and its comprehensive enforcement. In particular, Chile has a law that holds building owners accountable for losses in a building they build for 10 years. A second factor was the limited number of fires after the quake. Third, in many areas, the local emergency response was very effective. The fourth factor was the overall high level of knowledge about earthquakes and tsunamis the population. Some efforts look for anticipate the occurrence of mega earthquakes in the Andean subduction zone (Moreno et al., 2010). Table 1 Summarizes the Consequences of the 2010 Mega Earthquake.

Large undersea earthquakes usually cause tsunamis and tsunami waves travel fast. A tsunami warning was first declared for Chile and Peru. The warning was later extended to a Pacific Ocean-wide warning, covering all coastal areas on the Pacific Ocean except the west coast of the United States, British Columbia, and Alaska. Hawaiian media reported that tsunami-warning sirens first sounded at 06:00 local time. The U.S. Tsunami Warning Center issued advisories about potential tidal waves of less than 1m striking the Pacific Ocean coastline between California and most of Alaska late in the afternoon or through the evening 12 or more hours after the initial earthquake. Although the mega earthquake killed far fewer people than the Haitian earthquake less than 7 weeks prior, it was still devastating. Tsunamis tend to come in several waves, of which the first may not be the highest. The U.S. National Weather Service's Pacific Tsunami Warning Center issued a tsunami warning throughout a huge swathe of the Pacific region, including Antarctica. Figure 2 shows an energy propagation pattern of the 27 February 2010 tsunami calculated with MOST forecast model according to the National Oceanic and Atmospheric Administration (NOAA). Filled colors show maximum computed tsunami amplitude in cm during 24 hours of wave propagation. Black contours show computed tsunami arrival time..

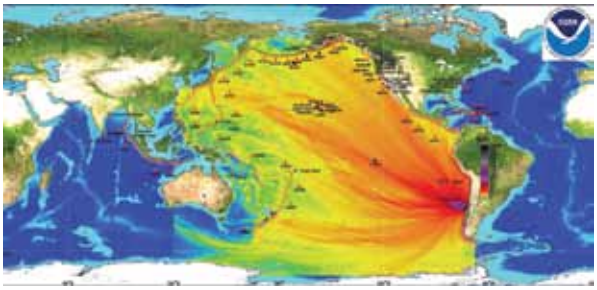

Figure 2: Energy Propagation Pattern of the 27 February 2010 Tsunami (NOAA, 2014).

Table 1: Consequences of the Disaster (American Red Cross Multi-Disciplinary Team, 2011).

Mega Earthquake and Tsunami	People Killed and Missing Persons	Estimated Population Affected	Homes and Buildings Affected	Estimated Economical Losses
The moment magnitude 8.8 Maule Mega Earthquake struck at 3:34 a.m. on Saturday, February 27, 2010. A Tsunami measuring up to 8 feet struck coastal areas between Concepcion and Valparaiso.	According to official information, 521 people were killed and 56 considered missing.	1.5 to 2 million affected	370,000 homes were destroyed or severely damaged. The quake affected 73 hospitals and 221 bridges. More than 3,049 schools, housing 1.25 million students were damaged or destroyed	$30 billion of US Dollars

3. The Mort and the Accident Analysis Techniques (Fault Trees)

Inside accident analysis techniques, fault trees extend concepts and relations from systems engineering to support the analysis of adverse incidents based on the idea that the causes of a complex event can be analyzed by a conjunction of simpler interrelated precursors.

This section presents a brief overview of the Management Oversight Risk Tree (MORT) tool that has been applied to the analysis of the mega earthquake. In addition, a summary of the main findings so far are presented in section 3.2.

3.1. The Accident Investigation Model (MORT)

The Management Oversight and Risk Tree (MORT) is an analytical procedure for determining causes and contributing factors. In MORT, accidents are defined as "unplanned events that produce harm or damage, that is, losses" (NRI-l, 2002). Losses occur when a harmful agent comes into contact with a person or asset. This contact can occur either because of a failure of prevention or, as an unfortunate but acceptable outcome of a risk that has been properly assessed and acted-on (a so-called "assumed risk"). MORT analysis always evaluates the "failure" route before considering the "assumed

risk" hypothesis. In MORT analysis, most of the effort is directed at identifying problems in the control of a work/ process and deficiencies in the protective barriers associated with it. These problems are then analyzed for their origins in planning, design, policy, etc. In order to use MORT key episodes in the sequence of events should be identified first; each episode can be characterized as: (a) a vulnerable target exposed to; (b) an agent of harm in the; (c) absence of adequate barriers.

The "Barrier analysis" is intended to produce a clear set of episodes for MORT analysis. It is an essen¬tial preparation for MORT analysis. The barrier analysis embraces three key concepts, namely: (a) "energy"; (b) "target"; and (c) "barrier". "Energy" refers to the harmful agent that threatens or actually damages a "Target" that is exposed to it. "Targets" can be people, things or processes - anything, in fact, that should be protected or would be better undisturbed by the "Energy". In MORT, an incident can result either from exposure to an energy flow without injuries or damage, or the damage of a target with no intrinsic value.

MORT may be regarded as an analytical technique that has been widely used in accident analysis of socio-technical systems MORT is in essence a graphical checklist that contains generic questions that the analysts attempt to answer using available factual data. MORT technique helps to identify multiple causal factors that contribute to an undesirable event or incident, i.e., a natural disaster. Fig. 3 shows the basic structure of the MORT chart.

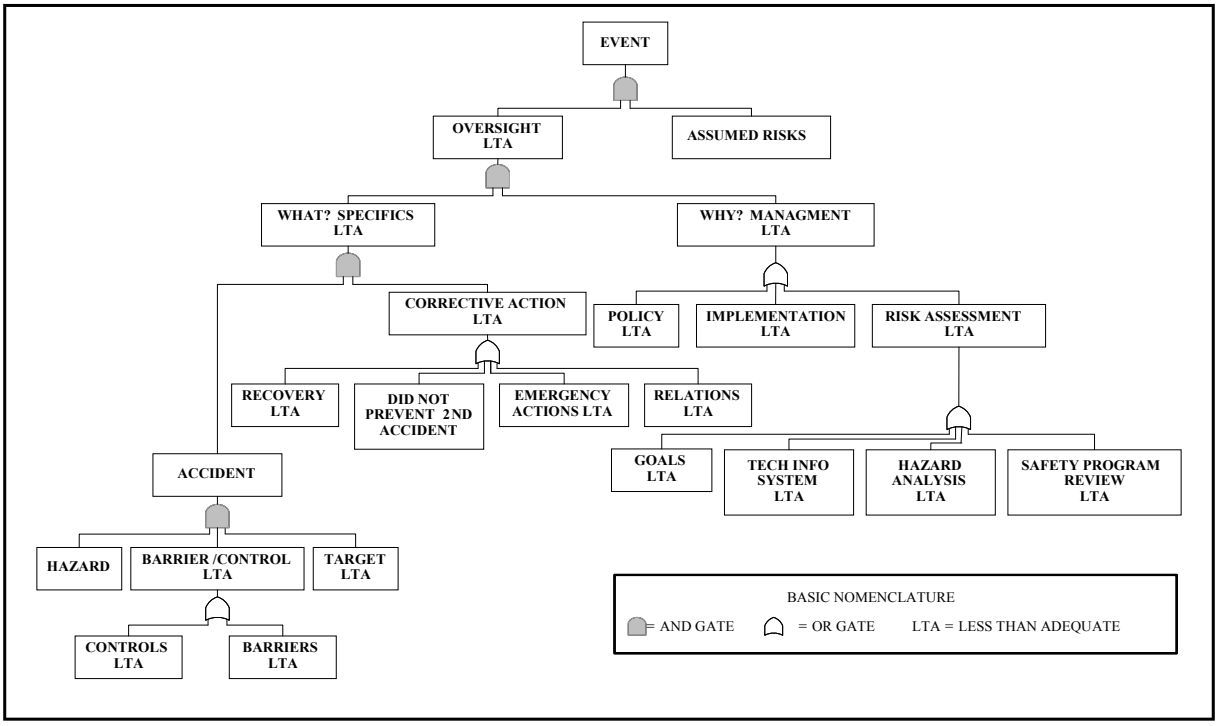

Figure 3: Overview of the Basic Structure of MORT (Adapted from NRI-1, 2002).

In MORT, accidents are defined as "unplanned events that contribute to a mishap and produce harm or damage, that is, losses" (NRI-1, 2002) as shown in Fig. 1. "The losses" represent the top event (T), beneath which are its two alternative causes; i-e. (a) "Oversight and omissions", and (b) "Assumed risks". In MORT all the contributing factors in the accident sequence are treated as "Oversights and Omissions unless they are transferred to "Assumed Risk" branch of the tree. "Specific Control Factors LTA" (S) and "Management System Factors LTA" (M) are inputs to the "Oversights and omissions" event (S/M).

Moreover, both inputs are through and AND logic gate; this means that problems manifest in the specific control of work activities, necessarily involve issues in the management process that govern them. Furthermore, both "Specific Control Factors LTA" and "Management System Factors LTA" are broken down into further events that should be look at when analyzing accidents (see NRI-1, 2002) for further details about these.

3.2. The Analysis

MORT is a generic technique, in MORT analysis, most of the effort is directed at identifying problems in the control of a "work/process" and deficiencies in the protective barriers associated with it. These "problems" are then analyzed for their origins in planning, design, policy, etc. A color code has been used to conduct the analysis; i.e., if an event was considered to be deficient or "Less Than Adequate-LTA", then it was marked 'red'; an event that is 'satisfactory' was marked green. On the other hand, if an issue is considered to be relevant but there is not enough information to assess it, then this was marked blue.

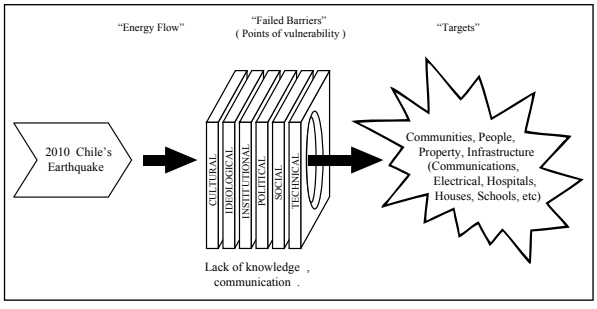

Figure 4: Barrier Analysis in 2010 Chile´s Mega Earthquake.

In order to conduct the analysis of the disaster by applying MORT, a "barrier analysis" needs to be conducted. The "barrier analysis" is intended to produce a clear set of episodes for MORT analysis embraces three key concepts. "Energy", "Target" and "Barrier", "Energy" refers to the harmful agent that threatens or actually damages a "target" that is exposed to it. Fig. 4 illustrates the three concepts that have been considered for the analysis applying the accident investigation model (MORT). "Targets" have been defined as the population, infrastructure, etc. that should be protected or would be better undisturbed by the "Energy" (i.e., a mega earthquake). "Barriers", on the other hand, may be regarded as the means by which "Targets" are kept safe from "Energies". Figures 5 and 5.1, show the initial and condensed results of the diagnostic for the Energy Flow obtained from the barrier analysis.

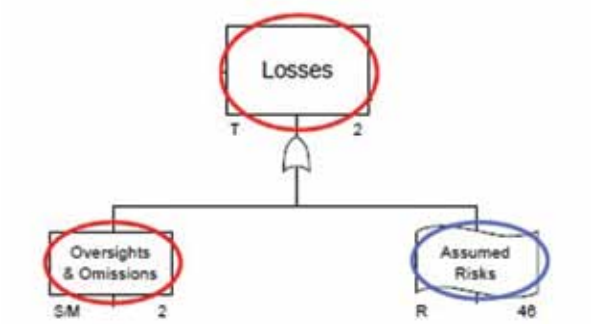

Figure 5: Initial Results of the Diagnostic for the Energy Flow Obtained from the Barrier Analysis. (Red: problems that contributed to the outcome. Blue: need more information. Green: is judged to have been satisfactory) (Adapted from NRI-2, 2002).

Examples of the branches of the tree shown in the above are presented in following Figs. 6 and 7. For example, Figure 6 shows the deficiencies and/or omissions (in red) that were found when assessed the branch indicated as "SB1-Flow of Energy or Harmful Condition." On the other hand, deficiencies found when assessed the branch indicated as "SA2-Stabilisation and Restoration" are shown in Fig. 7. This branch has been used to assess whether actions have been preplanned as opposed to occurring fortuitously at the time of the disaster.

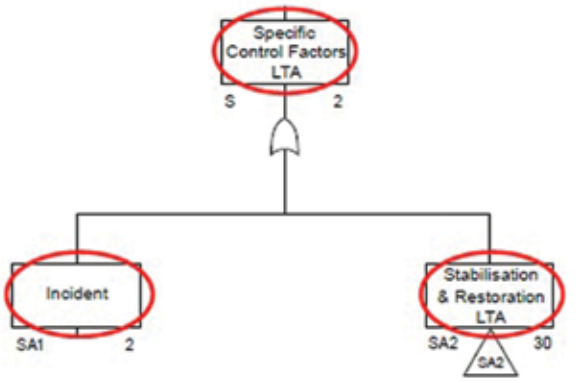

Figure 5.1: Specific Control Factors Branch: Condensed Results of the Diagnostic for the Energy Flow. (Red: problems that contributed to the outcome. Blue: need more information. Green: is judged to have been satisfactory (Adapted from NRI-2, 2002).

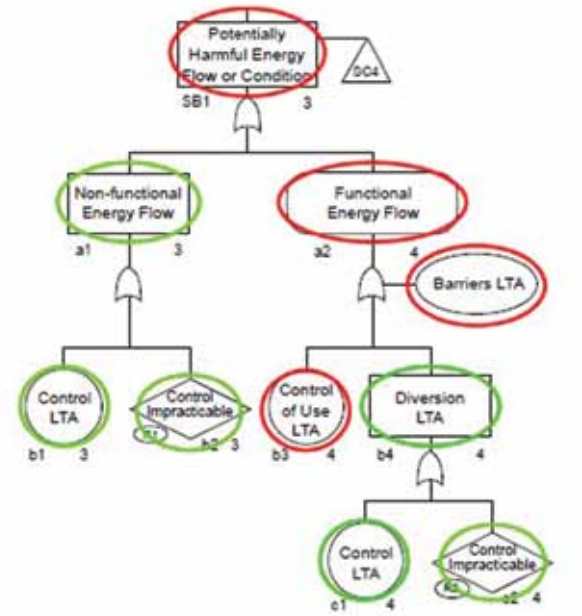

Figure 6: Branch Indicated as "SB1-Flow of Energy or Harmful Condition."

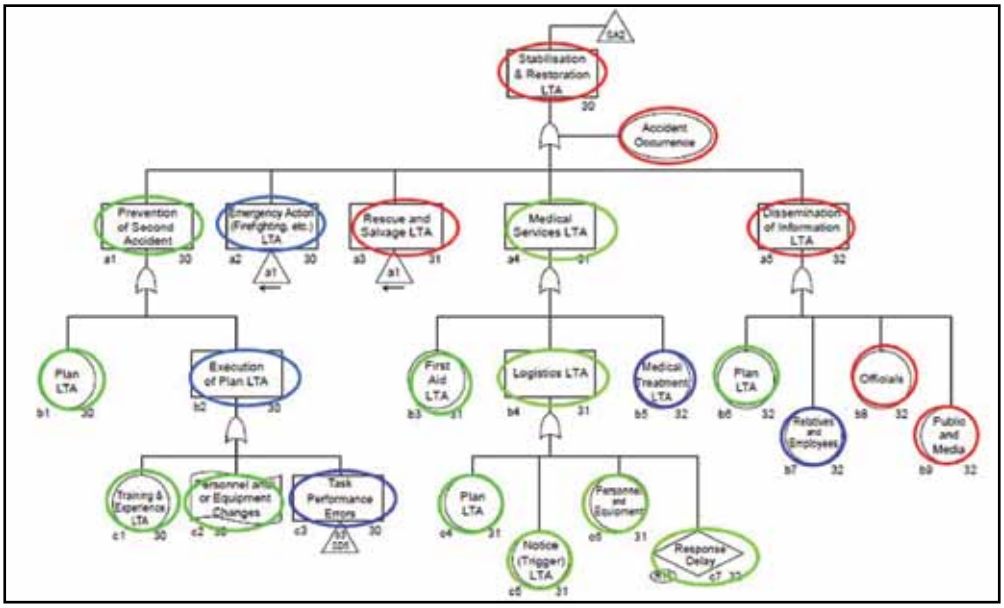

Figure 7: Branch Indicated as "SA2-Stabilisation and Restoration LTA."

Table 2: Some of the Causal Factors Identified on the what? Branch of MORT

No.	Description
1	Some barriers failed at the time of the disaster; i.e. there were not adequate early warning systems. Moreover, in some cases building codes aiming at reducing the vulnerability of buildings to earthquakes were not adequately followed. Furthermore, some key organizations dealing with natural disasters were damaged and had to be restructured.
2	Inadequacy of technical information related to early warning, etc.
3	Lack of knowledge from codes and manuals regarding the construction of buildings. Furthermore, people did not know exactly what to do under such circumstances; i.e. how to act and evacuate from buildings, homes, etc.
4	There have been a number of mega earthquakes and tsunamis in the past. However, lessons were not adequately learned from them.
5	Inadequacy of communication knowledge of the disaster severity amongst the authorities, local civil protection and the population.
6	Deficiencies of the internal communication; i.e. the population did not know exactly what to do and there was confusion.
7	The "operational readiness" was not assured at the time of the disaster; i.e. the population has not been well prepared how to act when earthquake and a tsunami of such magnitude struck.
8	Inadequate coordination amongst key organizations involved in dealing with disasters at the time.
9	Deficiencies in the process of evacuation and rescue. Organizations such as explicit "civil protection" failed at the time of the disaster.
10	Without evidence of decision-making based on risk assessment.

4. Conclusions and Future Directions

This paper discusses the application of an accident investigation model to the case of natural disasters. Some preliminary results of the 2010 Chile's mega earthquake that occurred in February 27, 2010, at 03:34 local time, have been presented. The approach has been the application of the Management Oversight and Risk Tree (MORT) accident investigation model. The MORT accident investigation model has highlighted a number of causal factors leading to the earthquake. It may be argued that most of the causal factors identified by the application of the model can be broadly grouped within the 'hazard analysis process', based on Briscoe´s categories (Briscoe, 1991; Johnson, 2003), and has the potentiality (and presumably other accident analysis techniques) to be used to identify causal factors to the case of natural and technological disasters. MORT has been used extensively to the analysis of failure of socio-technical systems (i.e., nuclear, oil and gas, transport, petrochemical, etc.). For example, to identify why the factors pointed on the what-branch of MORT happened (see Table 2). Also, it may be argued that a prepared community response saves lives. However, further research is needed in order to draw some final lessons and conclusions from the 2010 Chile´s mega earthquake. This may be achieved by applying other accident analysis approaches, such as PRISMA (Van der Schaaf ,1996), Accimap (Rasmussen, 1997; Hopkins, 2000) and the SDMS model (Santos-Reyes and Beard, 2010), and others that could be relevant. The present paper argues that by analyzing past mega earthquake disasters, such as the 2010 Chile's mega earthquake, lessons can be learnt so that the consequences of similar events can be mitigated and it is hoped that by conducting such analysis the resilience capacity can be improved in the future to reduce natural disasters impact.

Acknowledgements

The authors wish to express their sincere thanks to NOAA and USGS Agencies (Among others). This project was funded by SEP, CONACyT, TESCI and IPN (www.ipn.mx).

References

[1] Absolon, P., 1994. Risk Management in a TQM environment, Stanley Thornes, Cheltenham, England.

[2] Alexander, D.E., 2012a. Mortality and morbidity risk in the L'Aquila, Italy, earthquake of 6 April 2009 and lessons to be learned. In R. Spence, E. Ho and C. Scawthorn (eds) Human Casualties in Earthquakes. Advances in Natural and Technological Hazards Research no. 29, Springer, Berlin, Ch. 13.

[3] Alexander, D.E., 2012b. An evaluation of the medium-term recovery process after the 6 April 2009 earthquake in L'Aquila, central Italy. Environmental Hazards: Human and Policy Dimensions.11.

[4] Alvarado-Corona, R., and Santos-Reyes, J., 2012. Applying MORT to the analysis of the Haiti's earthquake. Disaster advances, 5(4), 102-109.

[5] American Red Cross Multi-Disciplinary Team, 2011. Report on the 2010 Chilean earthquake and tsunami response: U.S. Geological Survey Open-File Report 2011-1053, v. 1.1, 68 p., available at http://pubs.usgs.gov/of/2011/1053/ (Accessed: 19/05/2014).

[6] BBC, 2010a. Earthquakes. http://.news.bbc.co.uk/2/hi/science/nature. (Accessed: 15/09/2010).

[7] BBC, 2010b. Floods. http://.news.bbc.co.uk/2/hi/science/nature. (Accessed: 15/09/2010).

[8] BBC, 2010c. Haiti cholera outbreak spreads to Port-au-Prince prison. http://www.bbc.co.uk/news/world-latin-america-11800143. (Accessed: 19/11/2010)

[9] BBC, 2010d. Hundreds die in west China quake. BBC NEWS: http://news.bbc.co.uk/go/pr/fr/-/hi/world/asiapacific/8619135.stm (Accessed: 14/04/2010).

[10] Briscoe, G.J., 1991. MORT-based risk management. Technical Report Working Paper 28, System Safety Development Centre, E.G.and G Idaho, Inc., Idaho Falls, USA.

[11] Chui B. S., 2011. A Risk Management Model for Merger and Acquisition. International Journal of Engineering Business Management, 3, 37-44.

[12] Cullen, W. D., 1990. The Public Inquiry into Piper Alpha Disaster. HMSO, London, UK. Federal Emergency Management Agency (FEMA), 2004. Flooding: America's #1 Natural Hazard! News Release No. 1530-027. August 16, 2004, Department of Homeland Security, US.

[13] Deng, X., Yuan, S., Si, Q., Li, Y., Pei, J., and Yuan, J., 2014. 1209. Seismic response analysis of residual heat removal pump considering transient fluid excitation force in 1000-MW nuclear power plants. Journal of Vibroengineering, 16 (2).

[14] Farías, M., Vargas, G., Tassara, A., Carretier, S., Baize, S., Melnick, D., and Bataille, K., 2010. Land-level changes produced by the Mw 8.8 2010 Chilean earthquake. Science, 329(5994), 916-916.

[15] Gavious, A.; Shlomo Mizrahi, S.; Yael Shani, Y.; Minchuk Y., 2009. The cost of industrial accidents for the organization: developing methods and tools for evaluation and cost-benefit analysis of investment in safety. Journal of Loss Prevention in the Process Industries, 22, 434-438.

[16] Grant, Will, 2010. Chileans bitter about quake response. BBC NEWS: http://news.bbc.co.uk/go/pr/fr/-/1/hi/world/americas/8548774.stm (Accessed: 12/04/2010).

[18] Hale, A.; Wilpert, B.; Freitag, M., 1997. After the Event: From Accident to Organizational Learning Pergamon, New York.

[19] Hopkins, A., 2000. Lessons from Longford – The Esso Gas Explosion. CCH, Australia.

[20] Jeynes, J., 2002. Risk Management: 10 principles, Butterworth-Heinemann, Oxford.

[21] Johnson, C. W., 2003. A handbook of Incident and Accident Reporting, Glasgow University Press, UK.

[22] Johnson, W. G., 1980. MORT Safety Assurance System Marcel Dekker, New York, USA.

[23] LaBelle, J. E., 2000. What do accidents truly cost? Professional Safety 45, 38-42.
[24] Leverson, N. G., 2004. A New Accident Model for Engineering Safer System. Safety Science 42 (4).
[25] Lewis, D., 1973. Counterfactuals. Oxford University Press Oxford, UK.
[26] Lewis, D., 1986. Philosophical Papers, vol. II. Oxford University Press, New York, USA.
[27] Mackie, J. L., 1993. Causation and Conditions. In: Sosa, E., Tooley, M. (Eds.), Causation and Conditions. Oxford University Press, Oxford, UK, 33-56.
[28] Moreno, M., Rosenau, M., and Oncken, O., 2010. Maule earthquake slip correlates with pre-seismic locking of Andean subduction zone. Nature, 467 (7312), 198-202.
[29] NEIC (National Earthquake Information Center)., 2010. NEIC-United States Geological Survey. 2010 Página de internet http://earthquake.usgs.gov/regional/neic/ (Accessed: 12/01/2010).
[30] NOAA Center for Tsunami Research. http://nctr.pmel.noaa.gov/chile20100227/fmaxamp.png (Accessed: 05/05/2014).
[31] NRI-1, 2002. MORT user´s manual. For use with the Management Oversight and Risk Tree analytical logic diagram (NRI-2). Noordwijk Risk Initiative Foundation (NRI). The Netherlands.
[32] NRI-2., 2002. MORT chart. For use with the MORT users' manual (NRI-1). Noordwijk Risk Initiative Foundation (NRI). The Netherlands.
[33] Olla P., and Patel, N. V., 2002. A Value Chain Model for Mobile Data Service Providers. Telecommunications Policy, 26 (9-10), 5551-5571.
[34] Rasmussen, J., 1997. Risk Management in a Dynamic Society: A Modelling Problem Safety Science, vol. 27. Elsevier Science Ltd., 183-213.
[35] Rupakhety, R. and Sigbjornsson, R., 2010. A note on the L'Aquila earthquake of 6 April 2009: Permanent ground displacements obtained from strong-motion accelerograms. Soil Dynamics and Earthquake Engineering, 30, 215-220.
[36] Santos-Reyes, J., Alvarado-Corona, R., and Olmos-Peña, S., 2010. Learning from Tabasco's floods by applying MORT. Safety science, 48(10), 1351-1360.
[37] Santos-Reyes, J., and Beard, A. N., 2010. A systemic approach to managing natural disasters. In Asimakopoulou, E., and Bessis, N. Eds., Advanced ICTs for Disaster Management and Threat Detection: Collaborative and Distributed Frameworks. New York: Information Science Publishing.
[38] Siu-Lun Ting, Jacky; Siu-Keung Kwok; Hing-Choi Tsang Albert, 2009. Hybrid Risk Management Methodology: A Case Study. International Journal of Engineering Business Management, 1, 25-32.
[39] Tak Ming, Lam, 2011. Value Chain flexibility with RFID: A case Study of the Octopus Card. International Journal of Engineering Business Management, 3, 44-49.
[40] USGS, 2010. Magnitude 7.0- Haiti region-2010. http://earthquakes/eqintthenews/2010/us2010rja6/ (Accessed: 12/04/2010).
[41] Van der Schaaf, T.W., 1996. PRISMA: A Risk Management Tool Based on Incident Analysis. International Workshop on Process Safety Management and Inherently Safer Processes, October 8-10, Orlando, FL, USA, 242-251.
[42] Vigny, C.; Socquet, A.; Peyrat, S.; Ruegg, J. C.; Métois, M.; Madariaga, R.; Morvan, S.; Lancieri, M.; Lacassin, R.; Campos, J.; Carrizo, D.; Bejar-Pizarro, M.; Barrientos, S.; Armijo, R.; Aranda, C.; Valderas-Bermejo, M. C.; Ortega, I.; Bondoux, F.; Baize, S.; Lyon-Caen, H.; Pavez, A.; Vilotte, J. P.; Bevis, M.; Brooks, B.; Smalley, R.; Parra, H.; Baez, J. C.; Blanco, M.; Cimbaro, S. and Kendrick, E., 2011. 'The 2010 Mw 8.8 Maule mega-thrust earthquake of Central Chile, monitored by GPS', Science 332 (6036) , 1417—1421.
[43] Zhao, B., Taucer, F., and Rossetto, T., 2009. Field investigation on the performance of building structures during the 12 May 2008 Wenchuan earthquake in China. Engineering Structures, 31, 1707-1723.

JJEES

Volume 6, Number 1, September, 2014
ISSN 1995-6681
Pages 9- 14

Jordan Journal of Earth and Environmental Sciences

Adsorption of Hexavalent Chromium Cr(VI) by Using Local Jordanian Sand (LJS) and Iron Dust-Sand Mixed Adsorbents

Aymen Abdul-Salam M. Awad

Middel East University – MEU, Jordan

Faculty of Engineering and Technology - Head of Civil Engineering Department

Received 27 November, 2013; Accepted 7 September, 2014

Abstract

Hexavalent chromium is a known carcinogen. It is generated during the electroplating, leather tanning, mining, and photography industries cause harm to the environment and water resources. An attempt for cost effective adsorbent was made by utilizing sand and iron-sand mixed adsorbents. Sand adsorbent was found to exhibit remarkable adsorption capacity for hexavalent chromium. The extent of Cr(VI) removal was found to be dependable on the solution pH, Cr(VI) initial concentration, contact time, sand adsorbent dosage, and the iron content in iron-sand mixed adsorbent. The optimum pH for the removal was found to be 2. The highly removed concentrations by sand adsorbent ranged from 0 to 40 mg/l. It was found that as contact time increases the removal efficiency of Cr(VI) increases. Variation in sand adsorbent dosages indicated that as the adsorbent dosage increases the removal efficiency increases and it was reached to 65% at 40 hours. On the other hand, the effect of iron mixed with sand adsorbent was examined at two stages; first, at low Cr(VI) concentration solution of 20 mg/l, and, second, at high initial concentration of Cr(VI) up to 1000 mg/l. By using the optimal iron dosage, the removal efficiencies were increased to 99% within 1 to 3 hours at 20, 61, 171, 345 and 1000 mg/l of Cr(VI) initial concentrations.

Keywords: Hexavalent chromium, adsorbent, adsorption, Sand adsorbent (LJS), iron-sand mixed adsorbent, removal.

1. Introduction

Wastewater from metal finishing industries contains contaminants such as heavy metals, organic substances, cyanides, and suspended solids, at levels which are hazardous to the environment. One of these heavy metals pollutants generated from the industry is hexavalent chromium [Cr(VI)]; the pollutant of greatest concern because of its toxicity (Kirk and Othmer, 1980; and Costa and Klein, 2006). Concentrations as low as 0.5 ppm in solution and 5 ppm in soils can be toxic to plants; in contrast Cr(III) is generally only toxic to plants at very high concentrations and is necessary in animal nutrition. Chromate or Cr(VI) is 100 times more mobile and more toxic than Cr(III), (Sang et al., 2002). A number of treatment methods for the removal of metal ions from aqueous solutions have been reported, mainly reduction, ion exchange, electrodialysis, electrochemical precipitation, evaporation, solvent extraction, reverses osmosis, chemical precipitation and adsorption, (Patterson, 1985).

One potential strategy is to use low-cost natural materials as sorbents for the contaminants of concern. Due to their low cost these materials could be disposed of directly when their sorptive capacity is exhausted rather than regenerating and reusing them (Bajpai, 2001; Matin et al., 2003; and Vikrant and Pant, 2006).

Studies conducted by Schmidt, 1977 and Ellis, 1985 revealed a significant removal of water-borne heavy metals by sand filtration. These preliminary findings were later confirmed by several workers, who thoroughly investigated the adsorption of heavy metals on sand and other similar materials. Ghanayem, 1989, reported that soil and soil materials such as clay minerals could play an important role in eradicating various heavy metals. Similarly, Muhammad, et al., 1997. found that passing wastewater containing heavy metals through a slow sand filter may produce effluents complying with the world health organization (WHO) guidelines for drinking water. Very high removal efficiencies of Cr (VI) were also achieved by adsorption on kaolinite and illite (Ward, 1990). The transport and mobility of hexavalent chromium in soils were found mainly to be controlled by adsorption and reduction processes. Reduction of Cr (VI) is caused by the magnetite present in the soil as concluded by (Azizian, 1993).

Using iron in different states under especial techniques have been considered to reduce the content of chromium ions from industrial and wastewater effluents. Abdo et al. (1998) used scrap iron to reduce hexavalent chromium to trivalent chromium with simultaneous generation of electrical energy using a divided parallel plate cell and fixed bed electrodes. It was also reported that the reduction of hexavalent chromium to trivalent chromium using pure iron wire is effective in reducing Cr(VI) to Cr(III) under pH conditions of 2-3 as concluded by (Gould, 1982). Later, El-Shazly et al., 2005 studied the reduction of hexavalent chromium and its kinetics by using a fixed bed of scrap bearing iron spheres and they concluded that such technique reduces Cr(VI) to trivalent state successfully. Rodriguez and Martinez (2005) concluded that a high and fast reduction of hexavalent chromium from wastewaters was according to a study in a tubular electrochemical reactor utilizing the oxidation of iron to Fe(II) in acid solution to aid the overall process at different pH levels.

It is a matter of fact that searching for a new non-conventional water resource in Jordan has the first priority. This research will focus on examining a potential lower cost treatment technique of the industrial wastewater for reuse applications or for a safe disposal of treated industrial wastewater.

2. Materials and Methods

A local Jordanian sand sample (LJS) of 25 kg was prepared by washing and dried at 104ºC and then used for all experimental investigations, while, the iron dust was obtained from a dust collection system of a steel shot blasting facility. A 3000 ppm stock solution of hexavalent chromium Cr(VI) was prepared by dissolving the required quantity of solid chromium trioxide in distilled water. Solutions of the desired concentrations were then prepared by diluting the appropriate volumes of the stock solution using distilled water. 1N hydrochloric acid was utilized for washing and rinsing of lab equipments used in the current study. Meanwhile 0.1N sulfuric acid and A lab grade of 0.1M sodium hydroxide solution were used for adjustment of pH of Cr(VI) solutions investigated. Four sets of batch experiments were carried out to investigate the effect of the solution acidity, adsorbate initial concentration, adsorbent dosage and iron dust-sand ratio. All batch experiments were carried out at room temperature and a rotation speed of 150 rpm. An analytical digital balance (Mettler AE200, USA), with 0.1 mg readability and 205 gram capacity was used to weigh the required amounts of chromium trioxide as well as sand and iron dust.

Prior to analysis, samples of Cr(VI) solution were filtered through a 0.45 µm membrane filter and their pH was adjusted to a value of 8.5 so that trivalent chromium would form an insoluble precipitate (i.e., chromium hydroxide, $Cr(OH)_3$), which could then be easily removed, and thus the solution becomes with the lowest total chromium concentration. This acidity (8.5) is the optimum pH value at which the solubility of chromium hydroxide is minimal. The filtrate was then analyzed colorimetrically for the determination of the remaining concentration of Cr(VI) according to the Standard Methods for the Examination of Water and Wastewater, 15th edition and using a direct reading spectrophotometer (HACH, model DR2000) (APHA 1989). All reagents used were of AR grade (HACH, USA). A microprocessor pH meter (model pH 3000.WTW) was used to measure the pH.

3. Results and Discussion

3.1. Effect of solution pH

Figure (1) shows the variation of hexavalent chromium concentration with contact time at different starting pH values while Figure (2) represents the percentage removal with time at the same pH values.

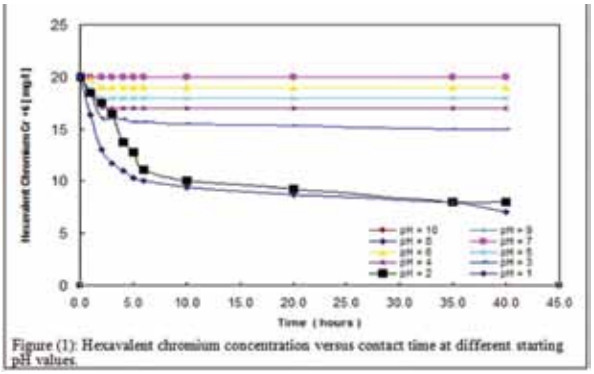

Figure (1): Hexavalent chromium concentration versus contact time at different starting pH values.

The removal of Cr(VI) from solution increases as the solution pH decreases. This increase lessens as the pH increases until no removal achieved at pH values above 7. The top line in Figure (1) as well as the bottom one in Figure (2) represent a concurrence of four lines of pH values of 10, 9, 8, and 7, which reveals that almost no removal of Cr(VI) takes place at these pH values. At pH 6, there is a slight removal of Cr(VI). Furthermore, the results indicate that the rate of removal of Cr(VI) significantly increases at pH values below 3 until it reaches maximum at pH 1 while the time required to reach equilibrium conditions increases. For example, a removal percentage of 5% was achieved at pH 6, while 45% removal was obtained at solution pH 1, at contact time of 3 hours (see Figure 2).

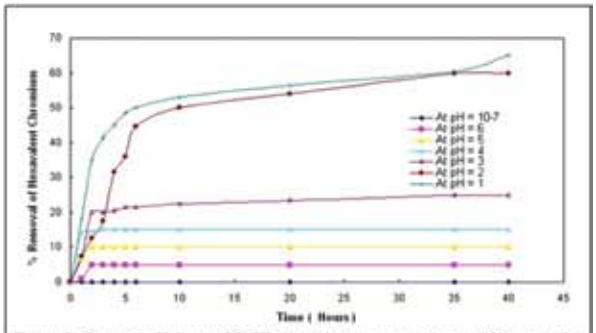

Figure (2): Removal efficiency of Cr(VI) by sand versus contact time at different starting pH values.

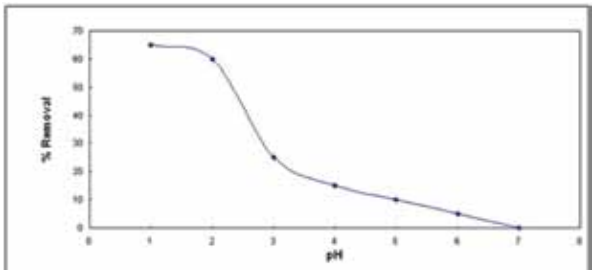

Figure (3): Percent removal of Cr(VI) versus solution pH after 40 hours contact time.

It is clear from that the maximum attainable removals of Cr(VI) occur at pH range of 1 to 2, which indicates that no significant removals are achieved by lowering the pH further, as shown in Figure (3).

3.2. Effect of contact time

At a given pH, as can be seen in Figures (2) and (1), as the contact time increases the remaining Cr(VI) concentration rapidly decreases. As time elapsed, this behavior becomes less pronounced until a state of equilibrium is reached. Similarly, both the removal efficiency and chromium uptake firstly increase as treatment time increases until equilibrium conditions are approached, which means that further increase in contact time results in an insignificant metal removal or uptake. This practically implies no more chromium removal takes place (see Figure 2). The percentage removal of Cr(VI) from aqueous solution increases rapidly and reaches a removal efficiency of 50% within 5 to 6 hours from the beginning of treatment process which implies that most of removal was achieved first, After that time, the percentage removal of Cr(VI) increases slowly by time increasing, reaches a maximum of 65% till 40 hours. This means that a further increase in contact time has a negligible effect on the percentage removal or metal uptake.

3.3. Effect of Cr(VI) initial concentration

The remaining Cr(VI) concentration was plotted against contact time as shown in Figure (4). As Cr(VI) initial concentration decreases the remaining concentration at equilibrium conditions decreases. Most of the removal of Cr(VI) occurred within the first 6 hours of the experiment.

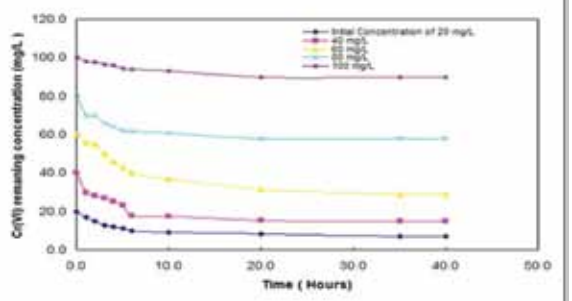

Figure (4): Effect of hexavalent chromium initial concentration versus time at an initial pH 2.

As exhibited by Figure (4), the high removal of Cr(VI) at low initial concentration could be due to the availability of a sufficient number of free adsorption places onto adsorbent surface compared to the concentration of the adsorbate, which necessarily lead to prompt chromium removal from solution. Minor reduction in total removal efficiency (2.5%) is observed at 40 mg/l. As the initial concentration increases, the number of vacant adsorption sites becomes progressively less sufficient and subsequently the removal of the metal considerably decreases. Furthermore, as evident by Figure (4) equilibrium conditions (i.e., maximum chromium removal) are approached faster as the initial concentration of Cr(VI) increases, probably because the concentration of adsorbate specie tends to far exceed the available adsorption sites, which are likely become completely occupied by chromium specie, thus, decreasing the driving force for further adsorption.

Table 1: shows the removal percentage (Rem %), metal uptake, sand capacity and the remaining concentrations of Cr(VI) at equilibrium conditions.

Table (1): Removal percentage (Re %), metal uptake (q_t), adsorption capacity and equilibrium concentrations for sand adsorbent using different Cr(VI) initial concentrations (20, 40, 60, 80 and 100 mg/l).

C_o (mg/L)	C_e (mg/L)	Removal Efficiency (R_{em} %)	Metal uptake(q_t) (mg/g)	Adsorption Capacity (L/g)*
20	7	65	0.104	0.008
40	15	62.5	0.200	0.008
60	29	51.67	0.240	0.008
80	58	24.44	0.176	0.008
100	90	10	0.080	0.008

* Adsorption capacity = $(q_t) / [C_o - C_t]$.

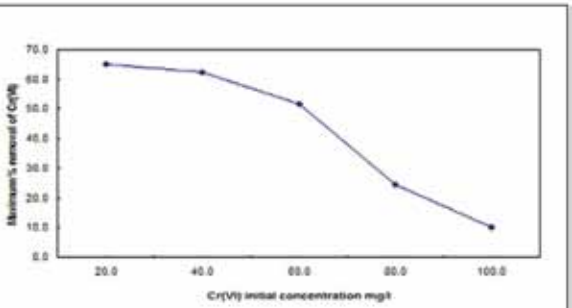

Figure (5): Cr(VI) initial concentration versus percentage removal (R_{em}(%)) by sand. [Sand dose 125 g/l, and initial solution pH is 2].

Removal efficiency (%) versus Cr(VI) initial concentration (mg/l) was illustrated in Figure (5). The highest removal percentages occurred in the range of 20 to 40 mg/l of Cr(VI) initial concentrations, and this may be due to the increase in the adsorption gradient which is generated between the adsorbent as solid phase and adsorbate (i.e, Cr(VI) solution) as a results of high availability of chromium ions in liquid phase. This implies that, high adsorption capacity is considered to be maximized at a Cr(VI) initial concentration of 40 mg/l, similar results were obtained by Santhy and Selvapathy (2004) who studied the removal of heavy metal adsorption onto activated carbon. The low removals of hexavalent chromium observed at high initial concentrations may be attributed to the limited number of adsorption sites available at the sand surface which is the key factor in the treatment process rather than Cr(VI) initial concentration. The repulsion among the chromium species at high initial concentrations may also play a role in the reduced removals obtained at high initial concentrations. These results are in agreement with those reported by (Lalvani et al., 1998; Santhy and Selvapathy, 2004; Baig et al., 2003; and Banerjee et al., 2004). As the initial concentration further increases, the removal efficiency rapidly declines until it reaches about 10% at an Cr(VI) initial concentration of 100 mg/l. This results in agreement with the findings reported by Lalvani et al. (1998) and Santhy and Selvapathy (2004). A plot of the metal uptake against the initial concentration is shown in Figure (6).

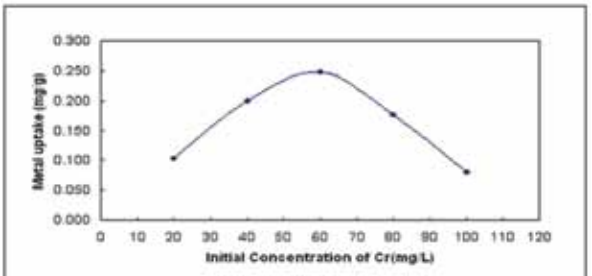

Figure (6): General relationship between initial concentration of Cr(VI) and metal uptake at equilibrium concentration adsorbed by tested sand at sand adsorbent dosage 125 g/l.

Such plot has a prime importance in practice, since it provides means of finding the optimum combination of initial concentration and contact time in order to achieve the removal of Cr(VI) required to comply with effluent standards. Figure (6) shows that, at first, the uptake varies linearly with the initial concentration until a maximum value is attained where further increase in the initial concentration results in a substantial reduction in the uptake. As shown, the metal uptake increases with the initial concentrations from 20 to 60 mg/l and then it starts to decline at higher Co values. This means that the maximum uptake of sand adsorbent is 0.248 mg/g at initial solution pH of 2 and an initial Cr(VI) concentration of 60 mg/l.

3.4. Effect of adsorbent dosage

Twelve sand adsorbent samples were tested. An initial adsorbent dose of 10 g/l was experimented and then gradually increased by 10 g/l each time up to 125 g/l. An initial solution pH of 2 was used throughout the ten experiments. The experimental results are displayed in Table (2).

Table (2): Adsorbent dose, Cr(VI) removal %, Equilibrium Concentrations (C_e) and uptake (q_e). [In batch reactor where Cr(V) Co is 20 mg/L, pH is 2 and liquid volume is 2 liters].

Experiment No.	Sand dose (g/l) (1)	Amount of sand (g) (Adsorbent) (m_s) (2)	Equilibrium concentration (C_e) (mg/l) (3)	Removal % (4)	Uptake adsorbed of Cr (IV) $q_e = (C_o-C_e)*V/m_s$ (mg /g) (5)
1	**10**	**20.00**	**18.00**	**10.00**	**0.200**
2	20	40.00	16.70	16.50	0.165
3	30	60.00	15.00	25.00	0.166
4	40	80.00	14.00	30.00	0.150
5	50	100.00	13.00	35.00	0.140
6	60	120.00	12.00	40.00	0.133
7	70	140.00	11.00	45.00	0.128
8	80	160.00	9.80	51.00	0.127
9	90	180.00	8.70	56.50	0.125
10	100	200.00	8.40	58.00	0.116
11	112.5	225.00	7.60	62.00	0.110
12	**125**	**250.00**	**7.00**	**65.00**	**0.104**

Metal uptake of chromium was maximized at low adsorbent doses. A metal uptake of 0.200 mg/g sand was obtained using 20 g/l of adsorbent compared to an uptake of 0.104 mg/g sand by a dose of 125 g/l. The literature reviewed reveals that the metal uptake was found to decrease with increasing adsorbent dose, which is in compliance with the results of the present study (Fadali et al., 2004 and Gupta and Babu, 2006). As seen in Figure (7), there should be a critical adsorbent dose that results in a maximum removal efficiency, which ought to be seeked for a given adsorbate concentration, (Fadali et al., 2004; Gupta and Babu, 2006; and Santhy and Selvapathy, 2004).

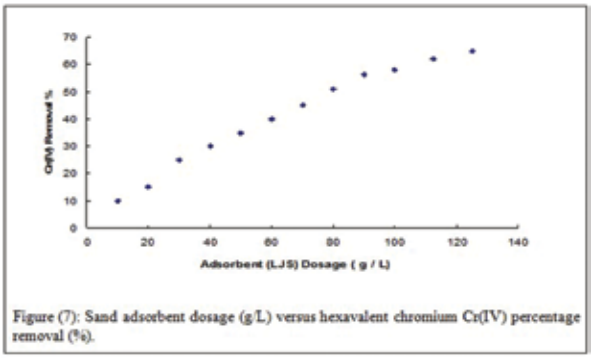

Figure (7): Sand adsorbent dosage (g/L) versus hexavalent chromium Cr(IV) percentage removal (%).

3.5. Effect of iron dose

Due to the previously demonstrated incompatibility of sand as an adsorbent for highly concentrated hexavalent chromium solutions, iron dust (in certain proportions) was mixed with sand in order to enhance the removal of Cr(VI). Iron and its compounds are the most commonly encountered reductants for the treatment of Cr(VI)-containing liquid effluents (Carl and PuIs, 1994; Chang, 2004; Eary and Rai, 1988; and Scott et al., 1998). Two sets of experiments were carried out. In the first set, a low initial concentration was tested while in the second one highly concentrated solution was treated. The overall iron-sand dose was always kept constant at 125 g/l throughout the experiments. The concentrations of the solutions treated and the iron doses studied as well as the results obtained at Cr(VI) initial concentration of 20 mg/l are displayed in Table (3).

Table (3): Effect of iron dust dose on Cr(VI) adsorption. [Cr(VI) C_o is 20 mg/L, solution pH of 2].

	Iron content							
	Mixture No 1	Mixture No 2	Mixture No 3	Mixture No 4	**Mixture No 5**	Mixture No 6	Mixture No 7	Mixture No 8
Iron dose (g/L)	6.25	12.50	18.75	25.00	**31.25**	37.50	43.75	50.00
Iron amount in 2L (g)	12.50	25.00	37.50	50.00	**62.50**	75.00	87.50	100.00
Time (Hours)	Hexavalent Chromium Concentration Cr(VI) (mg/L)							
0	**20**	**20**	**20**	**20**	**20**	**20**	**20**	**20**
1	**1.00**	**0.90**	**0.70**	**0.30**	**0.10**	**0.09**	**0.08**	**0.05**
2	*0.80*	*0.80*	*0.30*	*0.20*	*0.09*	*0.08*	*0.08*	*0.04*
3	0.70	0.50	0.30	0.10	0.90	0.08	0.05	0.02
4	0.70	0.40	0.20	0.09	0.07	0.07	0.05	0.01
5	0.60	0.30	0.10	0.09	0.07	0.07	0.04	0.01
6	0.40	0.30	0.09	0.09	0.05	0.05	0.03	0.01
10	0.30	0.20	0.09	0.06	0.04	0.04	0.02	0.01
20	0.15	0.10	0.08	0.06	0.04	0.03	0.02	0.01
35	0.15	0.10	0.08	0.06	0.04	0.03	0.02	0.01
40	**0.15**	**0.10**	**0.08**	**0.06**	**0.04**	**0.03**	**0.02**	**0.01**

It was founded that Cr(VI) removal of 96% at initial concentration (Co) of 20 mg/l can be achieved in 2 hours by utilizing iron-sand system (dust dose 6.25 g/l) compared to about 65% removal in 40 hours using the same quantity of sand. The high removals obtained, in case of iron-sand system, can be mainly attributed to the chemical reduction of Cr(VI) to Cr(III) and adsorption of Cr(VI) by iron metal. In addition to its high reaction affinity to Cr(VI), iron dust (it is composed of very fine particles) expectedly provides very large reactive surface area, thus, enhancing further eradication of hexavalent chromium from solution. The reduction reaction of dichromate by iron is a heterogeneous reaction and pH dependent. It can also be quantitative and extremely fast (Carl and PuIs, 1994; Chang, 2004; and Eary and Rai, 1988).

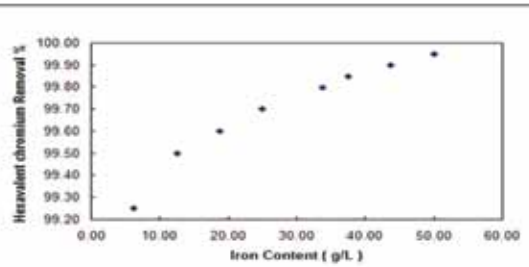

Figure (8): Cr(VI) Removal percentage (%) versus iron content (g/L) in iron-mixed adsorbent.

Figure (8) shows that as the iron content increase in adsorbent mixture Cr(VI) in the overall metal removal increases with the enhancement of the removal being less pronounced at high iron doses. The flat part of the curve in Figure (8) at high iron contents shows that equilibrium conditions are reached or no reaction takes place due to the depletion of Cr(VI) ions.

Table (4) shows the effect of employing the hybrid system on the remaining concentration of Cr(VI) using an iron dose of 31.25 g/l and different initial concentrations (20-1000 mg/l). The iron dose of 31.25 g/l was chosen for treating highly concentrated solutions because higher doses result in an insignificant enhancement in the Cr(VI) removal as clearly seen from Table (3).

Table (4): Effect of iron dust mix with sand on high concentration of Cr(VI) adsorption. [Batch reactor, solution pH is 2, and iron-sand adsorbent dose is (31.25 gram iron & 93.75 gram of sand)].

Time (Hours)	Hexavalent chromium concentration Cr(VI) (mg/L)				
0	20.0	61.0	171.0	345	1000
1	0.8	1.0	1.2	2.2	4
2	0.90	0.95	0.9	2	2
3	0.70	0.82	0.4	1.8	1
4	0.50	0.70	0.2	1.2	0.9
5	0.02	0.03	0.81	1	0.8
6	0.02	0.03	0.10	1	0.8
10	0.02	0.03	0.10	1	0.8
20	0.02	0.03	0.10	0.5	0.8
35	0.02	0.03	0.10	0.5	0.8
40	0.02	0.03	0.10	0.5	0.8

As can be seen, the iron–sand system can also be the very effective for the treatment of highly concentrated Cr(VI) solutions. All Cr(VI) initial concentrations are reduced to at least 4% of their initial concentrations in the first hour of the treatment. Also, almost complete removals of Cr(VI) are a achievable for initial concentrations of 20 and 1000 mg/l in 3 and 4 hours respectively.

Figure (9) compare the removal efficiencies of Cr(VI) at different retention times by using sand and iron-sand systems at the same initial Cr(VI) concentration of 60 mg/l. Again, results confirm the advantages of using the hybrid system over the sole sand adsorbent.

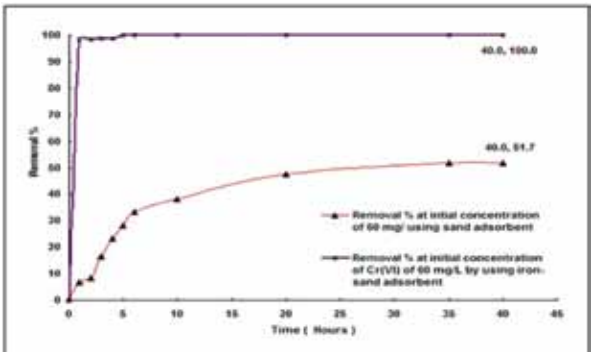

Figure (9): Removal effiiciencies (%) versus treatment time at initial concentrations of 60 mg/L, by using sand and iron sand mix adsorbents at 40 hours.

The process of Cr(VI) removal by using different iron types was classified as a physiochemical process (Carl and PuIs, 1994; Gang et al., 2005; and Rodriguez and Martinez 2005). This implies that these types of processes involve both chemical reduction reaction and physical adsorption at the same time. Cr(VI) is usually adsorbed onto outside the surface of iron before being reduced in the presence of electrons donated by the metal (Chang, 2004; and Eary and Rai, 1988). Accordingly, iron can be considered as a good adsorptive material in addition to being a very strong reductant.

4. Conclusion

Several conclusions can be drawn from this work. Up to 65% removal of Cr(VI), from dilute solutions, could be achieved by using the sand investigated as an adsorbent. Cr(VI) removal was found to depend upon solution pH, contact time, adsorbent dosage as well as Cr(VI) initial concentration. The removal of chromium was found to be pH dependent. Maximum removals were obtained at pH range of 1-2. The removal of Cr(VI) was found to initially increase with time elapsed until equilibrium conditions are approached. 50% of the removal occurs in the first five hours of treatment. The metal uptake was also found to similarly vary with increasing contact time. The removal efficiency of hexavalent chromium (i.e., adsorption and/or reduction-precipitation) was found to decrease with increasing Cr(VI) initial concentration over concentration range studied. In addition, it was found that the equilibrium concentration of Cr(VI) increases with increasing initial concentration. Furthermore, the metal uptake linearly varies with the increasing initial concentration up to a point after which it becomes inversely proportional to initial concentration. The removal efficiency of Cr(VI) was found to almost linearly vary with the adsorbent quantity whereas the metal uptake as well as Cr(VI) equilibrium concentration decrease with increasing sand dose

Much higher removals of Cr(VI) (up to 99%) could be gained by the iron dust to the adsorbing medium due to the reduction and different adsorption mechanisms of hexavalent chromium by iron metal.

References

[1] Abdo, M.S.E., and G.H. Sedahmad., 1998. "A new technique for removing hexavalent chromium from wastewater and energy generation via galvanic reduction with scrap iron".

[2] Azizian, M.F., 1993. "Experimental evaluation and chemical modeling of hexavalent chromium adsorption, desorption and reduction in a natural soil". Oregon State University.

[3] Bajpai S.K, 2001. “Removal of hexavalent chromium by adsorption onto fireclay and impregnated fireclay”. Department of chemistry-government Science College, India Separation Science and Technology.

[4] Baig M.A., Bilal Mehmood and Asif Matin, 2003. “Removal of chromium from industrial effluents by sand filtration”. Institute of environmental science and engineering (IESE), National university of science and technology (NUST), Tamizuddin road, Rawalpindi-46000, Pakistan.

[5] Banerjee. S. S, M. V. Joshi, and R. V. Jayaram1, 2004. "Removal of Cr(VI) and Hg(II) from Aqueous Solutions Using Fly Ash and Impregnated Fly Ash". Applied Chemistry Division, Institute of Chemical Technology, University of Mumbai, Matunga, Mumbai, India ICI India Research and Technology Center, Thane, India

[6] Carl D.Palmer, and Robert W.PuIs., 1994. “Natural Attenuation of Hexavalent Chromium in Groundwater and Soils”. EPA Ground Water Issue.

[7] Chang L.Y., 2004. "CHROMIUM REDUCTION BY ZERO-VALENT IRON AND BACTERIA", Lawrence Berkeley National Laboratory Conference, Tucson AZ February 29 - March 4.

[8] Costa Max and Catherine B. Klein., 2006. "Toxicity and Carcinogenicity of Chromium Compounds in Humans". Department of Environmental Medicine, NYU School of Medicine, New York, New York, USA Taylor and Francis Group, LLC.

[9] Eary L.E, and Rai D., 1988. “Kinetics of Chromate Reduction by Ferrous Ions Derived from Hematite and Biotite at 25ºC”. Amer. J. Sci., 289:180-213.

[10] Ellis K.V, 1985. “Slow sand filtration”. Critical reviews in environmental control, Vol. 15 (4), pp 315-354.

[11] El-Shazly A.H, A.A. Mubarak, and A.H. Konsowa, 2005. “Hexavalent chromium reduction using a fixed bed of scrap bearing iron spheres”. Desalination 185, 307-316, ELSEVIER.

[12] Fadali O. A., Y. H. Magdy, A. A. M. Daifullah, E. E. Ebrahiem, and M. M. Nassar, 2004. "Removal of chromium from tannery effluents by adsorption". Chemical engineering department, El-Minia University, El-Minia, Egypt, Hot Lab and Waste Management Center, Atomic Energy Authority, Cairo, Egypt.

[13] Gang, Qin., McGuire, Michael J., Blute, Nicole K., Seidel, Chad., and Leighton Fong., 2005. "Hexavalent Chromium Removal by Reduction with Ferrous Sulfate, Coagulation, and Filtration": A Pilot-Scale Study. Environmental Science and Technology; 8/15/2005, Vol. 39 Issue 16, p6321-6327, 7p.

[14] Ghanayem Mohamed Farid., 1989. "Removal of heavy metals from aqueous solutions by soils". The University of Texas at Dallas, 209 pages; AAT 8923168.

[15] Gould J.P, 1982 "The kinetics of hexavalent chromium reduction by metallic iron". School of Civil Engineering, Georgia Institute of Technology, Atlanta, GA 30332, U.S.A. Water Research 01/1982; DOI: 10.1016/0043-1354(82)90016-1.

[16] Gupta S, and Babu B.V., 2006. "Adsorption of Chromium (VI) by a Low-Cost Adsorbent Prepared from Tamarind Seeds". Chemical Engineering Group, Birla Institute of Technology and Science, (CEG-2006), BITS-Pilani, September 1-3.

[17] Kirk-Othmer., 1980. "Encyclopedia of Chemical Technology". Second edition, John Wiley and Sons, Inc.

[18] Lalvani S. B., A. Hubner, and T. S. Wiltowski, 1998. "Chromium adsorption by lignin". Southern Illinois University, Taylor and Francis, USA.

[19] Matin Asif, M. Ali Awan, and M. Masud Aslam., 2003. "A cost-effective treatment method for the removal of iron from water and wastewater". Electron. J. Environ. Agric. Food Chem. EJEAFChe, 2 (5).

[20] Muhammad N, Parr J. Smith M.D, and Wheatley A.D., 1997. "Removal of heavy metals by slow sand filtration". 23rd Wedc conference Durban, South Africa, Wedwater and sanitation for all partnerships and innovations.

[21] Patterson, J. W., 1985. "Industrial Waste Water Treatment Technology "; Ann Arbor,Science Pub. Inc.: Ann Arbor, Mich., 53.

[22] Rodriguez Miriam.G. and Sergio A.Martinez., 2005. "Removal of Cr (VI) from wastewaters in a tubular electrochemical Reactor".

[23] Sang D. Kim, Kyeong S. Park, and Man B. Gu., 2002. "Toxicity of hexavalent chromium to Daphnia magna: influence of reduction reaction by ferrous iron", Journal of Hazardous Materials A93, 155–164.

[24] Santhy K., and P. Selvapathy., 2004. "Removal of Heavy Metals from Wastewater by Adsorption on Coir Pith Activated Carbon". Center for Environmental Studies, Anna University, Chennai, India.

[25] Schmidt K., 1977. "Behaviour of special pollutants in slow and filters used in artificial recharge of ground water". Paper presented at the XVII Congress, Baden-Baden August 15.

[26] Scott, M. J., F. B. Metting, J. S. Fruchter, and R. E. Wildung, 1998. "Groundwater Cleanup". Research Investments Pays Off. Soil and October:6-13.

[27] Vikrant Sarin, and Pant K.K., 2006. "Removal of chromium from industrial waste by using eucalyptus bark". Bioresource Technology; Vol. 97 Issue 1, p15-20, 6p.

[28] Ward Nancy Erica, M.S., 1990. "Adsorption of hexavalent chromium on kaolinite and illite". The University of Arizona, 122 pages.

JJEES

Volume 6, Number 1, September, 2014
ISSN 1995-6681
Pages 15- 20

Jordan Journal of Earth and Environmental Sciences

Evaluation of Qanat Subsidence Potential Map in West of Mashhad City NE of Iran

Fahimeh Salehi Moteahed *, Mohammad Ghafoori, Gholam Reza Lashkaripour and Naser Hafezi Moghaddas

Department of Geology, Ferdowsi University of Mashhad, Iran

Received 11 April, 2013 ; Accepted 19 February, 2014

Abstract

Qanat systems (underground water galleries, kariz) have been used for extracting groundwater in many parts of Iran over centuries. There are 63 Qanat suits in Mashhad city (NE of Iran). In the past, these Qanats were used for extraction of groundwater; however, most of them have dried out today. Cases of land subsidence have been reported due to the collapse of these Qanats in Urban areas. In this paper, the Qanats in the western part of Mashhad city has been studied. The exact locations of Qanats vertical shafts has been determined by aerial photographs with scale of 1:20000 and 1:6000. Qanat characteristics include depth of Qanat underground tunnel and vertical shaft`s diameter has been investigated. The significant factors in Qanats collapse phenomena are soil properties, groundwater table, loadings due to the surface structures, density of vertical shafts and Qanat depth. In this study using of Qanat characteristics and loadings due to the surface structures, a potential map of Qanat collapse hazard and subsidence is presented. According to the field study, several cases of subsidence were recognized in high potential zone that introduced in the potential map.

Keywords: Qanat system, collapse hazard, subsidence, potential map, land use.

1. Introduction

Qanat systems are artificial underground water galleries with up to 3000 years old that used in arid Middle East. This system has been used in Iran for extracting groundwater over centuries (Reyhani and El Naggar, 2006). In Fact, Qanats are gently sloping tunnels dug far enough into alluvium or water bearing sedimentary rock. The Qanat tunnels pierce the underground water table and penetrate the aquifer beneath. Water from the aquifer filters into the upper reaches of this tunnel, flows down their gentle slope and emerges as a surface stream of water at or near a village or settlement (English 1998).

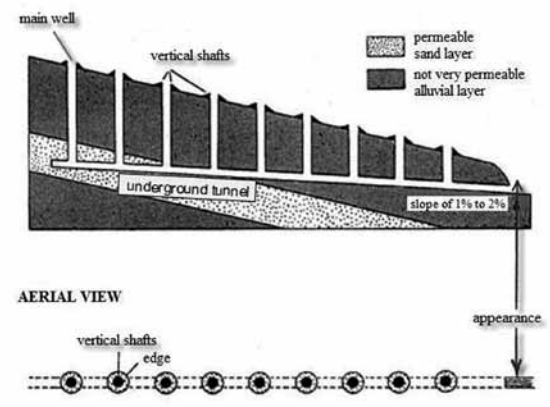

Figure 1: Longitudinal section and different parts of a Qanat suit (Hill and Al-Hassan, 1997)

Figure 1 shows a schematic profile of a Qanat system. In process of Qanat construction some vertical shafts are used for removing of the demolition soil and air conditioning. Qanat is usually dug in regions where there is not sufficient run off (Salih, 2006). In the past decades, huge withdrawal of groundwater using the deep and semi-deep wells led to the decline of groundwater level and dryness of more than 20,000 Qanat suits in Iran (Beckman et al., 1999. Yoshimura et al., 2006). The collapsing of underground tunnel of dry or out of service Qanats will be results to significant subsidence in urban area. The diameter of Qanat vertical shaft is about 1-1.5 meter. But in non-cohesive soils the shafts diameters could be increase up to 10 meters due to repeated collapsing of soil. By development of city over the Qanat suits, vertical shafts are filled by loose and uncompact soil and caused severe damage to surrounding buildings and lifelines.

There are some reports on Qanats collapsing and land subsidence in Iran and other countries (Lightfoot, 1996; Atapour and Aftabi, 2002; Shariatmadari and Fazelian, 2002; Amini Hossein et al., 2004; Hashemi and Hashemi, 2005; Pellet et al., 2005, Reyhani and El Nagger, 2006; Stiros, 2006). This phenomenon is also observed in Mashhad city. Due to the high distribution density of Qanat shafts and the deep Qanat tunnels in the western part of Mashhad city, most of land subsidence happened due to Qanat shafts rather than underground Qanat tunnels. The only support for Qanat shafts and underground tunnels are oval baked clay hoops called “caval”. Thus these Qanats are very vulnerable if confronted with earthquake forces which can lead to the destruction of shafts, and Qanat tunnel as well. Similar cases of Qanat damage were happened

* Corresponding author. e-mail: fahimehsalehi@ymail.com

in December 26, 2003 by Bam earthquake (south-west of Iran). 40% of Qanats systems around the Bam city were either destroyed or damaged seriously during this earthquake (Amini Hossein et al., 2004). Moreover, Qanat tunnels in urban areas are likely convert to a sewage channel so these underground tunnel lead to pollution of groundwater (Kazemi, 2010).

2. The effective factors on Qanat instability

The most effective factors on instability of Qanats are geotechnical properties of soil, groundwater table, loadings due to surface structures and Qanat properties including Qanat depth and Qanat distribution density (Reyhani and El Naggar, 2006). Qanat is similar to a tunnel system. In order to evaluate the stability of Qanats which have not been studied extensively yet, the data regarding tunnels dug in soils were employed. One of the most effective factors on instability of tunnels (such as Qanat underground tunnels) in soft materials is the type and properties of the soil (Vacher et al., 2004).

Figure 2: Soil texture map of the depth of 30 m (average depth of Qanat's well)

Figure 2 shows the soil texture map of the region to the depth of 30 m (Hafezi Moghaddas, 2008). The soils in the study area mostly consist of coarse-grained and low cohesion material of gravel and sand. Huge withdrawal of groundwater led to the decline of groundwater level and dryness of Qanats in the study area. Qanat vertical shafts were commonly filled with demolition wastes which will lead to land subsidence in future especially when saturated. The depth of groundwater in the area is about 60 to 100 m and Qanat suits in the study area are above the groundwater table.

3. Methodology

The main aim of this paper is preparing the collapse hazard and subsidence potential map of the area by GIS software based on two parameters: Qanat properties (include location of vertical shaft and underground tunnel depth) and land use; however geotechnical properties of soil and groundwater table did not considered in this map due to homogeneity of soil and high depth of groundwater. Locations of vertical shafts in study area (District 11 of Mashhad city) were determined by aerial photographs scale of 1:20000 and 1:6000 (National Geographical organization 1966 and 1975). Usually in non-cohesive soil the diameters of vertical shafts increased up to 10 meters by repeat of fall and soil collapse. The uncompact soil filling of vertical shafts lead to land subsidence. In this study the depth of Qanat underground tunnels are calculated by length of Qanat suits and main well depth (the last deepest vertical shaft of Qanat is main well or mother well). In the western part of Mashhad city most of Qanat underground tunnel are situated in high depth; so they rarely collapse. Another effective parameter using in potential map is land use which indicates the pressure of structures. Furthermore, the rupture of water network as the superficial sign of subsidence in the region was employed to correlate the effect of Qanat collapse with land subsidence. The research method is summarized in Flow chart below.

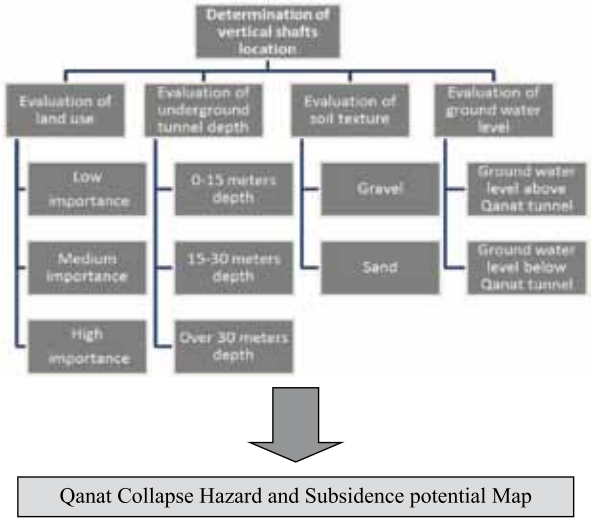

4. Results and discussion

4.1. Evaluation of Qanat systems in the study area:

Mashhad city is considered the second metropolis to Iran. The city area is about 320 km2 and according to statistical survey of 2011, its population is 2,772,287. This city has had a mild growth of population in the last 50 years and a rapid growth in last two decades. Figure (3) shows the development in Mashhad city between 1956 and 2006. As shown in this Figure most of this growth has been toward west and north-west of Mashhad city. Based on this Figure the study area in west of Mashhad city is funded in 1986.

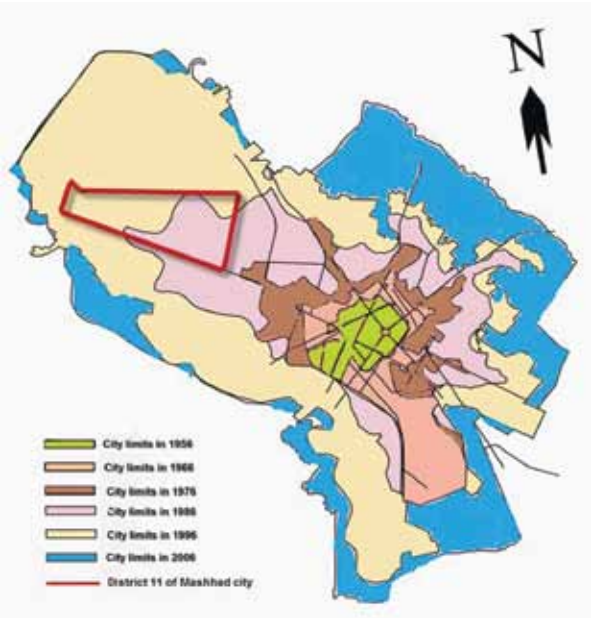

Figure 3: Development of Mashhad city (Khorasan-e-Razavi Housing and Urban development organization 2006)

Based on the aerial photographs and report on Mashhad plain Qanats (Khorasan-e-Razavi regional water company 1964), there are 63 Qanat suits in Mashhad city. Although, these Qanats had been used for many years, currently, only two Qanat suits are active. During the last 50 years, 95% of Qanats in Mashhad city area have dried out. The average depth of main wells of these Qanats (the deepest Qanat vertical shaft is called the mother or main well) is 45 m while the average length of Qanat suits is 5 kilometers. The longest and the deepest one is "Bahrabad Qanat" which has 22 kilometers length and its main well has 133 m depth (Khorasan-e-Razavi Regional water company 1964). Figure (4) shows Qanats in Mashhad city which are determined through the location of their vertical shafts on aerial photographs. Also location of study area has been determined in this map.

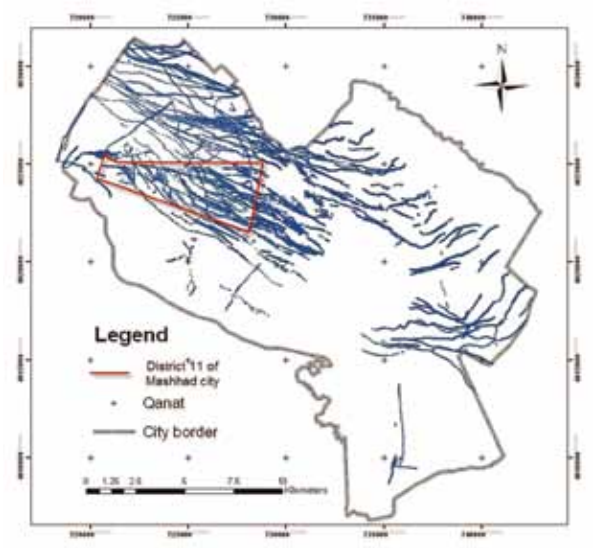

Figure 4: Qanat suits in Mashhad city

There are 19881 Qanat vertical shafts in the region. As shown in Figure (4), most of these Qanats are located in the western parts of the city and the general direction of Qanat suits is from North-west to south-east. Several cases of land subsidence due to Qanat instabilities have been reported in west of Mashhad city. As a noticeable example, a number of residential structures on Andisheh Street in Ghasem abad (west of Mashhad city) which are built on the Qanat shafts have subsequently been damaged (Hafezi Moghaddas et al., 2012) (Figure 5).

Figure 5: A crack in the wall of a building (left part) and tilting a wall (right part)on Andisheh Street west of Mashhad city (Hafezi Moghaddas et al., 2012)

Because, there are no Qanat establishments after 1970, the exact location of the Qanat shafts in study area have determined by the large scale and ancient aerial photographs of 1972 with scale of 1:6000. Figure 6 shows the distributions of Qanat suits and Qanat shaft in the region. The density of Qanats in the eastern part of the study area is higher than the western parts. They extend mostly from north-west to south-east.

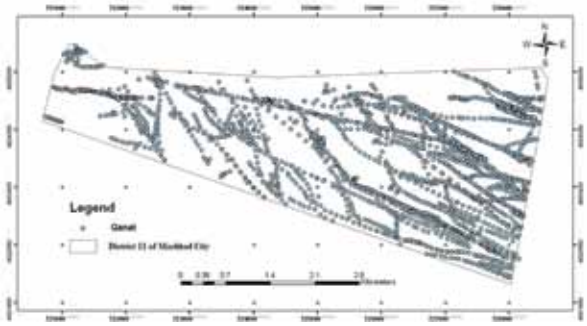

Figure 6: Qanats in District 11 of Mashhad City

Table 1: Characteristics of all Qanats located in Mashhad District11

Qanat name	Absarde	Farah abad	Neka	Mil karez	Sanabad	Nokhodak	Ghasem abad	Malek abad	Saad abad
Depth of main well (m)	65	71	90	80	65	75	43	80	70
Length of Qanat chain (m)	11000	6100	18000	13000	7000	17000	2300	8500	7000
Inflow (L/s) in 1963	45.7	42	8	Dry	9.4	52.59	20	40	Dry

There are 9 main Qanat suits in the area whose properties are mentioned in Table 1. The average depth of main wells of the Qanats in the area is 70 m. The average length of Qanat suits (the distance between main well and appearance of Qanat that water coming out) is 10 kilometers. The average diameter of vertical shafts is about 1-1.5 m and the diameters of underground tunnels are about 1 to 1.2 m. The distances between vertical shafts in the region are varying dramatically, but the average distance between vertical shafts of the area is about 40 m. based on the soil texture in the region, the distance between vertical shafts is longer in coarse grained soils. The average distance between vertical shafts in gravelly soils is 50 m and in sandy soils is 27m.

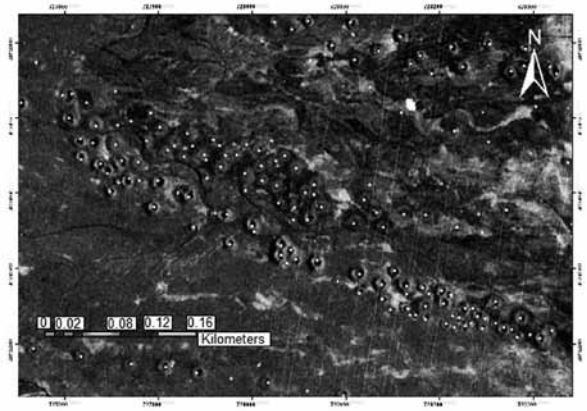

Figure 7: Qanats of the north-east of District 11 in an aerial photograph

The abundance of Qanats in the area is shown in Figure 7. This Figure shows an area of 252,000 m2 in north-east of District 11 on an aerial photograph. Every whit spot in the Figure is an indicator of a vertical shaft. As shown in this Figure in some cases the distance of the shafts is less than 10 m.

4.2. Collapse hazard and subsidence potential map

The collapse hazard and subsidence potential map of the area is prepared based on land use, Qanat shafts density and Qanat depth. Soil properties due to homogeneity in the study area are not considered as effective factors. The land uses in the study area include residential, educational, commercial, health, governmental and cultural and also green and resort areas.

Figure 8: Land use map of the area

In Figure 8 a simplified classification of land use importance in the study area is shown. This classification is based on two parameters: first one is the pressure inverted to the earth by structures. This parameter is determined by height of buildings. The second one is related to the density of population which has a high risk of damaging. The first class is low important regions which includes low density residential areas as well as green and resort areas. The second class is medium important regions includes residential areas with medium density and main streets. The third group with the highest level of importance includes residential areas with high density and educational, commercial, health, governmental and cultural zones. These areas are considered as the most important regions due to their significance and high population. According to Figure 8, regions with high levels of importance cover about 50% of the area.

In order to prepare the potential map, the area was divided into square cells with an area of 10,000 m2 each. Based on the distribution density of Qanat shafts the area was classified into three groups: (1) without Qanat shaft, (2) 1 to 3 Qanat shafts and (3) more than 3 Qanat shafts (Figure 9). Based on this classification, 47.5 % of the cells does not have any shafts, 41% have 1 to 3 and 11.5% have more than 3 Qanat shafts. Although the last group has the lowest area, but these cells usually have 8 to 10 Qanat shafts and in some cases there are 20 Qanat shafts in one cell. One of the cells with high Therefore, the rate of land subsidence due to Qanat collapse in deep Qanat underground tunnel is less than shallow Qanat tunnel. The distribution density of Qanat (about18 Qanat shafts) in the aerial photograph is shown at Figure 9.

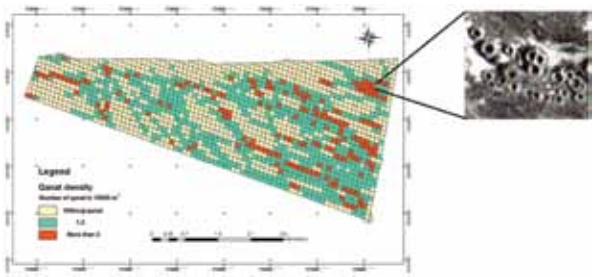

Figure 9: Classification based on the number of Qanat shafts. The photo in the right part shows high distribution density of Qanats

The last effective factor on Qanat instability is Qanat depth. Peck (1969) has expressed that the relation between the depth of a tunnel and land subsidence due to the digging of a tunnel is reverse. According to the depth of Qanat, the study area is categorized into three groups (Figure10).

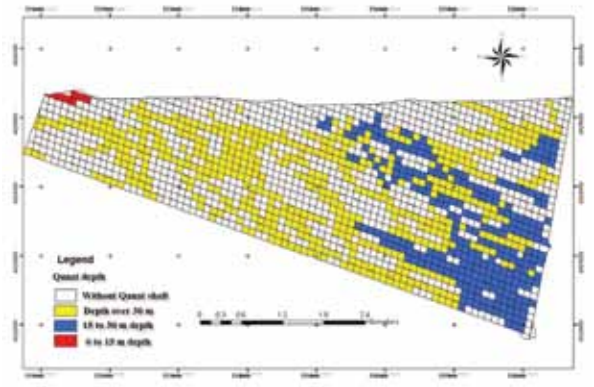

Figure 10: Classification of the area based on the depth of Qanats

The first group of Qanats is at the depth of more than 30 m. The second one is at the depth of 15 to 30 m and the third one is at the depth of less than 15 m. It is assumed that the shallow Qanats have the highest risk of collapsibility.

Table 2: Characteristics of all Qanats located in Mashhad District 11

Land use Number of Qanat shaft in every block	Low importance	medium importance	high importance
No-Qanat shaft	I	I	I
1 to 3 Qanat shafts	II	IV	V
More than 3 Qanat shafts	III	V	VI

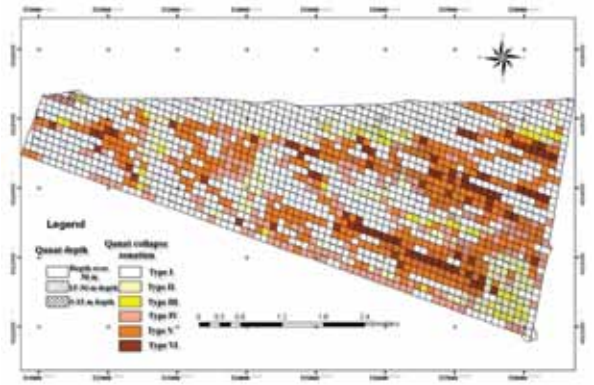

Figure 11: Collapse hazard and subsidence potential map of Qanats in Mashhad District 11

The potential map is prepared by overlaying the three maps of land use, Qanat distribution density and Qanat depth. In Figure 11 the area is categorized into 6 groups based on Qanat collapse hazard and subsidence potential. Groups of type I- VI summarized in Table 2.

The land subsidence and collapse hazard increases from group I to VI, respectively. Cells type I have no collapse hazard. Due to high number of Qanat shafts in cells type VI, these cells categorized in high risky areas. They also have a high risk from point of land use criteria. Cells type VI includes high population centers and their land uses are high density of residential, educational, commercial, health and governmental areas as well as cultural ones. The depth of Qanats has been evaluated in potential map separately (Figure11). As shown in the potential map, half of Qanats of type VI have medium depth. So the risk of collapse in these cells is more than cells with deep Qanats. 47% of total cells of the area are classified in group I, 10% in group II, 2.5% in group III, 12.5 % in group IV, 22.5% in group V and 5.5 % in group VI. Cells type IV, V and VI have the highest Qanat collapse hazard and subsidence potential and cover 40% of the area.

4.3. Reliability of Qanat collapse hazard and subsidence potential map

Field study was conducted in risky areas with high density of Qanats. These areas have been categorized in cells type VI in the potential map and some subsidence has been observed in these areas (Figures 12 and 13).

Figure 12: Round shaped subsidence formed in high-risky cells in potential map

Figure 13: Crescent and round shaped subsidence in risky area with high distribution density of Qanat

Land subsidence due to collapse of Qanat shafts and Qanat underground tunnel in urban area could cause damages in the drinking water network of the city. The location of cracks in main pipes of drinking water has been studied along with Qanat collapse hazard and subsidence potential map (Khorasan-e-Razavi water and Wastewater Company 2009). As Figure 14 shows, most of cracking in water pipes occurred in areas with highest Qanat collapsibility hazard (cells type IV, V, and VI).

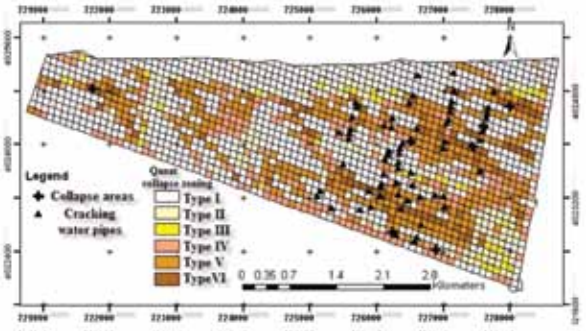

Figure 14: The location map of the main water pipes breaks and collapses in Mashhad District 11

5. Conclusions

In District 11 of Mashhad municipality nine main Qanat suits have been identified with an average of 10 kilometer length and 70 m depth for the main well. Seventy six percentages of the Qanats in the area are deep (more than 30 meters depth) and the others have medium (15 – 30 meters depth) or low depth. The soil texture in the area is non-cohesive coarse grained soil which results to falling of Qanats shafts. The filling of these shafts with disturbed soils and demolition wastes are vulnerable to collapse. Based on Qanat depth, land use and Qanat distribution density, the Qanat collapse hazard and subsidence potential map is prepared and the area is categorized into six groups. Cells of type IV, V and VI in the Qanat collapse hazard and subsidence potential map have the highest risk of collapsibility and cover about 40% of the area. In high-risk areas, many cases of subsidence and collapse have recognized. Also, the damage in urban water pipes has increased in these areas.

Acknowledgements

The authors would like to gratefully acknowledge the support of district 11 of Mashhad municipality and for their useful suggestions and for providing the researchers with the related data.

References

[1] Atapour, H., and Aftabi, A., 2002, Geomorphological, Geochemical and Geo-environmental Aspects of Karstification in the Urban Areas of Kerman City, Southeastern, Iran, Environmental Geology, 42, 783-792.

[2] Beckman, C.S., Weigand, P.C., and Pint, J.J., 1999, Old World Irrigation Technology in a New Contact: Qanats in Spanish Colonial Western Mexico, Antiquity, 73, 440-446.

[3] English, P.W., 1998, Qanats and Life worlds in Iranian Plateau Villages, New Haven: Yale University Press.

[4] Hafezi Moghaddas, N., Nekoodel, M., Qezi, A., 2012, Evaluation of Land Subsidence Due to Consolidation of Demolition Waste in West of Mashhad city, Journal of Engineering Geology Kharazmi University of Tehran, 6(1) 1373-1386 (in Persian).

[5] Hafezi Moghaddas, N., 2008. Seismic Micro Potential of Mashhad city, the Ministry of Housing and Urban Development of Khorasan-e-Razavi, Geological Survey of Iran, North-East Branch, (in Persian)

[6] Hashemi Sahi, H., V., and Hashemi Sahi, M., 2005, Qanat, Soil Settlement and Construction Problems, International Symposium of Qanat. Kerman, 701-707 (in Persian).

[7] Hill, D., Y. Al-Hassan, A., 1997, History of Science and Technology in Islam Part one: Engineering in Arabic-Islamic Civilization. Roshdi Rashed, Paris.

[8] Kazemi, G. A., 2010, Impacts of Urbanization on the Groundwater Resources in Shahrood, Northeastern Iran: Comparison with other Iranian and Asian cities, Physics and Chemistry of the Earth, 36, 150-159..

[9] Khorasan-e-Razavi Housing and Urban Development Organization, 2006, Report of Comprehensive Plan Development and Renovation of Mashhad city, 1991-2006.

[10] Khorasan-e-Razavi Regional Water Company, 1964, Report on Mashhad Plain Qanats.

[11] Khorasan-e-Razavi Water and Wastewater Company, 2009, Report of Statistical Data of Exploitation, Mashhad, (2007-2009).

[12] Lightfoot, D. R., 1996, Syrian Qanat Romani: History, Ecology, Abandonment, Journal of Arid Environments, 33, 321-336.

[13] Peck, R., 1969, Deep Excavations and Tunneling in Soft Ground, Proceeding of 7th International Conference on Soil Mechanics and Foundation Engineering, Mexico, State-of-the-art Volume, 225-290.

[14] Pellet F., Amini Hosseini, K., Jafari, M. K., Zohra Zerfa, F., Mahdavifar, M. R., and Keshavarz Bakhshayesh, M., 2005, Geotechnical Performance of Qanats During the 2003 Bam, Iran, Earthquake, Earthquake Spectra, 21, S137-S164.

[15] Reyhani, M. H. T., and El Naggar, M. H., 2006, Collapse Hazard Zonation of Qanats in Greater Tehran Area, Journal of Geotechnical and Geological Engineering, 25, 327-338.

[16] Salih, A., 2006, Qanats a Unique Groundwater Management Tool in Arid Regions: The Case of Bam Region in Iran, Proceedings of the International Symposium on Groundwater Sustainability, Alicante/Spain, 79-87.

[17] Shariatmadari, N., and Fazelian, A. F., 2002, Stability Analysis of Underground Spaces in Kish Qanat, 3th International Symposium of Geotechnical Engineering and Soil Mechanic of Iran, (in Persian).

[18] Stiros, S. C., 2006, Accurate Measurements with Primitive Instruments: the ‘‘Paradox’’ in the Qanat Design, Journal of Archaeological Science, 33, 1058-1064.

[19] Vacher, C.A., Raine, S.R., and Loch, R.J., 2004, Strategies to Reduce Tunneling on Dispersive Mine Spoil Materials, In Conserving Soil and Water for Society: Sharing Solutions, Proceeding of 13th International Soil Conservation Organization Conference, Brisbane, Paper 139, 6pp.

[20] Yoshimura, K., Nakahashi, T., Saito, K., 2006, Why Did the Ancient Inhabitants of Palmyra Suffer Fluorosis? Journal of Archaeological Science, doi:10.1016/j.jas.2006.01.016, 33, 1411-1418.

JJEES

Volume 6, Number 1, September, 2014
ISSN 1995-6681
Pages 21- 28

Jordan Journal of Earth and Environmental Sciences

Shiraz Air Pollution: Dependency on Meteorology and Temporal Variability

Amir sasha Banankhah [1], Farhad Nejadkoorki [2] and Hamid Sodaeezadeh [3 *]

[1] Department of Environmental Engineering, Yazd University, Yazd, Iran
[2] Department of Environmental Engineering, Yazd University, Yazd, Iran
[3] Department of Soil Science, Yazd University, Yazd, Iran

Received 31 January, 2013; Accepted 20 August, 2014

Abstract

An effective policy on air quality control in urban areas requires a detailed understanding of how pollutants interact with meteorological conditions and an understanding of how variations of concentrations of air pollutants are affected at temporal and local scales. This paper analyses air pollution in Shiraz in terms of three considerations: meteorological effects; temporal variability and impacts recorded at two urban stations located in Shiraz. Results imply that meteorology has an effect on pollutant concentrations and their variations in different months and situations. Results indicate that dependency on meteorology for dust, ozone (O_3), nitrogen oxides (NO_x) and sulphur dioxide (SO_2) are more than that of carbon monoxide (CO). Temporal variations in different years showed that some pollutants, such as CO and SO_2, demonstrated a decreasing trend in recent years as a result of air quality control policies, but dust had an increasing trend because of natural events. The difference between the two stations for all pollutants that were analyzed was significant. The findings of this study confirm that human activity and natural events have an effective impact on urban air pollution.

Keywords: Air pollution, Urban areas, Meteorology, Temporal variability.

1. Introduction

Most cities of the world have serious problems concerning air quality, which have received increasing attention in last decade. Some of these problems can be attributed to urban population growth and changing land use that has resulted in larger urban areas (Fenger, 1999). The main goal for air quality improvement in urban areas is the protection of human health (Bigi and Harrison, 2010). One of the major metropolitan cities in southern Iran is Shiraz and its residents have been suffering from health problems related to air pollution during recent years (Hadad et al.,2005). Health concerns associated with air pollution include effects on the respiratory system such as reduced lung function, increased hospital admissions, chronic bronchitis and mortality (Kan and Chen, 2004). Emissions that contribute to air pollutants are from different sources, they can be categorized as follows; motor traffic, industry, power plants and domestic fuel (Fenger, 1999). Pollutants do not act independently in eliciting their effects; therefore, it is important to understand relationships between air pollutants and meteorological parameters (Bigi and Harrison, 2010).

It is well known that concentrations of air pollutants within a local environment are affected by meteorology (Pearce et al., 2010). But to fully understand these relations a thorough analysis of local and regional meteorology is required especially wind direction, wind speed, turbulence and atmospheric stability associated with concentrations of air pollutants (Elminir, 2005). Emitted air pollutants are dispersed and diluted in the atmosphere with chemical reactions and they are strongly influenced by meteorological conditions. Furthermore, topography and urban structures such as streets and canyons have a great effect on meteorological conditions. Chemical reactions depend on ambient weather conditions because they are influenced by short wave radiation, air temperature and relative humidity (Fenger, 1999). Understanding temporal variability in urban air quality is a key consideration for policy on air pollution and epidemiological studies. The temporal pattern of air pollutants is related to seasonal atmospheric processes and hydrological cycles, influenced by human activities and natural events (Bigi and Harrison, 2010).

Furthermore measured characteristics of air pollutants depend on the location of the measurement site with respect to the sources of that air pollution and its features (Stulov et al.,2010).

This paper investigates air pollution in Shiraz in three sections. The first section relates to the interrelation of air pollutant to meteorological parameters. Weather patterns and different meteorological conditions are classified. This analysis was done for the year 2009.

The second part shows the temporal variability for air pollutants in Shiraz for the period 2005-2010 that identifies concentrations of pollutants in different years and daily variations of average concentrations.

The third part shows significant differences of average concentrations of air pollutants between the two stations in Shiraz that monitor air quality for the period 2005-2010

* Corresponding author. e-mail: a.s.banankhah@gmail.com, f.nejadkoorki@gmail.com, hsodaei@yazdun.ac.ir

2. Materials and Methods

2.1. Case study

Shiraz is the capital city of Fars province, located in southern Iran; the city covers an area 40 km long and 15 to 30 km wide, a total of 1268 km^2. The geographical coordinates are 29.617° N and 52.533° E. It has moderate and mountainous climate zones with an average annual rainfall of 335 mm unevenly distributed throughout the year. Shiraz experiences rather cold winters and there is usually rainfall in autumn (November and December), winter (January, February and March) and spring (April and May), with the highest in February and March. Summer in Shiraz is hot. The height of Shiraz city is 1468 meters above sea level. The average annual temperature is 18°C and the warmest month is July (high average 38.1°C) and the coldest is January (low average -7°C). Monthly sunlight is 109 h. The average annual wind speed is 13ms^{-1}.

2.2. Methods

Monitoring air quality in Shiraz is already well established by the Department of Environment (DOE) of Iran. Air quality monitoring is continually active in the city. There are two stations located in the city center where traffic is highly concentrated. The first one, Falakeh-Setad Station is located at a major road junction with 29.655˚ N and 52.532˚E coordinates surrounded by commercial-official land use applications. The second station, Darvazeh-Kazaroon having coordinates of 29.609˚ N and 52.532˚E is at a five ways within residential-commercial land use applications surrounding (Figure 1). Therefore, the stations are exposed to urban road traffic mainly. The daily air pollutants under evaluation are carbon monoxide (CO), dust, nitrogen oxides (NO_x), sulphurdioxide (SO_2). Concentrations of these parameters were monitored by continuous monitoring equipment (gas filter correlation method for CO (Chen et al.,2005), ultraviolet fluorescence method for SO_2 (Chang et al.,2005), ultraviolet absorption method for O_3 (O'Keeffe et al.,2007), pressure-reduced hemi luminescence method for NO_x (Maghzal et al.,2012) and radioactive absorption method for dust (Rodriguez et al.,2012). Daily meteorological parameters such as relative humidity, temperature (°C), maximum wind direction and maximum wind speed (ms^{-1}) were taken from the Iranian meteorological organization. Due to malfunctioning of the system to take measurements of air pollutants for some of the time, some data was not available.

Figure 1: Shiraz city with two monitoring air pollutant stations.

The normality of data for statistical analysis was checked by the Kolmogrovsmirnov test (Baklizi, 2006). Pearson correlation coefficients (Wang et al.,2013) were used to obtain relationships between air pollutants and meteorological parameters. One-way analysis of variance (ANOVA) was used to evaluate differences for air pollutant concentrations between different years and the (T- STUDENT) test was carried out for differences in air pollutant concentrations between the two air quality-monitoring stations (Wheater and Cook, 2005). The statistical analysis was done by SPSS (version 16) and analysis each station was analyzed.

3. Results and Discussions

3.1. Meteorology

This section presents relations between air pollutants and metrological parameters. The results are divided into two categories; impacts of meteorological parameters on concentrations of air pollutants and correlations between air pollutants and meteorological data. Tables 1 and 2 summarize average values for concentrations determined within ambient air temperature ranges for each station. The results show that the highest average concentrations for O_3 and dust occurred at ambient air temperatures higher than 30ºC but for CO and NO_x the highest average concentrations occurred at temperatures less than 10ºC. This appears to be reasonable as Dust increases during daytime because soil gets dry which makes dirt more susceptible to be picked up by wind and/or wakes generated by motor vehicles. Ozone is a photosynthetic gas. Therefore, it is expected that its concentration will be higher around noon where air temperature is highest. The results for SO_2 varied between the two stations.

Table 1: Average concentrations values determined within ranges of temperature for station #1.

range	CO	DUST	NO_x	O_3	SO_2
	(ppm)	(µg/m^3)	(ppb)	(ppb)	(ppb)
National Standard	9	150	21	50	37
T≤10	3.5	97.9	136.02	7.9	80.27
T=10-15	3.18	115.2	96.22	9.96	27.57
T=15-20	3.03	134.09	98.23	11.34	16.44
T=20-30	2.59	197.61	69.42	19	16.2
T>30	2.83	269.78	65.75	19.42	17.06

At station #1 the maximum concentration of SO_2 occurred at air temperatures less than 10ºC but for station #2 maximum concentrations occurred at air temperatures higher than 30ºC. O_3 sources in the planetary boundary layer are photochemical generation in reactions with precursors (Tarasova et al.,2003). Therefore, surface ozone showed a clear trend of increasing with temperature. NO_x and CO decreased with air temperature (Pearce et al.,2010). This may be due to the improvement of air mixing, as mixing height is low in the morning and evening where air temperature is low. During daytime air temperature increases and mixing height increases as well which dilutes air pollutants and thus reduces their ambient concentrations.

Table 2: Shows average values for concentrations determined within ranges of temperature for station #2

range	CO	DUST	NO_x	O_3	SO_2
	(ppm)	(µg/m^3)	(ppb)	(ppb)	(ppb)
T≤10	2.33	43.1	124.88	11.95	69.97
T=10-15	1.86	51.37	87.2	12.76	86.38
T=15-20	1.72	58.86	83.07	17.62	119.82
T=20-30	1.38	86.37	62.33	21.71	141.66
T>30	1.39	123.98	66.88	30.24	163.82

The statistical analysis of daily air pollutants and daily values for relative humidity for the two stations are summarized in Tables 3 and 4.The highest average concentrations for O_3 and dust for both stations occurred at humidity less or equal to 40% and that can be mainly attributed to strong vertical mixing of the boundary layer air masses to the 3 km level (Elminir, 2005). This is not always true as strong vertical mixing height leads to low concentrations of air pollutants. It is very important to keep in mind that relative humidity is often collinear with air temperature; low relative humidity is associated with high air temperature.

Table 3: Average values for concentrations determined within ranges of relative humidity for station #1

range	CO	DUST	NO_x	O_3	SO_2
	(ppm)	($\mu g/m^3$)	(ppb)	(ppb)	(ppb)
R.H<40	2.71	202.57	74.09	17.56	17.04
R.H≥ 40-60	3.36	111.32	104.56	9.3	62.11
R.H> 60-80	3.33	97.58	141.34	8.67	40.45
R.H> 80	3.58	61.58	141	6	36.5

Concentrations of NO_x and CO increased with increasing relative humidity. High values of relative humidity are associated with low air temperatures in the morning and evening, which are associated with a weak mixing height. The results for SO_2 were varied at station #1 with maximum concentration in relative humidity of 40-60% and a reverse behavior after wards and for station #2 decreased pollutant concentrations are associated with increased humidity. The difference between two stations may be due to their locations having contribution of dissimilar sources.

Table 4: Average values of concentrations determined within ranges of relative humidity for station #2

range	CO	DUST	NO_x	O_3	SO_2
	(ppm)	($\mu g/m^3$)	(ppb)	(ppb)	(ppb)
R.H≤40	1.41	89.8	67.01	22.56	147.27
R.H=40-60	1.85	49.44	96.23	12.84	105.2
R.H=60-80	2.52	43.53	122.27	13.86	41.78
R.H>80	3.03	27.08	126.33	10	26.67

The wind directions that affect air pollutants are shown in Tables 5 and 6 for both stations. Comparing prevailing directions to concentrations of air pollutants closely reflects the geological structure of the region (Elminir, 2005).

Table 5: Average concentrations of air pollutants as a function of wind direction for station #1

Wind direction	CO(ppm)	DUST($\mu g/m^3$)	NO_x(ppb)	O_3(ppb)	SO_2(ppb)
E	3.58	79.62	139	8.13	52.88
ENE	2.39	98.07	86	11	66
ESE	3.56	149.75	161.44	9.82	22.06
N	2.34	273.14	73.57	18.11	16.11
NNE	2.64	117.58	68	21.33	17
NNW	2.94	141.14	91.29	14.73	41.16
S	3.3	155.77	87.94	11.8	47.56
SSE	3.53	115.88	126.75	12	52.15
SSW	3.31	179.11	105.32	11.33	29.38
W	2.81	140.81	81.22	13.07	40.17
WNW	2.86	169.62	91.56	15.71	29.79
WSW	3.11	164.15	100.55	11.76	24.78

Prevailing winds in the city of Shiraz are mostly from the south and southwest to north and northeast (Hadad et al.,2003); concentrations of dust for both stations where highest when the wind blew dust from the south to the north. NO_x concentrations were highest in the east and the southeast. SO_2 concentrations were highest in east, north east direction in station one and for station two were highest in north, north east direction and this could have been due to higher concentrations of SO_2 in the southern parts of Shiraz (Hadad et al.,2005).

Table 6: Average concentrations of air pollutants as a function of wind direction at station #2

Wind direction	CO (ppm)	Dust ($\mu g/m^3$)	NO_x(ppb)	O_3 (ppb)	SO_2 (ppb)
E	2.28	34.11	117.13	14.13	84
ENE	1.55	46.81	84.67	15.33	85
ESE	2.63	68.7	133.72	16.28	61.18
N	1.36	123.32	68.33	22.67	128
NNE	1.32	51.93	63.67	21.33	146.33
NNW	1.67	60.87	83.77	18.72	118.81
S	1.58	68.45	79.69	17.5	131.6
SSE	2.25	48.25	109.23	16.92	115.69
SSW	1.68	81.1	84.88	17.25	108.78
W	1.59	64.29	77.55	16.31	125.79
WNW	1.76	74.3	85.39	20.21	115.98
WSW	1.74	72.61	82.1	16.87	109.53

For CO the concentrations are almost identical in all aspects, indicating that this pollutant has uniform origin. Finally, the highest concentrations of O_3 occurred in north and northeast direction for station one and south to north for station two.

Table 7: Correlation matrix for air pollutants and temperature at station one

Pearson correlation	JAN	FEB	MAR	APR	MAY	JUN	JULY	AUG	OCT	NOV	DEC	yearly
CO	.124 NS	-.047 NS	.232 NS	.316 NS	-.243 NS	.596⋆⋆	.161 NS	-.003 NS	.224 NS	.048 NS	-.145 NS	-.387⋆⋆
Dust	.211 NS	.060 NS	.040 NS	.024 NS	-.095 NS	-.221 NS	-.263 NS	.218 NS	.080 NS	.332 NS	-.194 NS	.414⋆⋆
NO_X	-.001 NS	-.078 NS	.170 NS	.362⋆	.106 NS	.577⋆⋆	-.029 NS	-215. NS	.143 NS	-.122 NS	-.206 NS	-.447⋆⋆
O_3	-.053 NS	-.054 NS	-.314 NS	-.302 NS	.234 NS	-.562⋆⋆	.012 NS	.101 NS	.462 NS	.045 NS	.167 NS	.697⋆⋆
SO_2	.785⋆⋆	-.633⋆⋆	-.285 NS	.659⋆⋆	.304 NS	.254 NS	.351 NS	.219 NS	.268 NS	.381⋆	-.301 NS	-.447⋆⋆

NS: Not Significant, Degree of significant ($\star p < 0.05$, $\star\star p < 0.01$)

In order to study the relationships between air pollutants and temperature correlation further analyses was performed and the results are shown in Tables 7 and 8; the correlation matrix between temperature and corresponding data for CO, NO_x, dust, ozone and SO_2 concentrations are shown.

It is noteworthy that there is a negative weak relation between temperature and both CO and NO_x at both stations. There is a strong positive relation between ozone and temperature and a weak positive relation for dust. The relationship between SO_2 and temperature was different for each station; with a negative relation at station 1 and a positive relation at station 2.

Table 8: Correlation matrix for air pollutants and temperature at station #2

Pearson correlation	JAN	FEB	MAR	APR	MAY	JUN	JULY	AUG	OCT	NOV	DEC	yearly
CO	.093 NS	.058 NS	.264 NS	.477⋆	-.022 NS	.619⋆⋆	.137 NS	-.274 NS	-.174 NS	-.206 NS	-.136 NS	-.439⋆⋆
Dust	.295 NS	.017 NS	.007 NS	.132 NS	-.293 NS	-.119 NS	-.255 NS	.205 NS	.266 NS	.486⋆⋆	-.242 NS	.380⋆⋆
NO_X	-.092 NS	-.469⋆	.001 NS	.493⋆⋆	-.072 NS	.500⋆⋆	.240 NS	-.264 NS	.055 NS	-.206 NS	-.252 NS	-.561⋆⋆
O_3	.070 NS	-.146 NS	-.117 NS	-.321 NS	.234 NS	-.439⋆	.428⋆	.330 NS	.560 NS	.066 NS	.087 NS	.724⋆⋆
SO_2	-.031 NS	-.004 NS	.274 NS	.665⋆⋆	.318 NS	.528⋆⋆	.443⋆	.401⋆	.247 NS	.443⋆	-.264 NS	.500⋆⋆

NS: Not Significant, Degree of significant ($\star p < 0.05$, $\star\star p < 0.01$)

Positive relations are observed in April and June for CO at both stations and in June for NO_x. There is a negative relation in June for ozone, implying that strong positive relations are in January and April for SO_2 and there are negative relations at station one positive relations in April and June for SO_2 at station two. These results show that temperature has a high effect on photochemical production of ozone (Elminir, 2005).

Table 9: Correlation matrix for air pollutants and relative humidity at station #1

Pearson correlation	JAN	FEB	MAR	APR	MAY	JUN	JULY	AUG	OCT	NOV	DEC	yearly
CO	-.118 NS	.326 NS	-.219 NS	.019 NS	.052 NS	-.094 NS	-.208NS	-.217 NS	-.356 NS	-.428⋆	-.145 NS	.324⋆⋆
Dust	.070 NS	-.173 NS	.016 NS	-.226 NS	.526⋆⋆	-.248 NS	.317 NS	-.132 NS	-.407⋆	-.706⋆⋆	-.266 NS	-.377⋆⋆
NO_X	-.264 NS	.038 NS	-.230 NS	-.180 NS	-.125 NS	-.155 NS	-.101 NS	-.030 NS	.430⋆	-.420⋆	-.402⋆	.463⋆⋆
O_3	.180 NS	-.410⋆	-.028 NS	-.165 NS	-.520⋆⋆	.029 NS	.139 NS	-.352 NS	-.285 NS	.115 NS	-.156 NS	-.664⋆⋆
SO_2	.061 NS	.425⋆	-.474⋆	-.723⋆⋆	-.137 NS	-.310 NS	-.276 NS	-.505⋆⋆	-.683⋆⋆	-.799⋆⋆	-.558⋆⋆	.281⋆⋆

NS: Not Significant, Degree of significant ($\star p < 0.05$, $\star\star p < 0.01$)

The results in Tables 9 and 10 show correlations between air pollutants and relative humidity. There is a negative correlation between Ozone and relative humidity and weak negative correlation between relative humidity and dust, and barely positive relations for CO and NO_x at both stations. For SO_2 various functions can be seen in both stations; with a weak positive relation at station one and a strong negative relation at station two. In addition, a strong negative correlation is observed in November for dust and in May for ozone. SO_2 has significant negative correlations with relative humidity in April, October, November and December at station one and in April, October and December at station two. Significant correlations of air pollutants with relative humidity could be due to precipitation conditions of high moisture in air masses (Stulov et al.,2010).

Table 10: Correlation matrix for air pollutants and relative humidity at station #2

	JAN	FEB	MAR	APR	MAY	JUN	JULY	AUG	OCT	NOV	DEC	yearly
CO	-.062 NS	.072 NS	-.035 NS	-.377 NS	-.026 NS	-.088 NS	-.288 NS	-.099 NS	.013 NS	-.167 NS	-.104 NS	.520⋆⋆
Dust	.109 NS	-.183 NS	.022 NS	-.257 NS	.264 NS	-.175 NS	-.298 NS	-.186 NS	-.573⋆⋆	-.723⋆⋆	-.232 NS	-.343⋆⋆
NO_X	-.168 NS	.171 NS	.119 NS	-.547⋆⋆	.213 NS	-.234 NS	-.357⋆	-.418⋆	-.181 NS	-.377⋆	-.363 NS	.540⋆⋆
O_3	.185 NS	-.105 NS	-.339 NS	-.048 NS	-.619⋆⋆	.-.080 NS	-.026 NS	-.451⋆	-.448⋆	-.216 NS	-.399⋆	-.590⋆⋆
SO_2	-.386⋆	-.321 NS	-.466⋆	-.861⋆⋆	-.291 NS	-.379⋆	-.338 NS	-.132 NS	-.534⋆⋆	-.209 NS	-.525⋆⋆	-.658⋆⋆

NS: Not Significant, Degree of significant ($\star p < 0.05$, $\star\star p < 0.01$)

The relationship between air pollutants and maximum wind speed was determined and the results are shown in Tables 11 and 12 indicating positive significant correlations in May for dust at both stations, and significant negative correlations for ozone in this month, and these relations could be due to a high wind speed in this month.

Table 11: Correlation matrix between air pollutants and maximum wind speed at station #1

Pearson correlation	JAN	FEB	MAR	APR	MAY	JUN	JULY	AUG	OCT	NOV	DEC	yearly
CO	-.324 NS	-.001 NS	-.326 NS	.328 NS	.035 NS	-.366⋆	-.041 NS	-.263 NS	.065 NS	.038 NS	-.324 NS	-.216⋆⋆
Dust	-.301 NS	.108 NS	.314 NS	.051 NS	.644⋆⋆	.392⋆	-.249 NS	-.189 NS	-.011 NS	-.267 NS	-.301 NS	.140⋆⋆
NO_X	-.255 NS	-.302 NS	-.400⋆	.243 NS	-.191 NS	-.397⋆	.065 NS	.197 NS	.066 NS	.057 NS	-.255 NS	-.384⋆⋆
O_3	.232 NS	.206 NS	.213 NS	-.227 NS	-.518⋆⋆	-.057 NS	-.067 NS	.005 NS	-.265 NS	.176 NS	.232 NS	.221⋆⋆
SO_2	.254 NS	-.353 NS	-.384 NS	.419⋆	-.321 NS	-.271 NS	-.022 NS	-.302 NS	-.153 NS	-.145 NS	.254 NS	-.151⋆⋆

NS: Not Significant, Degree of significant ($\star p < 0.05$, $\star\star p < 0.01$)

The relationship between air pollutants and maximum wind speed was determined and the results are shown in Tables 11 and 12 indicating positive significant correlations in May for dust at both stations, and significant negative correlations for ozone in this month, and these relations could be due to the high wind speed in this month.

Table 12: Correlation matrix between air pollutants and maximum wind speed at station #2

Pearson correlation	JAN	FEB	MAR	APR	MAY	JUN	JULY	AUG	OCT	NOV	DEC	yearly
CO	-.257 NS	-.037 NS	-.274 NS	.097 NS	.109 NS	-.266 NS	.118 NS	-.047 NS	.100 NS	-.049 NS	-.067 NS	-.367⋆⋆
Dust	-.218 NS	.098 NS	.352 NS	.074 NS	.782⋆⋆	.266 NS	-.256 NS	-.172 NS	-.139 NS	-.181 NS	.003 NS	.142⋆⋆
NO_X	-.264 NS	-.490⋆⋆	-.449⋆	.235 NS	.266 NS	-.078 NS	.107 NS	-.215 NS	.170 NS	-.135 NS	.047 NS	-.401⋆⋆
O_3	.162 NS	.193 NS	.228 NS	-.242 NS	-.637⋆⋆	-.177 NS	-.178 NS	-.268 NS	-.281 NS	-.131 NS	-.303 NS	.026⋆⋆
SO_2	-.024 NS	-.204 NS	-.288 NS	.355 NS	-.201 NS	-.097 NS	.037 NS	-.329 NS	-.102 NS	-.155 NS	-.072 NS	-.225⋆⋆

NS: Not Significant, Degree of significant ($\star p < 0.05$, $\star\star p < 0.01$)

3.2. Temporal variability:

This section shows variations of air pollutants in different months and different years in the period 2005-2010 for both monitoring air quality stations in Shiraz city.

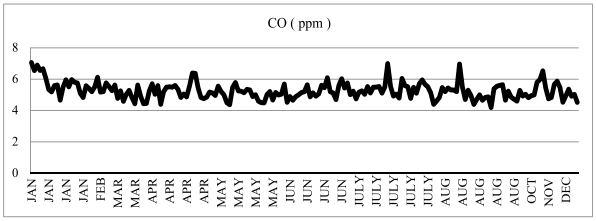

Figure 2: Daily variations of average CO concentrations for period 2005 – 2010 at station #1

Monthly variations of CO concentrations are shown in Figures 2 and 3 and these results imply that a slight fluctuation of CO is in January at both stations. This could be due to low temperature, low mixing depth, pollution inversion and traffic density (Elminir, 2005).

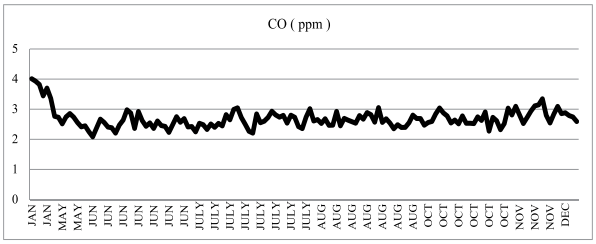

Figure 3: Daily variations of average CO concentrations for period 2005 – 2010 at station #2

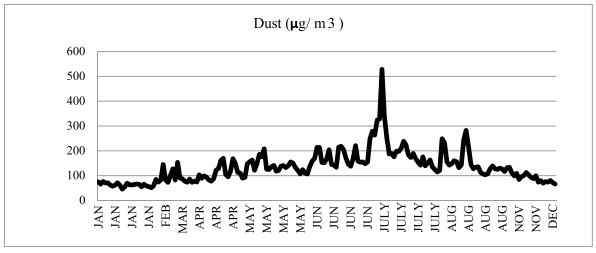

Figure 4: Daily variations of average dust concentrations for period 2005 – 2010 at station #1

Monthly dust variations are presented in Figures 4 and 5 at both stations, higher concentrations were evident in July with very clear variations in difference between months showing that particulate matter variations depend on the time of year and meteorology (Pearce, et al., 2010). Monthly variations for NO_x are shown in Figures 6 and 7; they indicate higher concentrations of NO_x in January at both stations and given that NO_x is a primary pollutant (Beaver and Palazoglu, 2010), with decreasing temperature in winter, its concentrations increased.

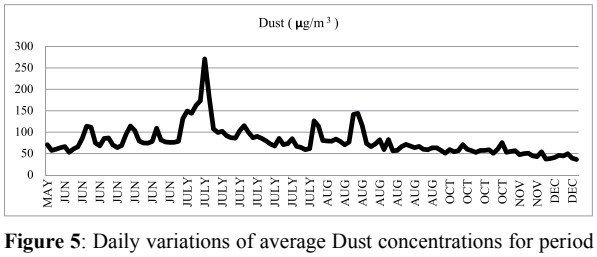

Figure 5: Daily variations of average Dust concentrations for period 2005 – 2010 at station #2

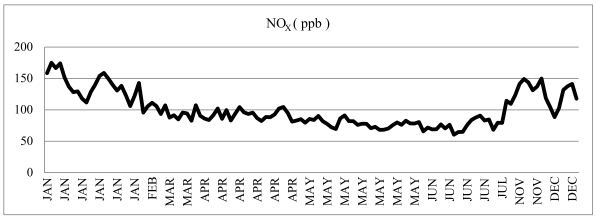

Figure 6: Daily variations of average NO_x concentrations for period 2005- 2010 at station #1

Ozone concentrations show clear variation across different months at both stations, as shown in Figures 8 and 9. There are higher concentrations of Ozone in June and July. The reason for this higher level of ozone is mainly due to the active photochemical production mechanism along with favorable meteorological conditions in summer months (Elminir, 2005).

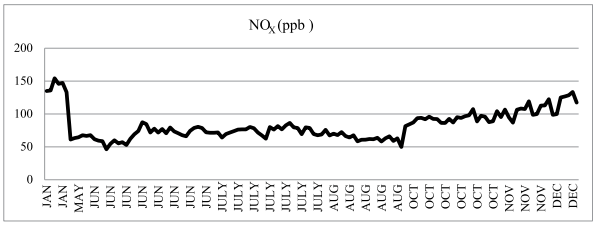

Figure 7: Daily variations of average NO_x concentrations for the period 2005 – 2010 at station #2

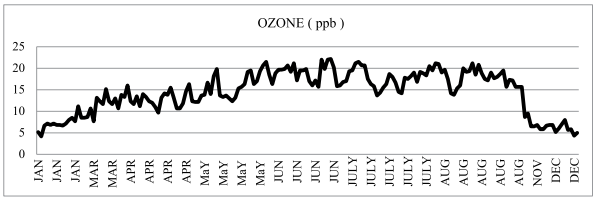

Figure 8: Daily variations of average O_3 concentrations for period 2005 – 2010 at station #1

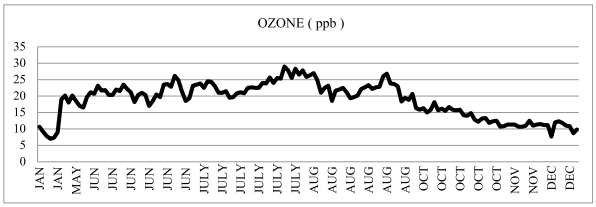

Figure 9: Daily variations of average O_3 concentrations for period 2005 – 2010 at station #1

Finally, monthly variations for SO_2 concentrations at both stations are presented in Figures 10 and 11. There is a steady trend at station one with higher concentrations in October at station two. Therefore, these results revealed the effect of weather conditions on the distribution pattern of air pollutants in different months.

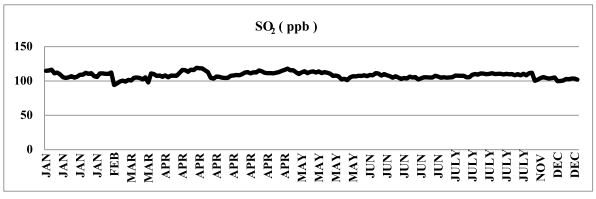

Figure 10: Daily variations of average SO_2 concentrations for period 2005 – 2010 at station #1

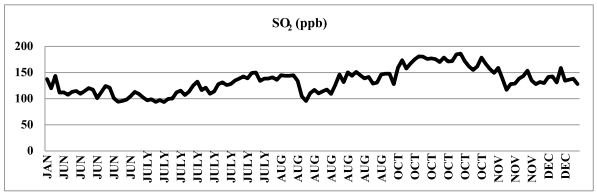

Figure 11: Daily variations of average SO_2 concentrations for period 2005 – 2010 at station #2

Variations of CO concentrations in different years are shown in Figures 12 and 13 for both stations. These results show that concentrations varied in different years, there is a decreasing trend at both stations that could be related to the air pollution control master plan and other strategies employed in the country especially those to control vehicles' emissions of CO. Some of these measures are improvements in fuel quality, limited promotion of alternative fuels, introduction of the auto emission inspection and some improvements in public transport (Atash, 2007). CO concentrations have increased slightly in 2010 at station two, which can be attributed to increasing concentrations of people and motor vehicle volume at this station.

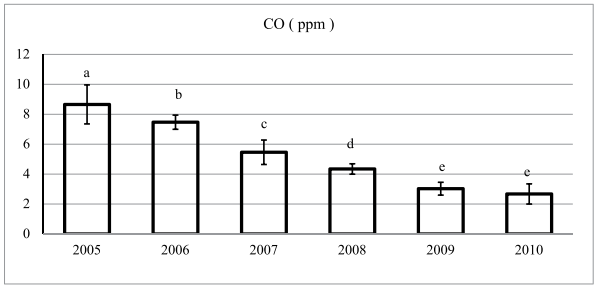

Figure 12: CO concentrations in different years at station #1, each bar represents ± SD, same letters indicate no significant difference at 5%, after applying the HSD test

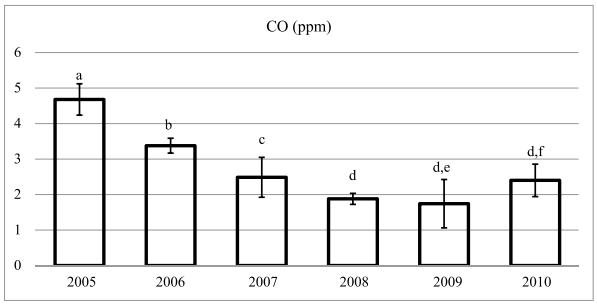

Figure 13: CO concentrations in different years at station #2, each bar represents ± SD, and same letters indicate no significant difference at 5%, after applying HSD test

Averages for concentrations of dust in different years for the period 2005 – 2010 are shown in Figures 14 and 15. These results show a relatively increasing trend for both stations, because the biggest source of dust is naturally occurring from the Iraqi dry deserts that have covered Fars province in recent years, especially in 2009 (Mansouri et al.,2011). With consideration of the effect of dust on public health it is important for policy makers and the Iranian government to restrict the entry of particulate matter to Iran.

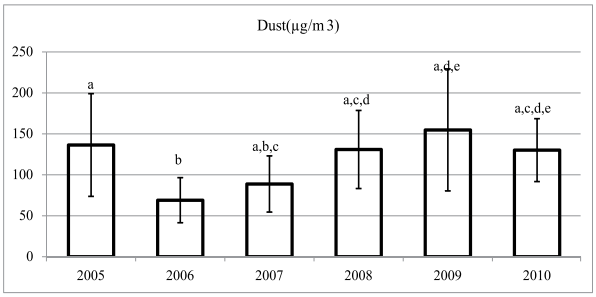

Figure 14: Dust concentrations in different years at station #1, each bar represents ± SD, same letters indicate no significant difference at 5%, after applying the HSD test

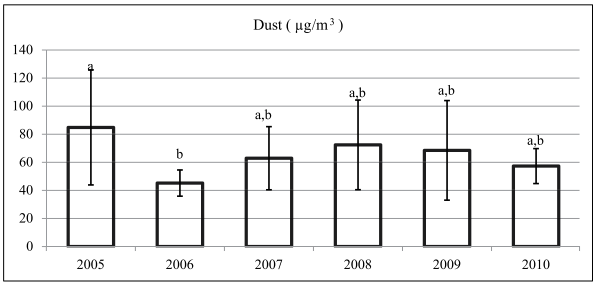

Figure 15: Dust concentrations in different years at station #2, each bar represents ± SD, same letters indicate no significant difference at 5%, after applying HSD test

Ozone average concentrations in different years are shown in Figures 16 and 17 for both stations. These results show a uniform trend at station one and a comparative increase for station two. This increase could be due to oxidation of atmospheric primary air pollutants that are emitted from motor vehicles and industries at station#2 (Fenger, 1999). Also average concentrations of Ozone at station two are higher than at station one for the period 2005-2010.

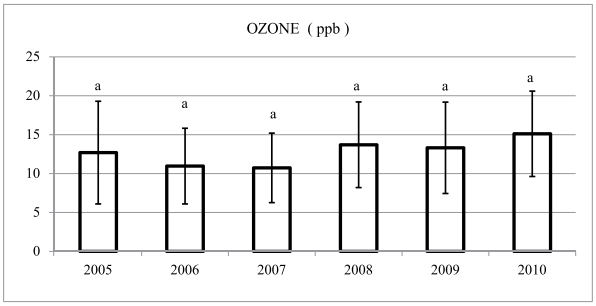

Figure 16: O_3 concentrations in different years at station #1, each bar represents ± SD, same letters indicate no significant difference at 5%, after applying the HSD test

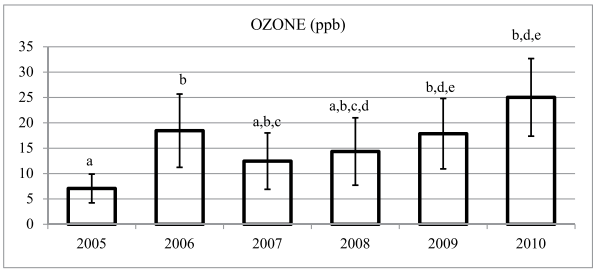

Figure 17: O_3 concentrations in different years at station #2, each bar represents ± SD, same letters indicate no significant difference at 5%, after applying the HSD test

NO_x average concentration variations in different years are shown in Figures 18 and 19. These results show a smooth increase for the period 2005–2010 especially during 2010 at both stations; this increase could be due to fuel combustion from motor vehicles and industries in recent years. Finally, SO_2 average concentrations in different years are shown in Figures 20 and 21 for both stations. The results have shown increasing trend up to the year 2008 and a decreasing trend in the years 2009 and 2010 for both stations.

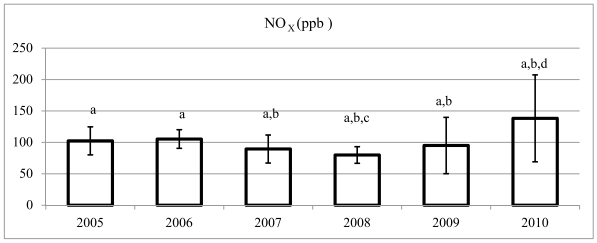

Figure 18: NO_x concentrations in different years at station #1, each bar represents ± SD, same letters indicate no significant difference at 5%, after applying the HSD test

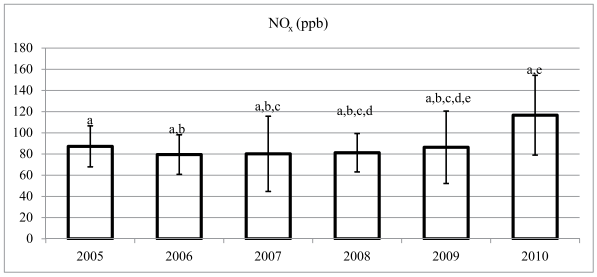

Figure 19: NO_x concentrations in different years at station #2, each bar represents ± SD, same letters indicate no significant difference at 5%, after applying the HSD test

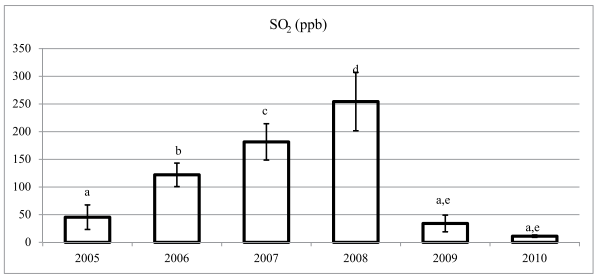

Figure 20: SO_2 concentrations in different years at station #1, each bar represents ± SD, same letters indicate no significant difference at 5%, after applying the HSD test

This fluctuating trend of increasing and decreasing could be due to the use of fuels with low sulphur content, for example natural gas or oil instead of coal or established desulphurization of the flue gas techniques in industries (Fenger, 1999).

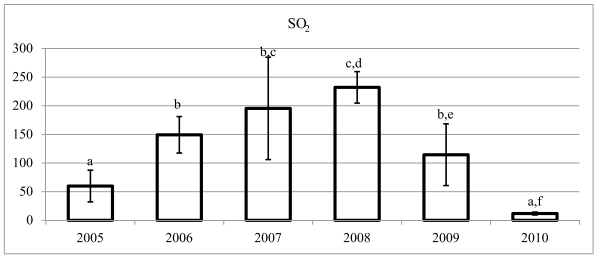

Figure 21: SO_2 concentrations in different years at station #2, each bar represents ± SD, same letters indicate no significant difference at 5%, after applying the HSD test

3.3. Stations differences:

This section shows differences of concentrations of air pollutants between two air quality monitoring stations in the city of Shiraz and results indicate that air pollutant concentrations are higher at station one than at station two for CO, dust and NO_x and for station two ozone and SO_2 are higher than at station one. These significant differences show that pollutants have different origins, the highest rate of CO, dust and NO_x at station one could be related to the heavy vehicle traffic and the highest rate of SO_2 and ozone at station two could be due to industrial activity, for example there is a cement factory in the southern part of Shiraz (Hadad et al.,2003).

4. Conclusion

This paper explored air pollution in Shiraz using meteorological parameters and concentrations of air pollutants in various temporal and spatial scales. The results make it obvious that meteorological conditions have an effect on pollutant concentrations in urban areas and air pollutant concentrations are variable according to months and situations and that this could be related to the interaction with meteorological parameters. These results also demonstrate that the affinities of some pollutants such as dust, Ozone, NO_x, and SO_2 on meteorology are more than that of carbon monoxide. Temporal variability shows that human activity and natural events have an effective role on concentrations of pollutants in different years and time scales, for example, dust had an increasing trend because of natural events and CO had a decreasing trend because of control measures in recent years. Significant differences between the two air quality monitoring stations implies that more air quality monitoring stations are needed to make monitoring air pollution in Shiraz more effective because of the city's urban structure.

Acknowledgements

The authors would like to thank Iran Department of Environment and Iran Meteorological Organization for providing the required data to carrying out this research.

References

[1] Atash, F., 2007. The deterioration of urban environments in developing countries: mitigation the air pollution crisis in Tehran, Iran. Elsevier.24:399-409.

[2] Baklizi, A., 2006. "Weighted Kolmogrov' Smirnov type tests for grouped Rayleigh data." Applied Mathematical Modeling 30(5): 437-445.

[3] Beaver, S. and A. Palazoglu, 2009. Influence of synoptic and mesocale meteorology on Ozone pollution potential for San Joaquin of California. Atmospheric Environment, 43: 1779-1788.

[4] Bigi, A. and R.M. Harrison, 2010. Analysis of the air pollution climate at a central urban background site. Atmospheric Environment, 44: 2004-2012.

[5] Chang, W., Y. Ono, M. Kumemura and T. Korenaga, 2005. "On-line determination of trace sulfur dioxide in air by integrated microchip coupled with fluorescence detection." Talanta, Nanoscience and Nanotechnology 67(3): 646-650.

[6] Chen, T., G. Su and H. Yuan, 2005. "In situ gas filter correlation: photoacoustic CO detection method for fire warning." Sensors and Actuators B: Chemical 109(2): 233-237.

[7] Elminir, H. K., 2005. Dependence of urban air pollutants on meteorology. Science of the total environment, 35: 225-237.

[8] Fenger, J., 1999. Urban air quality. Atmospheric Environment, 33: pp. 4877- 4900.

[9] Hadad, K., A Safavi and R. Tahon, 2005. Air pollution assessment in Shiraz by passive sampling techniques. Iranian journal of science and technology, 29. A3.

[10] Hadad, K., S Mehdizadeh and M. Sohrabpour, 2003.Impact of different pollutant sources on Shiraz air pollution using SPM elemental analysis. Environment International. 29: 39-43.

[11] Kan, H. and B. Chen, 2004. Particulate air pollution in urban areas of shanghaies china: health based economic assessment. Science of the total environment, 322: 71-79.

[12] Maghzal, G. J., K.-H. Krause, R. Stocker and V. Jaquet, 2012. "Detection of reactive oxygen species derived from the family of NOX NADPH oxidizes." Free Radical Biology and Medicine 53(10): 1903-1918.

[13] Mansouri, B., E. Hoshyari and A. Mansouri, 2011. Study on ambient concentrations of air quality parameters (O_2, SO_2, CO and PM10) in different months in Shiraz city, Iran. International journal of environmental sciences, 1(7).

[14] O'Keeffe, S., C. Fitzpatrick and E. Lewis, 2007. "An optical fiber based ultra violet and visible absorption spectroscopy system for ozone concentration monitoring." Sensors and Actuators B: Chemical 125(2): 372-378.

[15] Pearce, J. L., J. Beringer, N. Nicholls, R.J. Hyndman and N.J. Tapper, 2010. Quantifying the influence of local meteorology on air quality using generalized additive models. Atmospheric Environment, pp. 1-9.

[16] Rodriguez, S., A. s. Alastuey and X. Querol, 2012. "A review of methods for long term in situ characterization of aerosol dust." Aeolian Research 6(0): 55-74.

[17] Stulov, E. A., N.O. PlaudeandI.A. Monakhova, 2010. Weather effects on the aerosol characteristics in the surface layer of the atmosphere. Russian meteorology and hydrology, 35: 94-100.

[18] Tarasova, O. A., N.I. Elansky, G.I. Kuzentsov, I.N. Kuzenetsovaand I.A. Senik, 2003. Impact of air transport on seasonal variations and trends of surface Ozone at Kislovodsk high mountain station. Journal of atmospheric chemistry, 45: 245-259.

[19] Wang, G.-J., C. Xie, S. Chen, J.-J. Yang and M.-Y. Yang, 2013. "Random matrix theory analysis of cross-correlations in the US stock market: Evidence from Pearson's correlation coefficient and detrended cross-correlation coefficient." Physica A: Statistical Mechanics and its Applications 392(17): 3715-3730.

[20] Wheater, C. P. and P.A. Cook, 2005. Using statistics to understand the environment. Routledge introductions to environment series, pp.: 61-172.

JJEES

Volume 6, Number 1, September, 2014
ISSN 1995-6681
Pages 29- 35

Jordan Journal of Earth and Environmental Sciences

Influence of Urbanization on Water Quality Deterioration of Northern Wadi Shu′eib Catchment Area Springs, Jordan

Noor M. Al-Kharabsheh[1], Atef A. Al-Kharabsheh[2]

[1] Department of Engineering Geology and Hydrogeology, RWTH-Aachen University, 52064 Aachen, Germany
[2] Department of Water Resources and Environmental Management, Al-Balqa' Applied University, 19117 Salt, Jordan.

Received 5 May, 2012; Accepted 7 September, 2014

Abstract

This study investigates the effect of urbanization and informal residential settlements on the springs' water quality deterioration in Northern Wadi Shu′eib Catchment Area (NWSCA) that is mainly dominated by sedimentary rocks of the Upper Cretaceous Carbonate rocks. The present study examines ten representative springs out of twenty-two, in addition to the effluent of Salt Wastewater Treatment Plant (SWWTP). It also investigates the effect on water quality that is caused by urbanization and population growth around the recharge areas of the springs. It was found that the investigated springs are within the permissible limits of Jordanian Standards (JS) and World Health Organization (WHO) Guidelines for drinking-water quality for the parameters of pH, EC, turbidity, total hardness, total alkalinity, chloride, sulfate, sodium, potassium and iron. However, it exceeded the JS and WHO Guidelines for drinking-water quality for nitrate, phosphate, lead, Chemical Oxygen Demand (COD), Biological Oxygen Demand (BOD) and total Coliform.

Keywords: Urbanization, Wadi Shu′eib, Upper Cretaceous Carbonate rocks, Water Quality.

1. Introduction

Jordan is known to be one of the most water scarce countries in the world. More than 80% of the country is desert and about 90% of the annual rainfall is lost to evaporation with a share of 64% for agricultural purposes as irrigation water (MWI, 2004).

The growing demand for water supply is a result of the fast socio-economic development of Jordan and high population growth. Therefore, efforts were spurred to protect the quality of this limited water resource. NWSCA is mainly dependent on groundwater resources where water quality is at risk by groundwater hazards. It is experiencing rapid expansion with unsewered development and using septic tanks, thereby discharging to the unsaturated zone reaches groundwater where it affects water quality. Approximate times for septic effluent to pass the vadose zone to reach groundwater depend on the volume of effluent and the distance to water table. A septic plume in groundwater moves at a rate similar to the groundwater velocity (Robertson et al.,1991). The karst aquifer properties allow wastewater to recharge the springs very quickly and without any purification (Al-Kharabsheh and Ta'any, 2003). Therefore, the groundwater of the Upper Cretaceous Karst (carbonate) aquifer, which is prominent in the study area, is highly vulnerable. The inherent characteristics of the aquifer, namely, highly flow velocities, short residence time and fast hydraulic reactions accelerate groundwater pollution levels (Bender, 1974).

Werz (2006) found that highest risk intensity at Wadi Shu′eib area occurs in urban areas. The urban areas in the study area, often situated in karstified limestone's are not covered by auxiliary sediment or soil cover. This leads to a high vulnerable groundwater. Furthermore, the main contaminants are point source hazards caused by missing or leaking sewer systems, factor farms, manure heaps septic tanks and car service stations without unpaved floors and illegal waste dump.

McQuillan (2006) studied groundwater contamination by septic tanks effluents. He observed several health hazards from the contaminants, blue babies, neurotoxin and other specific outbreaks of disease. Furthermore, he suggested alternatives to conventional septic systems including advanced wastewater treatment units, which are like mini sewage treatment plants.

Foster (2001) investigated the interdependence of groundwater and urbanization in rapidly developing cities. He found that there are rather widespread indications of degradation of the groundwater resource-base caused by excessive exploitation and/or inadequate pollution control.

Minnesota Pollution Control Agency (1999) conducted a study to determine the effects of septic systems on groundwater quality in residential areas of Baxter, Minnesota. The agency reported that septic waste discharged to coarse-textured soils proceeds vertically through the unsaturated zone and into groundwater, through developing septic plume, which move with groundwater flow. It also found that median nitrate concentrations were significantly higher in areas with individual sewage treatment systems than in areas served by municipal sewers. Moreover, bacteria and Volatile Organic Compounds (VOCs) were found in septic effluent at all investigated sites.

The main objectives of this study are to determine the recent annual level of pollution fluctuations on these springs throughout the year, and classify the spring's′ water quality according to the biological and chemical properties. Furthermore, the interrelationships were pointed out between the results of the springs′ water analyses and recent pollution levels of these springs with the increased numbers of populations nearby of the springs′ catchment areas. Moreover, the urban expansion leads to increasing non-point source pollution with high effects on spring's′ water quality.

Therefore, in order to obtain the protection of the public health, it is essential to ensure water quality according to JS and WHO Guidelines for drinking-water quality. This is a strong motivation to lead this kind of study.

2. Study Area

NWSCA is located at the western part of Jordan, about 20 km northeast of the Dead Sea. It is located at 209-229 E and 144-165 N (according to Palestine grids) and covers a total area of approximately 185 Km^2 (Figure 1). A steep relief characterizes the area with elevations ranging from 1118 m above mean sea level (amsl) at El-Nabi Yousha′ to about 100 m below mean sea level (bmsl) at south Shoonah. The general shape of the catchment area is rectangular, with longer axis oriented NE-SW (Ta′any, 1992).

The study area is dominated by interstratification of karstic lime stones, marls and dolomites of the Upper Cretaceous Ajlun Group and lower part of the Balqa Group. Some main parts of the study area are intensively jointed and cut by faults (Figure 2). The joints are often enlarged by corrosion (Mikbel and Zacher, 1981).

In regard of the limestone of the formations, they are partially soluble in water and weak acid solution, thereby forming limestone pavements, potholes, centos, caves and gorges and then accelerating percolation rates to groundwater. Depending on the described geological situation, the vulnerability of groundwater is high.

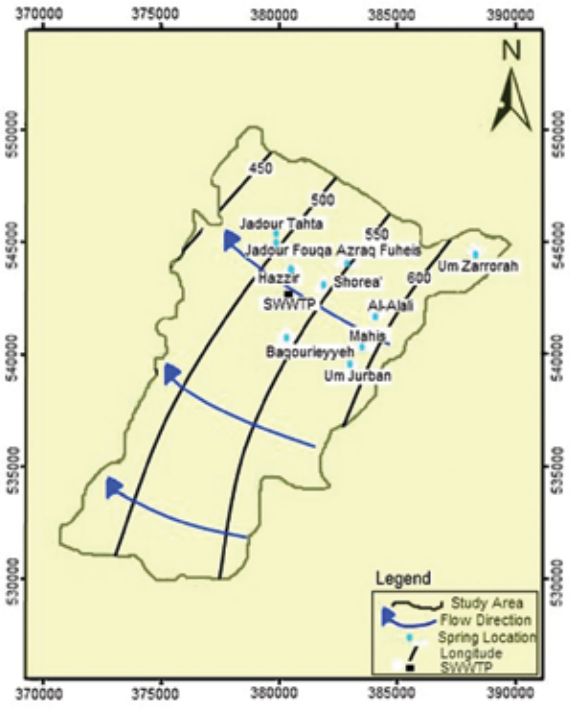

Figure 1: Locations of the studied springs and SWWTP in NWSCA and groundwater flow map of Wadi Shu′eib Catchment Area.

In some locations especially in Wadi Shu′eib area, intensive irrigation agriculture is possible during summer, whereas in the grabenshoulders, rain-fed agriculture exists. Because the Wadi Shu′eib watercourse itself has water all the year supplied by the outflow of the water treatment plant of Salt, some parts of the NWSCA have special crop situations. However, attention should be paid for the irrigation methods used in the study area, which are drip and subsurface irrigation systems (Salameh and Bannayan, 1993).

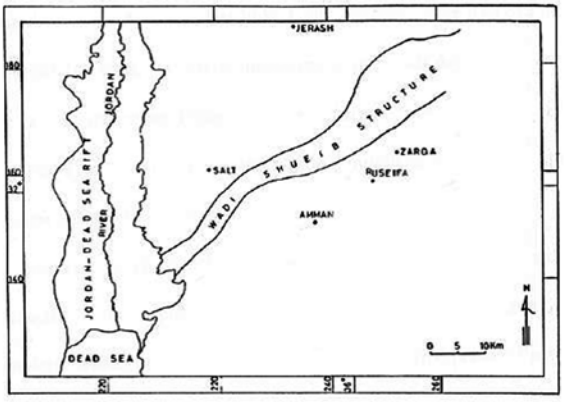

Figure 2: Location of the Wadi Shu'eib Structure (Werz 2006).

There are twenty-two major springs in the catchment area, nine springs emerge their water from Wadi Es-Sir Aquifer (A7), five from Hummar Aquifer (A4) and eight from Na′ur Aquifer (A1/2). Ten representative springs were selected for the purpose of this study. Figure (1) shows the locations of the selected springs and SWWTP in NWSCA. The discharge of these springs reaches to about 1000 (m3/hr) (Ta'any and Al-Kharabsheh, 2002).

The drainage path of the surface runoff follows the topography in NE-SW direction (Werz, 2006). However, the groundwater flow follows mainly the dipping of strata of the Na′ur, Hummar and Wadi Es-Sir aquifers separated by the lower permeability interstratifications of the Fuheis and Shu′eib formations as in Figure (2). Harter (2003) found that groundwater naturally flows at a speed that may range yearly from a few meters in poorly producing aquifers to a few thousand meters in very productive aquifers. However, in very sandy or gravelly aquifers and in some highly porous or cavernous volcanic and karstic aquifers, groundwater speed may be 3048 m per year or more.

According to Salameh and Bannayan (1993), the average natural flow of the wadi is 1.8 (MCM/year) as flood flow and 3.9 (MCM/year) as base flow. In addition to that, the effluent of the SWWTP, one of the best-functioning plants in Jordan, is discharged into the wadi. A dam was constructed in Wadi Shu′eib with a capacity of 2.3 MCM for irrigation purposes. Some parts of NWSCA, are located on the banks of Wadi Shu′eib course, have special crop situations due to supplementary water from the outflow of SWWTP during the year. At locations above the wastewater treatment plant and in the lateral valleys of the Wadi Shu′eib area mainly orchards exists.

Another two treatment plants are located in NWSCA; Fuheis and Mahis Wastewater Treatment plant, in addition to Fuheis Site SMART project. However, this study does not include them as a point of study because of low probability of pollution caused by these plants. More clarifications about both of them are within the context. The middle and northern parts of NWSCA are dominated by olive trees agriculture (Werz, 2006). Agriculture in the southern parts is limited to the existence of continuous soil cover. Built-up areas are mainly located in the northern and the northeastern areas that are characterized by a high population density, while sparsely populated parts are in the south of the study area. Open Files of the Department of Statistics of Jordan (2010) reported that the number of houses using septic tanks are 3664, 377 and 495 against 10474, 2208 and 1577 use sewer system; are serving 83202, 13171 and 12049 capita in the areas of Salt, Fuheis and Mahis, respectively. However, around 782 capita of

135 houses in Wadi Shu′eib totally use septic tanks systems. Consequently, 26%, 14.5%, 24% and 100% of population in Salt, Fuheis, Mahis and Wadi Shu′eib, respectively, depend on septic system to discharge their domestic wastewater.

According to the views at fieldwork, Hazzir, Shorea′, Baqouriyyeh, Mahis and Azraq Fuheis are used for drinking purposes and all of them are chlorinated by specialized parties. On the other hand, the springs of Um Jurban, Jadour Tahta and Um Zarrorah are used for drinking by residents without any kind of treatment. Jadour Fouqa spring is used for agricultural purposes and other domestic uses, but Al-Alai spring, which is under authority of Fuheis Cement Factory, is used for industrial purposes.

3. Materials and Methods

The examination of water quality is a determination of microorganisms, minerals and organic compounds contained in water. Physical analyses; pH and Electrical Conductivity, chemical analyses; major cations (Na^+, K^+, Ca^{2+} and Mg^{2+}), major anions (Cl^-, CO_3^{2-}, HCO_3^-, SO_4^{2-}, NO_3^- and PO_4^{3-}), heavy metals (Fe^{2+} and Pb^{2+}), Chemical Oxygen Demand (COD) and Biological Oxygen Demand (BOD), were carried out. Also biological analyses; total coliform as Most Probable Number (MPN) method were performed on springs water samples to determine their water quality.

The samples were taken before chlorination from ten representative springs in the study area as well as from the effluent of SWWTP. Samples were stored cool until analyses. The analyses of all parameters were carried out in the Laboratories of the Department of Water Resources and Environmental Management (DWREM) at the Faculty of Agricultural Technology, Al-Balqa′ Applied University, Salt, Jordan.

The samples were collected and analyzed on monthly basis for a whole year. Two thousand five hundred and eight analyses for nineteen parameters were carried out. The analytical techniques were performed according to the procedures mentioned in Standard Methods for the Examination of Water and Wastewater (Clesceri et al.,2005).

4. Results, Discussion and Conclusion

The average value of pH for the different springs ranges between 7.0 for Al-Alali and 7.5 for Shorea′, Um Zarrorah and Azraq Fuheis. Table (1) shows the average and standard deviation of all studied parameters of the representative springs and SWWTP in the study area. The pH value of Al-Alali spring confirms the existence of bicarbonate as a result of limestone dissolution. In all springs, the pH values are acceptable for drinking water according to JS and WHO Guidelines for drinking-water quality. According to Subramania classification (1997) of the pH, the water samples could be classified into two groups, the first is classified as springs of soft water including Jadour Fouqa, Jadour Tahta, Hazzir, Baqourieyyeh, Um Jurban, Al-Alali and Mahis springs and the second one as springs of hard water including Shorea′, Um Zarrorah and Azraq Fuheis spring.

The average value of Electrical Conductivity (EC) of springs′ water samples ranges between 540.3 (µS/cm) for Shorea′ spring and 1036.2 (µS/cm) for Al-Alali spring. According to JS and WHO Guidelines for drinking-water quality, all water samples are within the permissible limit of EC. High value of EC in Al-Alali spring confirms a high content of dissolved solids, which can be attributed to the leakage of sewer water from present or old septic tanks caused by the urban expansion along the recharge area of the spring. A considerable correlation is found between high concentrations of pollutants, come from seepage of sewer system such as Cl^- and Na^+, and the high value of EC of Al-Alali spring. The correlation coefficient values demonstrate a high positive relevance between them as 0.9745 and 0.9627, respectively. Whereas Shorea′ spring is located in an area surrounded by a few houses located faraway. Therefore, there are no continuous pollution sources near the recharge area of this spring and this may explain its low EC value. The addition of excess of agricultural fertilizers represented by the nitrogenous, phosphatic or organic fertilizers, to soil increases the value of leached chemical pollutants to springs′ water.

In Jordan there is a lack of information concerning fertilizers quantities, which are used and lead to potential groundwater hazards. Lists of number, type, location, and the size of industrial firms were not existing or available from public offices or ministries. This fact can be considered as normal for areas such as the study area. Precise and reliable information concerning infrastructural installations, such as wastewater, sewer systems or utilization ratio of streets, or the amount and nature of fertilizers or number of livestock in agriculture, is often difficult to obtain (Storz, 2004).

The average value of turbidity of the water samples ranges between 0.8 NTU for Jadour Fouqa, Mahis and Azraq Fuheis springs and 2.8 NTU for Hazzir spring. All springs have turbidity values within the permissible limit of JS and WHO Guidelines for drinking-water quality, except of Hazzir spring where two values in January and February were found out of the permissible limit. This may due to winter season rainfall that easily feed the Hummar formation where Hazzir spring emerges. During winter season, the high flow rate of leaked water through the formation of underground karstic limestone get the spring′s water to be turbid taking into account the dissolution process. Hence, once the rain reaches the ground, it passes through soil that can provide much more CO_2 to form a weak carbonic acid solution, which dissolves calcium carbonate as suspended matter causing turbidity of groundwater.

The average value of the total hardness of water samples ranges between 213 (mg/l) as $CaCO_3$ for Shorea′ spring and 392.9 (mg/l) as $CaCO_3$ for Al-Alali spring. All the studied springs have total hardness values within the permissible limit of JS and WHO Guidelines for drinking-water quality. The values of total hardness for both springs (Shorea′ and Al-Alali) agree with EC values, in addition to the positive relation between EC and dissolved metallic ions of calcium and magnesium (Shalash and Ghanem, 2008). A Significant correlation coefficient of 0.8926 is found between the EC and calcium values for both springs, which refer to a strong relation between the two parameters.

According to Freeze and Cherry classification (1979) of the total hardness, the water samples of springs can be classified into two groups; the first is hard water springs including Shorea', Azraq Fuheis and Baqourieyyeh and the second is very hard water springs including Um Zarrorah, Jadour Fouqa, Jadour Tahta, Hazzir, Um Jurban, Al-Alali, and Mahis. All concentrations of calcium are higher than magnesium concentrations for all springs. This is highly attributed to the dissolution of limestone that is mainly built of Ca-mineral.

The total alkalinity values of all examined springs are only represented by bicarbonate concentrations because pH values were less than 8.3. The average value of bicarbonate ranges between 179 (mg/l) for Shorea′ spring and 318.5 (mg/l) for Al-Alali spring. A positive relationship is found between EC

Table 1: The average and standard deviation of the analyzed parameters for the springs and SWWTP.

Analysis	Jadour Fouqa	Jadour Tahta	Hazzir	Shorea'	Baqourieyyeh	Um Jurban	Al-Alali	Mahis	Um Zarrorah	Azraq Fuheis
pH	7.4±0.2	7.4±0.2	7.2±0.2	7.5±0.2	7.3±0.2	7.2±0.2	7.0±0.2	7.2±0.2	7.5±0.2	7.5±0.2
EC (µs/cm)	934.6±13	944.9±11	895.8±34.8	540.3±19.9	674.9±34.1	988.2±13.6	1036.2±17.3	707.1±6.9	754.5±15.1	556.9±20.2
Turbidity (NTU)	0.8±0.4	1.5±0.5	2.8±2.5	1.8±0.9	1.2±0.9	1.7±0.9	1.4±1.5	0.8±0.6	0.9±0.7	0.8±0.7
Ca (mg/L)	94.9±6.1	98.9±8.6	101.5±12.3	66.4±7.1	80.8±4.1	121.6±11.2	137.3±14.6	88.2±4	103.1±13.6	70.9±3.8
Mg (mg/L)	22.2±4.6	17.9±4.3	16.9±4.3	11.5±4.2	15.9±6.2	17.0±2.4	12.2±3.5	21.4±6.1	11.5±5.7	13.4±2
T. H. as $CaCO_3$ (mg/L)	328±11.1	320.3±11.1	322.7±19.2	213±8.1	267±24.4	373.6±30.4	392.9±32.8	302.7±10.6	304.8±16.9	232.3±12.2
HCO_3^- (mg/L)	209±11.5	203.9±10.3	249.3±8.8	179±15.9	217.5±11.4	316.6±15	318.5±10	236.1±6.9	234.5±21.1	193±7.7
Cl^-(mg/L)	93.7±6	95.3±7.5	79.5±8	37.2±5.4	54.2±6.5	90±2.9	93.2±6.2	56.1±2.9	55.3±2.5	41.5±5.3
NO_3^- (mg/L)	95.8±12	103.7±17.9	73.2±20.1	30.2±9.9	33.6±4.2	58±10.2	46.5±3.3	35.5±5.9	61.6±9.4	27±6.9
PO_4^{3-} (mg/L)	0±0.1	0.1±0.1	0.7±0.8	0.1±0.1	0.1±0.1	0±0.1	0±0	0±0	0±0.1	0±0.1
SO_4^{2-} (mg/L)	33.5±7.3	27.2±10.7	25.4±3.2	16.2±8.5	25.2±7.1	27±7.3	59.8±8.3	24±5.3	28.7±7.1	20.3±4.1
Na^+ (mg/L)	42.7±6.1	40.5±6.7	33.8±6.1	15.6±5.8	22.8±6.8	45.6±13.3	51.9±9.4	20.7±3.5	23.3±7.9	19.1±3.6
K^+ (mg/L)	14.7±1.6	14.1±4.2	8.8±2.3	1.4±1.2	4.5±0.9	6.2±1.6	6.6±1.6	1.5±1.1	1.5±1.1	1.4±1.1
BOD (mgO_2/L)	26.5±18	25.3±16.3	29.3±17.6	26±17.9	23.8±16.4	27.7±16.6	27.8±18.4	25.8±19	28.3±17.4	16.1±16.3
COD (mgO_2/L)	45.7±29.7	42±27.4	51±30.2	42.5±28.6	41.8±29	48.1±27.8	48.4±29.3	42.6±32.2	48.5±26.1	23.8±27
T. Coliform (MPN/ 100 ml)	1008.4±920.1	1167.5±1386.7	2658.3±1815.8	678.3±793.8	133.3±39.2	721.7±605.7	1775±1123.4	120±193.6	11741.7±15000.4	10.1±8.2
Iron (mg/L)	0.1±0.1	0.2±0.1	0.1±0	0.1±0.1	0.1±0	0.1±0.2	0.1±0	0.1±0.1	0.1±0	0.1±0.1
Lead (mg/L)	0.1±0.1	0.1±0.1	0.1±0.1	0±0	0.1±0.1	0.1±0	0±0.1	0±0.1	0.1±0	0±0.1

and total alkalinity; hence, the highest value of bicarbonate of Al-Alali spring correlates with its highest value of EC. Furthermore, the lowest value of bicarbonate for Shorea′ spring accompanies with its lowest EC value. The relatively high values of bicarbonate for the springs are primarily due to the dissolution of limestone and marl of the region (Ta′any, 1992). All studied springs samples prove a high correlation between EC and bicarbonate values through a correlation coefficient value of 0.7111.

The average value of chloride ranges between 37.2 and 95.3 (mg/l) for Shorea′ and Jadour Tahta springs, respectively. Due to the effects of urbanization, the relatively high values of chloride for Jadour Tahta can be explained. The recharge area is contaminated by direct seepage of septic tanks or old sewer system. The dissolution of rocks and soils may also contribute in considerable amount of chloride constituents in the spring's′ water. All springs have chloride concentrations within the permissible limit of JS and WHO Guidelines for drinking-water quality. A significant correlation exists between chloride and sodium concentrations of spring's′ water of a correlation coefficient value of 0.9564. This indicates a high probability of wastewater as a source of contamination. It is well known, that septic tanks increase the risk of exceeding drinking criteria for nitrate and chloride. The higher is the nitrate content of a specific location, the higher is the chloride content of this location as found for Jadour Fouqa spring. A significant correlation exists between chloride and nitrate with a correlation coefficient equals to 0.8.

The average value of nitrate ranges between 27 (mg/l) for Azraq Fuheis spring and 103.7 (mg/l) for Jadour Tahta spring. Most of the springs have higher nitrate content during the months of February, March and April. This can be attributed to contribution of excess nitrogen fertilization and manure addition during the agricultural season. Jadour Fouqa, Jadour Tahta and Hazzir springs have high concentrations of nitrate exceed the JS and WHO Guidelines for drinking-water quality. These high concentrations indicate to high probability of presence of organic matter resulting from domestic wastewater or seepage from septic tanks. Particularly for Jadour Tahta spring, the partial disposal of Salt slaughterhouse in the catchment area of the spring can be regarded as a source of pollution. Management of groundwater quality in unsewered areas focuses on nitrate because it is the primary chemical of concern associated in septic systems. Nearly all nitrogen passing through the drain field converts to nitrate in the aerobic soil zone and eventually flow to the groundwater, especially through joints and faults of the Upper Cretaceous Limestone rocks (GWMAP, 1999).

Most of the studied springs have considerable concentrations of phosphate during the months of March, April and May, the period of soil fertilization. These are at Shorea′, Jadour Tahta and Baqourieyyeh springs which have phosphate average of 0.1 (mg/l) with a maximum average concentration of 0.7 (mg/l) for Hazzir spring. This relatively high value indicates an input of anthropogenic wastewater or agricultural fertilizer. Most phosphorous contained in the septic tank is in organic forms and mainly as orthophosphate (Wilhelm et al.,1994).

Koelle (2003) defined phosphate concentrations higher than 100 (µg/l) as a pollution indicator. According to that, Hazzir spring is polluted with phosphate but the following springs: Jadour Tahta, Shorea′ and Baqourieyyeh have the upper permissible limit of phosphate to still suitable for drinking water.

The average value of sulfate ranges from 16.2 (mg/l) for Shorea′ spring to 59.8 (mg/l) for Al-Alali spring. The sulfate composition is contained in groundwater because of chemical weathering of sedimentary rocks in the study area. Each of the springs has sulfate value within the permissible limit of JS and WHO Guidelines for drinking-water quality. The average value of sodium ranges from 15.6 (mg/l) for Shorea′ spring to 51.9 (mg/l) for Al-Alali spring. Relatively high concentrations may be found in brines and hard water and this explains the positive relation between total hardness (Ca^{2+} and Mg^{2+}), sodium and EC such as at Al-Alali spring as explained before. All springs have sodium values within the permissible limit of JS and WHO Guidelines for drinking-water quality.

The average value of potassium ranges between 1.4 (mg/l) for Shorea′ spring and 14.7 (mg/l) for Jadour Fouka spring. High values of potassium in Jadour Fouqa, Jadour Tahta and Hazzir springs can be attributed to the agricultural activities represented by the addition of the popular synthetic potassium nitrate fertilizers to soils used in the recharge areas of these springs. As an artificial plant supplement, KNO_3 is added for high-value crops. It is typically made by reacting potassium chloride with a nitrate source (IPNI, 2007). A significant correlation exists between the concentrations of nitrate and potassium of the three mentioned springs with a high considerable correlation coefficient value of 0.8992. However, all springs have potassium values within the permissible limit of JS and WHO Guidelines for drinking-water quality.

In the springs of Jadour Fouqa, Shorea′, Um Jurban, Mahis and Azraq Fuheis, iron was either not detected or under the detection value. The other springs have iron value of 0.1 (mg/l) which is still within the permissible limit of lead according to JS and WHO Guidelines for drinking-water quality. Upward and downward of Jadour Tahta, Hazzir, Baqourieyyeh, Al-Alali and Um Zarrorah springs catchment areas, there are pollution sources such as roads, where many drivers clean their cars using the spring′s unprotected water. In particular, for Jadour Tahta spring another pollution source is the slaughterhouse, which is closely located beside the catchment area of this spring. The permanent seepage output of animal blood residues can be observed on the soil surface. This definitely affects the water quality by raising the iron concentration of the spring′s water. We attribute the results, that the trace metal as iron is typically low in human waste (Wilhelm et al.,1994). Concentrations of trace inorganics may reach levels of concern in poorly buffered groundwater systems if the pH of groundwater samples is below than 6.0 (Robertson and Blowes, 1995). But this is not relevant for the present study, because pH samples′ readings ranged between (7.0 and 7.5).

Lead parameter values for Azraq Fuheis, Jadour Fouqa, Jadour Tahta, Hazzir, Baqourieyyeh, Mahis, Shorea' and Al-Alali springs were either not detected or under detection. However, lead values of 0.1 (mg/l) were detected for Um Jurban and Um Zarrorah springs and exceed the maximum allowable limit according to JS and WHO Guidelines for drinking-water quality.

The average value of COD ranges between 23.8 (mg/l) for Azraq Fuheis spring and 51.0 (mg/l) for Hazzir spring. Although Azraq Fuheis spring has the minimum value of COD it has to be considered as high value because of their use for drinking water abstraction. The COD value of drinking water should be less than 10 (mg/l) (WAJ Open Files, 2010). This high values could be attributed to the occasional disposal of wastewater tanks and seepage of agricultural wastewater that penetrate within the Wadi Es-Sir Limestone (A7) formation then reach the groundwater. The relative low value of Azraq Fuheis spring compared with other springs is assigned to the spring′s location. Only this spring is surrounded in two

directions by a few faraway houses. In comparison, Hazzir spring showing the highest COD value is close to urban expansion in its catchment area. Um Zarrorah, Al-Alali and Um Jurban springs that have catchment areas crossed with existence of septic tanks show high values of COD. The high COD values of Jadour Fouqa are caused by a lack of sewer system and the close urbanization to the springs catchment area. The pollution sources for other springs are variant. For Jadour Tahta, the presence of slaughterhouse near to its catchment area increases the probability of pollution resulted from cleaning high-polluted slaughtered equipments by spring′s water, in addition to throwing some slaughter wastes adjacent to its catchment area. According to Chan (2001) and Benka and Ojior (1995), a positive relation between the relatively high COD and BOD values with high values of NO_3^- and total coliform is a decisive indicator for the exposure to source of organic pollutant. Shorea′ and Baqourieyyeh springs are facing the same pollution source represented by the occasional disposal of wastewater tanks. However, Mahis spring also faces the effect of presence of old and present septic tanks in its catchment area.

The average value of BOD ranges between 16.1 (mg/l) for Azraq Fuheis spring and 29.3 (mg/l) for Hazzir spring. Drinking water should have BOD value less than 5 (mg/l) (WAJ Open Files, 2010). However, all BOD results of springs exceed 5 (mg/l). This indicates a high probability of presence of organic matter resulting from domestic wastewater seepage from septic tanks or decaying of agricultural residues. The joints and faults present in the Upper Cretaceous Limestone rocks that cover the catchment area of the springs accelerate the penetration rate of these objects to reach groundwater.

The average value of total coliform ranges from 10.1 (MPN/100 ml) for Azraq Fuheis spring to 2658.3 and 11741.7 (MPN/100 ml) for Hazzir and Um Zarrorah springs, respectively. All springs have total coliform values exceed the permissible limit according to JS and WHO Guidelines for drinking-water quality. These values are caused by contamination with total coliform from septic tanks wastewater seepage to the spring's′ sources. Furthermore, storm water runoff during high stream flow, which is often called non-point source pollution, contributes to groundwater quality problems. About 80% of houses within the borders of Fuheis Municipality have been connected with the sewer system (Fuheis Municipality, 2010), only 65% for Mahis Municipality (Mahis Municipality, 2010), whereas in Salt Municipality is 78% (Salt Municipality, 2010). Faecal coliforms analyses were not performed in this study, however, total coliform persistence may refer to faecal origin, (Edberg et al.,1998).

Most prominent factors that affect the recharge area of the springs are the informal settlement or irregular urbanization and unplanned land use around the recharge areas of the springs. This is accompanied by absence of primary services such as sewer system. Furthermore, high slope of the catchment area accelerates the pollution rate along the recharge area of the springs. Moreover, the geological formation of the Upper Cretaceous Limestone rocks covers the catchment area of the springs, also increases the pollution rate due to the presence of joints, faults and massive cliffs through it.

Acknowledgments

The authors would like to thank Al-Balqa′ Applied University for funding this research. Thanks also to the Journal′s reviewers for improving the original manuscript.

References

[1] Al-Kharabsheh, A. and Ta'any, R., 2003. Influence of urbanization on water quality deterioration during drought periods at South Jordan. Journal of Arid Environments 53, pp. 619-630.

[2] Bender, F., 1974. Geology of Jordan. Supplementary edition in english with minor revisions. Gebruder Borntraeger, Berlin, pp. 4-30.

[3] Benka-Coker. M.O. and Ojior O.O., 1995. Effect of slaughter house wastes on the water quality of Ikpoba River, Nigeria. Bioresource Technology 52 (1995), 5-12.

[4] Chan Ho Jeong, 2001. Effect of land use and urbanization on hydrochemistry and contamination of groundwater from Taejon Area, Korea. Journal of Hydrology 25, 2001, 194-210.

[5] Clesceri, L.S., Greenberg, A.E. and Trussell, R.R., 2005. Standard methods for the examination of water and wastewater, twenty-first edition. American Water Works Association, Washington, USA, pp. 80-1307.

[6] Department of Statistics of Jordan (DSJ), 2010. Department of Ecology Statistics Open Files. Department of Statistics, Amman, Jordan.

[7] Edberg, S.C., Allen, M.J. and Smith, D.B., 1998. National field evaluation of a defined substrate method for the simultaneous enumeration of total coliforms and Escherichia coli from drinking water: comparison with the standard multiple tube fermentation method. Applied Environmental Microbiology 54 (6), 1595-1601.

[8] Foster, S.S.D., 2001. The interdependence of groundwater and urbanization in rapidly developing cities. Journal of Urban Water 3 (3), 185-192.

[9] Freeze, R.A., Cherry, J.A., 1979. Groundwater. Prentice-Hall Inc, Englewood Cliffs, pp. 400-546.

[10] Ground water Monitoring and Assessment Program (GWMAP), 1999. Effects of septic systems on groundwater quality - Baxter, Minnesota. Published by Minnesota Pollution Control Agency.

[11] Harter T., 2003. Groundwater quality and groundwater pollution. Published by the Regents of the University of

[12] California, Oaklan, California.
International Plant Nutrient Institute (IPNI), 2007. Nutrient source specifics series. Norcross, Georgia, USA. Ref #11-
[13] 10071.
Koelle, W., 2003. Wasseranalysen-richtig beurteilt. WILEY-
[14] VCH Verlag, Weinheim, p. 315.
McQuillan, Dennis, 2006. Groundwater contamination by septic tank effluents. Online published report by New Mexico
[15] Water Resources Research Institute.
Fuheis Municipality, Ministry of Municipality Affairs of
[16] Jordan, 2010. Fuheis Municipality Open Files. Fuheis, Jordan.
Mahis Municipality, Ministry of Municipality Affairs of Jordan,
[17] 2010. Mahis Municipality Open Files. Mahis, Jordan.
Salt Municipality, Ministry of Municipality Affairs of Jordan,
[18] 2010. Salt Municipality Open Files. Salt, Jordan.
Ministry of Water and Irrigation (MWI), 2004. National water master plan of Jordan-water resources in Jordan. National Water
[19] Master Plan Directorate of MWI, Amman, Jordan, p. 200.
Mikbel, S. and Zacher, W. 1981. The Wadi Shu′eib Structure in Jordan. Neues jahrbuch für geologie und palaeontologie
[20] monatsheft 9, pp. 571-576.
Robertson, W.D. and D.W. Blowes. 1995. Major ion and trace metal geochemistry of an acidic septic-system plume in silt.
[21] Groundwater 33, pp. 275-283.
Robertson, W.D, J.A. Cherry, and E.A. Sudicky. 1991. Ground-water contamination from two small septic systems on sand
[22] aquifers. Ground Water 29, pp. 82-92.
Salameh, E. and Bannayan, H., 1993. Water resources of Jordan, present status and future potentials. Published by
[23] Friedrich Ebert Stiftung Amman, Jordan, pp. 25, 43.
Shalash, I., Ghanem, M., 2008. Hydrochemistry of the Natuf Drainage Basin in Ramallah Area/West Bank. Environmental
[24] Geology Journal 55 (2), 359-367.
Storz, R., 2004. GIS-based groundwater hazard mapping of the Wadi Shu′eib Catchment Area, Jordan. Master Thesis
[25] University of Karlsruhe, Karlsruhe (unpublished), p. 149.
Subramania, S.M., 1999. Environmental chemistry and analysis.
[26] Indian Institute of Technology Madras, India, pp. 53-89.
Ta'any, R.A. and Al-Kharabsheh, A.A., 2002. Effect of hydraulic characteristics of karst Springs on discharge magnitudes of Wadi Shu′eib Catchment Area, Jordan.
[27] Alexandria Science Exchange 23 (3), 275-294.
Ta'any, R.A., 1992. Hydrological and hydrochemical study of the major springs in Wadi Shu'eib Catchment Area. M.Sc.
[28] Thesis, University of Yarmouk, Irbid, Jordan, pp. 4-245.
Water Authority of Jordan (WAJ), 2010. Water Authority of
[29] Jordan Open Files. Water Authority, Amman, Jordan.
Werz, H., 2006. The use of remote sensing imagery for groundwater risk intensity mapping in the Wadi Shu′eib, Jordan. PhD. Thesis, University of Karlsruhe, Germany, pp.
[30] 3-110.
Wilhelm, S.R., S.L. Schiff, and W.D. Robertson. 1994. Chemical fate and transport in a domestic septic system: Unsaturated and saturated zone geochemistry. Environmental
[31] Toxicology Chemistry 13, pp. 193-203.
World Health Organization (WHO), 1997. Guidelines for drinking-water quality. Geneva-Switzerland, second edition 3, pp. 4-16.

JJEES

Volume 6, Number 1, September, 2014
ISSN 1995-6681
Pages 37- 43

Jordan Journal of Earth and Environmental Sciences

SRAD Radial Diagram: A New Way to Display Important Aspects of Fault-Slip Analysis Results

Alireza Yousefi Bavil*

Department of Geotectonics and Regional Geology, Geology Institute of Azerbaijan, Baku, Azerbaijan

Received 12 April, 2013; Accepted 7 September, 2014

Abstract

Aspects of stress inversion, such as angular deviation, stress ratio, orientation of the principal stress axes, and the normal and shear components of the resolved stress tensor on a fault plane, are given as output by many programs that address stress inversion. However, comparison of results becomes difficult when the number of stress states and associated parameters increases. A stress ratio–angular deviation radial diagram was constructed. The diagram provides simultaneous illustration of the above parameters and facilitates the comparison and interpretation of up to eleven various stress states. The application of the diagram is demonstrated by a worked example based on data obtained from the Tabriz North Fault in the Eastern Azerbaijan province NW of Iran.

Keywords: Angular deviation; Radial diagram; Stress ratio; Stress tensor, Tabriz North Fault

1. Introduction

Since the 1970s, various methods have been introduced to determine (paleo) stress conditions from homogeneous and heterogeneous fault-slip data (e.g. Carey and Brunier, 1974; Angelier, 1979, 1984; Etchecopar et al.,1981; Armijo et al.,1982; Simón-Gómez, 1986; Lisl,e 1987, 1988; Galindo-Zaldívar and González-Lodeiro, 1988; Huang, 1988; Hardcastle and Hills, 1991; Nemcok and Lisle, 1995; Fry 1999; Yamaji, 2000; Delvaux and Sperner, 2003). Recently, new methods have been introduced to analyze heterogeneous fault-slip data based on cluster analysis (Nemcok and Lisle, 1995), Fry's graphical procedure, 1999, or the multiple inverse method (Yamaji, 2000). Angelier,1994, Liesa and Lisle, 2004, and Célérier, et al., 2012. have scrutinized and reviewed most of the above-mentioned methods.

Stress inversion techniques treat faults and their slip vectors as paleostress gauges recording the direction of maximum resolved shear stress on the planes of the faults. The directional characteristics of shear stress on planes of different attitude are sufficient to constrain certain features of the geological stress condition, namely the orientations of the principal stress axes (σ_1, σ_2, σ_3) and stress ratio (Φ or R) (e.g. Wallace, 1951; Bott, 1959; Bishop, 1966; Angelier, 1979, 1984; Lisle and Orife, 2002; Delvaux and Sperner, 2003).

The majority of computer programs that deal with stress inversion techniques utilize some criteria of best fit. In this manner, such programs consider the lowest mean deviation or lowest mean-square deviation between the observed slickenlines and the direction of maximum shear stress predicted from the stress tensor, which is known as the deviation angle δ (hereafter, the first criterion). A mechanical criterion is typically used to check the reactivation compatibility of faults via restraining fault orientation to high shear stress τ and lower compressive normal stress σ_n (hereafter, the second criterion) (Célérier, 1988; Angelier, 1990; Ramsay and Lisle, 2000). A detailed review of these criteria has been presented by Célérier, et al., 2012.

Usually, depending on the heterogeneity of the data set, more than one set of stress conditions can result from a stress inversion analysis; these condition sets will typically exhibit some differences with respect to a given parameter or criterion. The opportunity for simultaneous consideration of the results of both the geometrical and mechanical criteria applied, as well as the other parameters resulting from stress inversion, can facilitate the study of various stress tensors. This permits better assessment of the suitability of a certain stress state for the reactivation of a set of fault-slip data and for the comparison of different stress inversion parameters. Here, a diagram is introduced that serves as a histogram and allows the study of the results of up to eleven various stress states simultaneously. Furthermore, it permits comparison of two criteria for individual stress states and allows comparison of all defined stress states with respect to these criteria and some other parameters that can be attributed to stress state.

* Corresponding author. e-mail: ayousefi@gia.ab.az

2. Diagram's constituent parameters

2.1. Angular deviation

Angular deviation, which results from different methods of stress inversion, is usually the principal parameter used for assessing the relation between a given stress state and a set of fault-slip data (Carey and Brunier, 1974; Angelier, 1979; Lisle, 1987; Ramsay and Lisle, 2000; Yamaji, 2000; Célérier et al.,2012). Depending on the precision desired, different angles (e.g. 10°, 20°, and 30°) are used as critical values to restrain the relation between fault-slip data and a driven stress state. Various methods can be used to represent δ, including stereograms, tables, Venn diagrams, and histograms. However, the first three methods can cause perplexity during the classification of δ and the determined stress tensors. In most programs applying inversion methods, histograms are usually used to represent the frequency of fault-slip data satisfying different criteria of δ. This type of histogram, together with an associated Mohr diagram, provides information about δ directly and Φ indirectly.

2.2. Stress ratio

A Mohr diagram shows the predicted levels of τ and σ_n, i.e., the Mohr point, for all the measured faults in relation to a sliding envelop and presents a visual appreciation of the suitability of a given tensor for explaining the observed slip on the faults. In the context of brittle failure and faulting, τ and σ_n are two resolved components of the stress vector on a given plane, which is a result of internal forces acting on imaginary surfaces of a body (Ramsay and Lisle, 2000). On a specified plane, the shear stress component τ is effective parallel to the plane, whereas the normal stress component σ_n is effective perpendicular to the plane. Their combination is one of the parameters controlling the characteristics of slip on a fault surface. As principal stress values are not obtained through stress inversion, the ratio of the differences between the principal stress values are determined relatively, which defines Φ (Bott, 1959; Célérier, 1995; Lisle and Orife, 2002). For example, according to Bishop (1966) and Angelier (1975), the value of stress ratio is determined by:

$$\Phi = (\sigma_2 - \sigma_3) / (\sigma_1 - \sigma_3) \quad (1)$$

where $\sigma_1 \geq \sigma_2 \geq \sigma_3$ and where the positive sign refers to compression. By definition, the value of Φ ranges between 0 and 1, represented by $\sigma_1 \geq \sigma_2 \geq \sigma_3$ and $\sigma_1 = \sigma_2 > \sigma_3$, respectively. The adoption of the above stress ratio is mentioned here because the inversion method in Yamaji's multiple inverse method (MIM) program is based on Bishop's version of stress ratio (Yamaji et al.,2010). However, there are different adoptions available, e.g. Nádai's μ (Nádai, 1931 p. 77), Carey's R (Carey and Mercier, 1987), and Lisle's R (Lisle, 1989). Their formulations are provided in Appendix A.

3. Diagram inputs and adopted criteria

Stress ratio and δ are the principal parameters upon which the diagram is established. The Mohr point parameters related to each defined stress state and the orientation of principal stress axes, e.g.$\overrightarrow{\sigma_1}$. , are also used in the diagram. Most of the above-mentioned parameters are usually provided as program output, e.g. for Yamaji's MIM program (Yamaji, 2000). The stress inversion results for analysis are placed in an Excel file, in which each row corresponds to the data of one fault slip; however, the first row is allocated to $\overrightarrow{\sigma_1}$. Considering the range of Φ (i.e., 0–1 with intervals of 0.1), 11 and 22 columns are required for δ and (σn, τ), respectively. In this work, values for δ, σ_n, τ, and $\overrightarrow{\sigma_i}$ are allocated for each fault-slip datum and each recognized stress state, respectively.

Three critical values of δ (i.e., 10°, 20°, and 30°) are chosen as the first criterion. Meanwhile, the Mohr point of the faults that satisf $\tau \geq \mu\sigma_n$ is adopted as the second criterion, where μ is the coefficient of residual friction for sliding on a pre-existing fault (Žalohar and Vrabec, 2007). The fault-slip data used in the example are collected from sandstones; thus, the value of μ is set at 0.51 (Schellart, 2000).

4. Establishment of stress ratio–angular deviation (SRAD) diagram

Code is written in MatlabTM to construct the SRAD radius diagram. The radial form is chosen both for easier visualization and for comparison of the statistics resulting from the stress inversion. Consequently, a circle formulation is used in the writing of the code. In an x–y Cartesian coordinate system, the circle with center coordinates (a, b) and radius r is a set of all points (x, y) in which:

$$(x-a)^2 + (y-b)^2 = r^2 \quad (2)$$

Any point (x, y) on the circle has length x–a and y–b. If the circle is centered at the origin (0, 0), then the equation can be written as:

$$x = r\cos t \quad (3)$$

and

$$y = r\sin t \quad (4)$$

where r is the angular deviation and t is the angle that the radius—with a given value of Φ—from (a, b) to (x, y) makes with the x-axis in the range of 0–90°, where 0° and 90° refer to Φ = 0 and 1, respectively.

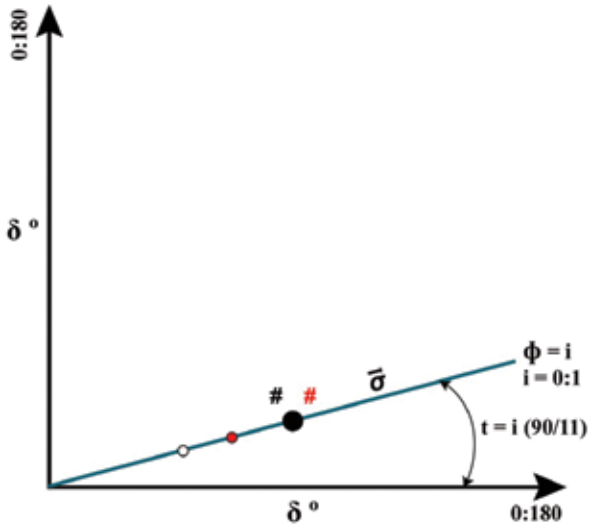

Figure 1: Components and basics of the SRAD diagram established based on the parameters of stress ratio Φ and angular deviation δ. A given stress state with a certain Φ value (i.e. i = 0 to 1, where i represents the Φ interval number) is represented by a ray that makes a given angle (t) with respect to the horizontal axis, calculated ast=i. (90/11). The ray length ranges between 0° and 180°, where the position of small circles (both white and red) denotes the δ value of each fault within the data set with respect to the defined stress state. White and red circles denote faults satisfying only the geometrical and both the geometrical and mechanical criteria, respectively. The black circle shows the position of a critical value of δ. Black and red # symbols denote the frequencies of faults, at a given critical value, that satisfy the first criterion and both criteria, respectively. Along a ray (i.e. a defined stress state), $\overrightarrow{\sigma}$ denotes the orientation of the principal stress axis that corresponds to the stress state.

The SRAD radial diagram consists of 11 radii. These radii are allocated to 11 intervals of Φ and each radius includes the values of δ for all fault-slip data with respect to a given defined stress state with a certain value of Φ (Fig. 1). Using three critical deviation angles, the values of δ are bounded as 0–10°, 0–20°, and 0–30° and the sum of the faults that meet the criteria are calculated for each bin. Also, of defined stress states with given Φ values are allocated to the same Φ radii (i.e., Φ interval) on the diagram.

The radial form of Φ intervals in the diagram evokes the diagram for representing stress tensors introduced by Ramsay and Lisle (2000); however, these diagrams are based on different concepts. Ramsay and Lisle's diagram is based on the parameters σ_1, σ_2, and σ_3 and displays the location (i.e., stress shape ratio and the differential stresses) of a stress tensor between Φ = 0 and Φ = 1. However, the diagram in this study is based on σ_n, τ, δ, and Φ and displays the attributes of correlation between a given stress state, a set of faults, and associated slip directions. In other words, in Ramsay and Lisle's diagram, Φ is output data, whereas in the diagram in this study, Φ is input data for the diagram.

5. Applications

During the comparison of different stress conditions (which can be determined under similar or different tectonic regimes and by different sources, i.e., geologic or seismic), in addition to the geometrical and mechanical criteria, it is sometimes important to consider those statistical criteria either adopted before applying the inversion or derived from it. Other stress field parameters can be involved in the comparison; however, these are approached in different ways, e.g. tectonic regime (γ) (Célérier, 1995). Unlike ordinary histograms, the SRAD radial diagram provides an opportunity to illustrate different parameters with different characteristics (e.g. orientation, frequency, eigenvector, and eigenvalue) and different value ranges (e.g. frequency, octahedral shear stress, and standard deviation).

The diagram allows the study and comparison of up to eleven stress tensors simultaneously and the simultaneous comparison of the geometrical and mechanical criteria for an individual state. Furthermore, the comparison can be expanded depending on the parameters allocated to the stress state, i.e., the tectonic regime parameter (γ) (Célérier, 1995), principal stress axes, differences between each tensor and the mean stress tensor, eigenvectors and eigenvalues of the stress state, octahedral shear stress (τ_{oct}) (Lisle and Orife, 2002; Orife and Lisle, 2003), and differences between angular stress distance (Θ), and mean angular stress difference (Θ^-). Moreover, regarding the MIM program, the diagram also allows the study of the enhance factor (EF), dispersion factor (DF), fault combination number (K), number of tensors plotted on each stereogram (N_p), number of different stress states output by the program (N_s), and standard deviation (SD) (Yamaji, 2000; Yamaji et al.,2010).

Depending on the parameters transferred to the diagram, it allows the display of two patterns of variation across different values of Φ (due to the 'across-ray' differences between various stress states) and δ (due to 'along-ray' changes in fault angular deviations with respect to an individual stress state).

6. A worked example

In this example, the parameters transferred to the diagram are δ, σ_n, τ, and $\overrightarrow{\sigma_1}$. The illustration of the across-ray differences allows the simultaneous comparison of the frequency of faults satisfying the following: (1) the first criterion, (2) both the first and second criteria, and (3) $\overrightarrow{\sigma_1}$. The illustration of along-ray changes allows the comparison of the frequency of faults satisfying the first criterion (δ) and both criteria (δ, σ_n, and τ) for a given critical value. This last illustration (i.e. along-ray changes) provides a similar function to an ordinary histogram.

The MIM program main processor (version 6) was used to apply a stress inversion on a real data set. The program allows the separation of deviatoric stresses using cluster analysis without a priori information on the stresses (Menke, 1989), which utilizes a form of self-correlation of data (Yamaji, 2000).

6.1. Geological setting

Fault-slip data (i.e., the attitude of faults and associated slickenlines) were collected from an area around the NW segment of the Tabriz North Fault (TNF), which is an area on the Ayanli Mountain between the Aji-chay and Arpa-dere rivers (Fig. 2). The study area is covered both by the youngest lithological units of the Miocene, i.e., red sandstone with marl, and by Quaternary sediments. The layers are almost horizontal (dip angle is about 6°). The deformation and uplift of these lithological units are ascribed to epeirogenic activity during the Pliocene–Quaternary Pasadenian structural stage (Geological Survey of Iran, 1993). Right-lateral displacement along this strand of the TNF is conspicuous by the deflection of drainage channels on the Quaternary sediments (Karakhanian et al.,2004). Within the study area, faults with both NW–SE and NE–SW trends cross cut and displace each other; however, the cross cutting of the NE–SW-trending faults by the NW–SE-trending faults are more frequent. Slickenlines' superposition is not found in the sampled faults (37 fault-slip data). The tectonic setting mentioned above suggests low heterogeneity of the data set.

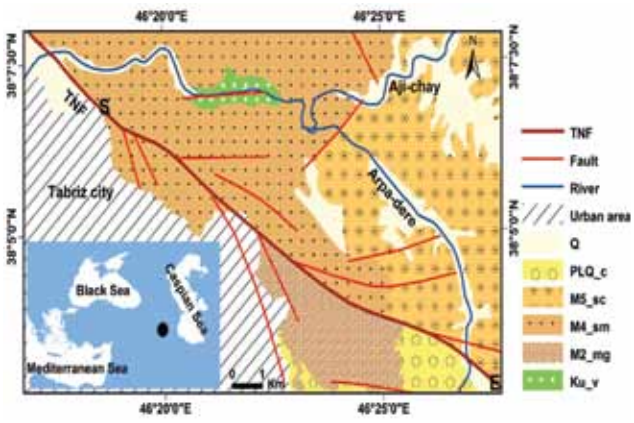

Figure 2: Geologic map around the NW segment of the TNF, showing red conglomerates with sandstone (M_5^{sc}), red sandstone with marl (M_4^{sm}), gypsiferous marl (M_2^{mg}), and basic and ultrabasic rocks (K_u^v). The black solid circle in the inset denotes the location of the study area. S and E define the start and end points of the swath profile. Tabriz city is located on the SW slope of the Aynali Mountain, which is located mainly to the NE of the TNF

6.2. Inversion procedure and results

At the first attempt at inversion, seven fault-slip data were found incompatible with any of the defined stress states and their separate inversion did not reveal a stable stress tensor. Therefore, these data were considered spurious and were excluded from the data set. The results of the secondary inversion, on the remaining 30 fault-slip data (Fig. 3a), did not change dramatically; therefore, the defined stress tensors are oriented almost coaxially.

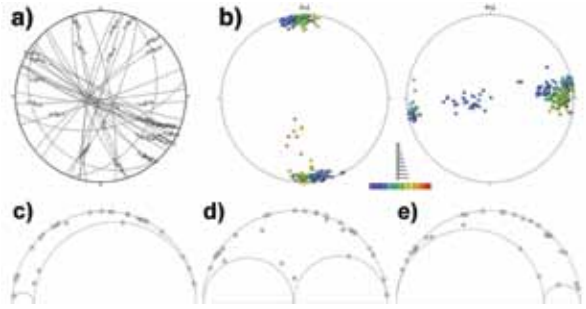

Figure 3: (a) Stereographic projection of fault-slip data and (b) recognized stress tensors. Fault-slip data were collected around the NW segment of the TNF. Stress tensors have been recognized by applying the multiple inverse method (program MIM) to the fault-slip data. In part (b), each square delineates the attitude of σ_1 (in the left stereogram) and σ_3 (in the right stereogram). Tensor colors show the Φ value: violet (Φ = 0), red (Φ = 1). Mohr points (τ and σ_n) of collected fault-slip data are illustrated with respect to three determined stress states: (c) Φ = 0.12, (d), Φ = 0.49, and (e) Φ = 0.8.

To treat the stress tensors (each square in the stereogram) recognized by MIM (Fig. 3b) objectively, to be precise about the location of the defined stress state(s), and to study the differences and their significance, the parameters of all defined states were calculated by the program, without any human intervention at this stage. Therefore, those stress states including all values of Φ, regardless of whether they formed a cluster, were taken into account. The inversion yields nine stress states with differing cluster densities, which include all tensors with different Φ values, i.e., 0.1–0.9 (Fig. 4).

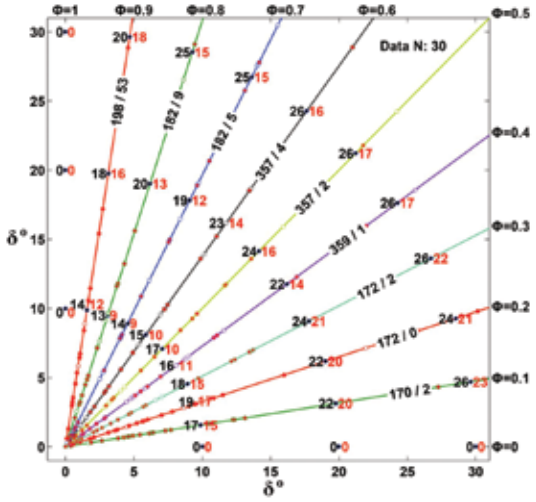

Figure 4: SRAD diagram illustrating the results of stress inversion on 30 fault-slip data collected along the NW segment of the TNF (modified after Yousefi Bavil and Moayyed, in press, 2015). Each ray is related to the defined stress state with a certain Φ value and involves the deviation angle δ of all fault-slip data (faults with values of δ greater than about 30–35° cannot be seen in the diagram) with respect to that state, whereas each circle on each radius indicates a fault's δ. The basics and parameters of the diagram have been described in Fig. 1.

Note that, in this study, three terms are used in the different stages of inversion analysis. (1) 'Recognized stress tensor' refers to a given tensor calculated by the MIM program (Fig. 3b, each square in the stereogram). (2) 'Defined stress state' refers to a given state composed of different stress tensors with the same Φ interval value, chosen objectively with no human interference based on their Φ values (Fig. 4). (3) 'Determined stress state' refers to a given stress state composed of one or more defined stress states—similar stress states, but with different Φ values. The last identified state is based on human decision. In this context, the SRAD diagram helps extend the objective stage of the decision-making procedure during the investigation of defined states with respect to various parameters.

6.3. Observations from the SRAD diagram

Surveying the diagram and the across-ray variation pattern obtained in this example (Fig. 4) demonstrates the following:

(1) For all critical values (δ = 10°, 20°, and 30°), the frequency of those faults that satisfy only the first criterion (black frequency numbers) is greater than that of those that satisfy both criteria (red frequency numbers). According to the first criterion, each of the defined stress states with Φ = 0.1 to 0.8 causes instability in more than 80% of faults where δ = 30°.

(2) The frequency of faults that satisfy both criteria generally decreases as Φ increases. This frequency is greater for states with Φ = 0.1 to 0.3 comparing other stress states. The value, i.e., frequency, reaches more than 70% of all faults with respect to the stress states with Φ = 0.1 to 0.3. Furthermore, even though some fault-slip data do not meet the first criterion exactly, i.e., δ > 30°, they are suitable for reactivation with regard to both criteria, where δ is slightly more than 30° (i.e., in cases with Φ = 0.2, 0.5, 0.7, and 0.8).

(3) A stress state with Φ = 0.9 has a different $\overrightarrow{\sigma_1}$ compared with other stress states.

(4) Among the stress states with Φ = 0.1 to 0.8, the value of Δ (which results from the difference between the frequency of faults satisfying the first criterion and both criteria at a given critical δ value) is lower for stress states with Φ = 0.1 to 0.3 than for stress states with other Φ values.

6.4. Stress state differences

The STRESSTAT program (Lisle and Orife, 2002) was used to compare the differences of the defined stress states. According to Orife and Lisle (2003), the difference between two normalized tensors can be expressed by a single parameter, the 'tensor difference' D. They introduced four terms with an accompanying range of values: Very similar, D < 0.66; Similar, D = 0.66 to 1.01; Different, D = 1.01 to 1.71; and Very different, D > 1.71. These terms can be used for the qualitative description of stress difference between any two stress tensors.

The differences between nine defined states show that the maximum value of D (D_{max}) among all defined stress states is equal to 1.0189, which corresponds to the difference between states with Φ = 0.1 and 0.9 (Table 1, number 4). Among eight stress states (Φ = 0.1 to 0.8) with similar principal stress axes, D_{max} is equal to 0.8696, which indicates their similarity (Table 1, number 1). Furthermore, among three stress states with proximity in terms of Φ (i.e., 0.1 to 0.3) and frequency number, D_{max} is equal to 0.2508, suggesting that the tensors are very similar (Table 1, number 2).

Table 1: Parameters of seven determined stress states in different Φ ranges. σ_1, σ_2, and σ_3 are orientations of three principal stress axes (where $\sigma_1 \geq \sigma_2 \geq \sigma_3$); Φ denotes the stress ratio according to Bishop's adoption; D_{max} and Nrt indicate the maximum stress tensor difference and number of recognized tensors in the stereogram for the constituent states of determined stress states, respectively.

Determined stress state		Parameters of mean stress tensor					
Number	Φ range	σ_1	σ_2	σ_3	Φ	D_{max}	N_{rt}
1	0.1–0.8	174.5 / 0.1	264.9 / 77.8	84.4 / 12.2	0.32	0.8696	270
2	0.1–0.3	170.9 / 1.3	273.4 / 84.1	80.8 / 05.8	0.12	0.2508	147
3	0.9	198.4 / 52.7	344.7 / 32.4	85.6 / 16.5	0.91	-	5
4	0.1–0.91	174.5 / 0.2	265.4 / 77.5	84.5 / 12.5	0.33	1.0189	275
5	0.0–0.330	170.9 / 1.3	273.4 / 84.1	80.8 / 05.8	0.12	0.2508	147
6	0.331–0.660	357.7 / 2.0	259.7 / 75.8	88.2 / 14.1	0.49	0.2656	99
7	0.661–1.0	182.0 / 8.8	303.9 / 73.8	89.9 / 13.6	0.80	0.3669	29

6.5. Interpretation

According to Orife and Lisle (2003), the absolute value of the stress ratio is a first approximation to the tensor difference measure (D), where the principal axes of stress tensors are coaxial. This is the case for the constituent states of the first determined stress state (Table 1, number 1), where the defined states with Φ = 0.1 to 0.8 are approximately coaxial and only their values of Φ are different. However, considering that, among the states, D_{max} = 0.8696, and according to the ranges introduced by Orife and Lisle (2003), the Φ difference of the states is insufficient to classify them as different stress states. The inclusion of states with Φ = 0.1 to 0.2 within the first determined state is preferred (rather than the inclusion of the state with Φ = 0.9) because, except for the last state, the others are coaxial and refer to the same tectonic setting (i.e., strike-slip). Therefore, two significant stress states are determined with respect to the stress difference measure D (Table 1, numbers 1, 2).

The average parameters of the two determined states refer to the strike-slip tectonic setting; however, the defined states of the second determined state are the most significant regarding the satisfaction of both criteria (Fig. 4) and the cluster density of the recognized stress tensors (Fig. 3; Table 1). In addition, the frequency of faults satisfying both criteria decreases as Φ increases (Fig. 4). This deduction, which has been facilitated by the diagram, allows the more accurate restraining of the average stress tensor during its determination. Furthermore, the similar lithological units without superposition of slickenlines on collected fault surfaces, indicating a single structural phase, in conjunction with the similarity of the stress states, demonstrate that the determined states belong to the modern stress phase.

The strike-slip tectonic setting and the trend of $\overrightarrow{\sigma_1}$ are also consistent with: (1) the results of the fault plane solutions of Talebian and Jackson (2002) and Moradi et al. (2011), showing an approximate NNW–SSE-trending compressive stress; (2) the N–S shortening trend and the right-lateral displacements deduced from GPS measurements by Vernant et al.,(2004).

The classification of defined stress states with respect to their stress ratios and cluster densities (Table 1, numbers 5–7) also reveals that the fault displacements are mainly a result of compressional rather than extensional stress regimes, i.e., only about 11% of the recognized tensors are extensional (Fig. 3c–e). This deduction is supported by geomorphic and tectonic geomorphology evidence. In this regard, the elevated area on the NE side of the TNF, in comparison with the lower area on the SW side of the fault (Fig. 2 and 5), indicates an intensified uplift history on the NE side. In this respect, measurement of elevation changes along a swath profile (Fig. 5) reveals the average elevation range (i.e., maximum elevation - minimum elevation) to be 266 m. Furthermore, according to Yousefi Bavil (2012), the responses of streams flowing on the Aynali Mountain, in respect to the relative vertical displacements along their longitudinal profiles, reveal unstable and nearly linear or convex longitudinal profiles that indicate ongoing uplift and young orogenic activity.

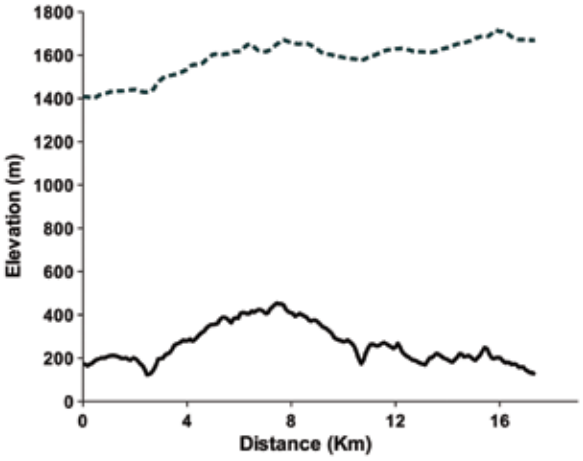

Figure 5: Elevation changes between the NE and SW sides of the TNF along a swath profile with length and width of approximately 17 and 5.3 km, respectively. The start and end points of the swath profile (i.e., S and E) are shown in Fig. 2. The solid line represents the elevation range (maximum elevation - minimum elevation) and the dashed line denotes mean elevation. The average value of the elevation range is 266 m.

The above-mentioned evidence (i.e., lithologic, kinematic, tectonic geomorphology, seismic, and remote sensing evidence) combined with the statistical results (i.e., very low-stress tensor cluster density) does not support the presumption that extensional stress states with $\Phi > 0.66$ (Table 1, number 7) are significant stress states responsible for the brittle deformation within the study area.

7. Conclusions

The SRAD diagram established on the parameters of stress ratio and angular deviation allows the following:

(1) the simultaneous illustration of the different parameters resulting from a stress inversion analysis;

(2) a reduction in classification perplexity of δ caused by conventional clustering methods, e.g. stereograms and Venn diagrams;

(3) an increase in the number of parameters available for mutual comparison (it also facilitates the illustration and, therefore, the comparison of parameters with different characteristics and value ranges); and

(4) the comparison and interpretation of up to eleven various stress states, including the entire range of Φ.

Acknowledgements

Thanks go to the two anonymous reviewers whose comments and suggestions were helpful in improving the manuscript. The author is grateful to Bernard Célérier for his suggestion on the mechanical criterion that helped to improve the quality of the criterion.

Appendix A

In addition to Bishop's Φ, which is the most common version of stress ratio, there are other adoptions of stress ratio formulated by different authors, including the following.
Nadai's $\mu = (2\sigma_2 - \sigma_1 - \sigma_3)/(\sigma_1 - \sigma_2)$ (Nádai 1931 p. 77)

Carey's $R = (\sigma_1 - \sigma_2)/(\sigma_1 - \sigma_3)$ (Carey and Mercier 1987)

Lisle's $R = (\sigma_2 - \sigma_3)/(\sigma_1 - \sigma_2)$ (Lisle 1989)

References

[1] Angelier, J., 1975. Sur l'analyse de mesures recueillies sans des sites faillés: l'utilité d'une confrontation entre les méthodes dynamiques et cinématiques. Comptes Rendus de l'Académe des Sciences, Paris D281, 1805–1808.

[2] Angelier, J., 1979. Determination of the mean principal directions of stresses for a given fault population, Tectonophysics, 56(3–4):T17–T26.

[3] Angelier, J., 1984. Tectonic analysis of fault slip data sets, Journal of Geophysical Research, 89:5835–5848.

[4] Angelier, J., 1990. Inversion of field data in fault tectonics to obtain the regional stress—III. A new rapid direct inversion method by analytical means, Geophysical Journal International, 103: 363–376.

[5] Angelier, J., 1994. Fault slip analysis and palaeostress reconstruction. In: Hancock, P.L., (Ed.), Continental Deformation, Pergamon, New York, pp. 53–101.

[6] Armijo, R., Carey, E., and Cisternas, A., 1982. The inverse problem in microtectonics and the separation of tectonic phases, Tectonophysics, 82:145–160.

[7] Bishop, A.W., 1966. The strength of soils as engineering materials, Géotechnique, 16:91–128

[8] Bott, M.H.P., 1959. The mechanisms of oblique slip faulting, Geological Magazine, 96:109–117.

[9] Célérier, B., 1988. How much does slip on a reactivated fault plane constrain the stress tensor? Tectonics, 7(6):1257–1278.

[10] Célérier, B., 1995. Tectonic regime and slip orientation of reactivated faults, Geophys. J. Int., 121:143-161.

[11] Célérier, B., Etchecopar, A., Bergerat, F., Vergely, P., Arthaud, F., and Laurent, P., 2012. Inferring stress from faulting: From early concepts to inverse methods, Tectonophysics, 581:206–219.

[12] Carey, E., and Brunier, B., 1974. Analyse théorique et numérique d'un modèle mécanique élémentaire appliqué à l'étude d'une population de failles, Comptes Rendus Hebdomadaires des Seances de l'Academie des Sciences, D279:891–894.

[13] Carey, E., and Mercier, J.L., 1987. A numerical method of determining the state of stress using focal mechanisms of earthquake populations: applications to Tibetan teleseismicity and microseismicity of S. Peru. Earth and Planetary Science Letters 82, 165–179.

[14] Delvaux, D., and Sperner, B., 2003. New aspects of tectonic stress inversion with reference to the TENSOR program. In: New Insights into Structural Interpretation and Modelling, edited by D.A. Nieuwland, Geol. Soc. Spec. Publ., 212, 75-100.

[15] Etchecopar, A., Vasseur, G., and Daignieres, M., 1981. An inverse problem in microtectonics for the determination of stress tensors from fault striation analysis, Journal of Structural Geology, 3:51–65.

[16] Fry, N., 1999. Striated faults: visual appreciation of their constraint on possible palaeostress tensors, Journal of Structural Geology, 21:7–21.

[17] Geological Survey of Iran, Tehran, 1993, Eastern Azerbaijan, Tabriz, 1:100000 geological series, sheet 5266, Geological Survey of Iran, Tehran.

[18] Galindo-Zaldívar, J., and González-Lodeiro, F., 1988. Faulting phase differentiation by means of computer search on a grid pattern, Annales Tectonicae, 2:90–97.

[19] Hardcastle, K.C., and Hills, L.S., 1991. Brute3 and Select—QuickBasic 4 programs for determination of stress tensor configurations and separation of heterogeneous populations of fault-slip data, Computers and Geosciences, 17:23–43.

[20] Huang, Q., 1988. Computer-based method to separate heterogeneous sets of fault-slip data into sub-sets, Journal of Structural Geology, 10:297–299.

[21] Karakhanian, A.S., Trifonov, V.G., Philip, H., Avagyan, A., Hessami, K., Jamali, F., Bayraktutan, M.S., Bagdassarian, H., Arakelian, S., Davtian, V., and Adilkhanyan, A., 2004. Active faulting and natural hazards in Armenia, eastern Turkey and northwestern Iran, Tectonophysics, 380:189–219.

[22] Liesa, C.L., and Lisle, R.J., 2004. Reliability of methods to separate stress tensors from heterogeneous fault-slip data, Journal of Structural Geology, 26(3): 559–572.

[23] Lisle, R.J., 1987. Principal stress orientations from faults: an additional constraint, Annales Tectonicae, 1:155–158.

[24] Lisle, R.J., 1988. Romsa: a Basic program for palaeostress analysis using fault-striation data, Computers and Geosciences, 14:255–259.

[25] Lisle, R.J., 1989. The statistical analysis of orthogonal orientation data. Journal of Geology 97, 360–364.

[26] Lisle, R.J., and Orife, T., 2002. STRESSTAT: a Basic program for numerical evaluation of multiple stress inversion results, Computers and Geosciences, 28:1037–1040.

[27] Menke, W., 1989. Geophysical data analysis: discrete inverse theory. Academic Press, San Diego 289.

[28] Moradi A.S., Denis Hatzfeld, D., and Tatar M., 2011. Microseismicity and seismotectonics of the North Tabriz fault (Iran), Tectonophysics, 506:22–30.

[29] Nádai, A., 1931. Plasticity. McGraw-Hill, New York, 367pp.

[30] Nemcok, M. and Lisle, R.J., 1995. A stress inversion procedure for polyphase fault/slip data sets, Journal of Structural Geology, 17:1445–1453.

[31] Orife, T., and Lisle, R.J., 2003. Numerical processing of palaeostress results, Journal of Structural Geology, 25:949–957.

[32] Ramsay, J.G. and Lisle, R.J., 2000. The Techniques of Modern Structural Geology, Vol.3, Applications of Continuum Mechanics in Structural Geology. Academic Press, London 1061pp.

[33] Schellart, W.P., 2000. Shear test results for cohesion and friction coefficients for different granular materials:

scaling implications for their usage in analogue modelling, Tectonophysics, 324:1–16.

[34] Simón-Gómez, J.L., 1986. Analysis of a gradual change in stress regime (example from the eastern Iberian Chain, Spain), Tectonophysics, 124:37–53.

[35] Talebian, M., and Jackson, J.A., 2002. Offset on the Main Recent Fault of the NW Iran and implications for the late Cenozoic tectonics of the Arabia-Eurasia collision zone, Geophys. J. Int., 150:422–439.

[36] Vernant, P., Nilforushan, F., Hatzfeld, D., Abbasi, M.R., Vigny, C., Masson, F., Nankhali, H., Martinold, J. Ashtiani, A. Tavakoli, F. and Chery, J. 2004. Present-day crustal deformation and plate kinematics in the Middle East constrained by GPS measurements in Iran and northern Oman, Geophys. J. Int., 157:38–398.

[37] Wallace, R.E., 1951. Geometry of shearing stress and relation to faulting. Journal of Geology, 59:118–130.

[38] Yamaji, A., 2000. The multiple inverse method: a new technique to separate stresses from heterogeneous fault-slip data, Journal of Structural Geology, 22:441–452.

[39] Yamaji, A., Sato, K., and Otsubo, M., 2010. Multiple inverse method software package (user's guide). <http://www.kueps.kyoto-u.ac.jp/~web-bs/tsg/software/mim> Accessed 21 March 2013.

[40] Yousefi Bavil, A., 2012. Longitudinal Profiles of Bedrock Rivers around North Tabriz and North Misho Faults: Implications for Geomorphic Fault Segmentation (Eastern Azerbaijan Province, Iran); ASM Sci. J., 6(2): 107–121.

[41] Yousefi Bavil, A., and Moayyed M. Paleo and modern stress regimes of central North Tabriz Fault (Eastern Azarbaijan province, NW Iran), Journal of Earth Science, China, (in press: vol 25, no 3, 2015).

[42] Žalohar, J., and Vrabec, M., 2007. Paleostress analysis of heterogeneous fault-slip data: The Gauss method, Journal of Structural Geology, 29:1798–1810.

المملكة الأردنية الهاشمية

الجامعة الهاشمية

المجلة الأردنية
لعلوم الأرض والبيئة

JJEES

مجلة علمية عالمية محكمة

http:// jjees.hu.edu.jo/

ISSN 1995-6681

المجلة الأردنية لعلوم الأرض والبيئة

مجلة علمية عالمية محكمة

المجلة الأردنية لعلوم الأرض والبيئة: مجلة علمية عالمية محكمة ومفهرسة ومصنفة، تصدر عن الجامعة الهاشمية وبدعم من صندوق البحث العلمي– وزارة التعليم العالي والبحث العلمي، الأردن.

هيئة التحرير

ترسل البحوث إلى العنوان التالي:

رئيس تحرير المجلة الأردنية لعلوم الأرض والبيئة

عمادة البحث العلمي والدراسات العليا

الجامعة الهاشمية

الزرقاء ١٣١٣٣ – الأردن

هاتف ٣٩٠٣٣٣٣–٥–٩٦٢+ فرعي ٤١٤٧

Email: jjees@hu.edu.jo, Website: www.jjees.hu.edu.jo

المملكة الأردنية الهاشمية

الجامعة الهاشمية

المجلة الأردنية
لعلوم الأرض والبيئة

JJEES

مجلة علمية عالمية محكمة

تصدر بدعم من صندوق دعم البحث العلمي

http://jjees.hu.edu.jo/

المجلد (٦) العدد (١) ISSN 1995-6681 أيلول ٢٠١٤ / ذو الحجة ١٤٣٥